The *Periaxin* gene in human and mouse demyelinating peripheral neuropathy.

Anna C. Williams

Ph.D. Thesis

The University of Edinburgh

2002

DECLARATION

I declare that I wrote this thesis, and the work described in it is my own except where indicated. The work has not been submitted for any other degree or professional qualification.

Anna C. Williams

July 2002

ACKNOWLEDGEMENTS

My thanks go to Professor Peter Brophy, in whose laboratory I have carried out this work. I want to thank the members of the 'Brophy lab', past and present, who have supported me with help, ideas, technical assistance and friendship: Felipe Court, Mary Davie, Linda Ferguson, Stewart Gillespie, Frank Gunn-Moore, Mandy Jackson, Richard Johnson, Shona Melrose, Diane Sherman, Steven Tait and Sylvia Vasiliou. Special thanks go to Stewart Gillespie, without whom the *PERIAXIN* gene would not have been successfully sequenced, Felipe Court, who took the confocal microscope pictures, Richard Johnson, computer hero and Sylvia Vasiliou, who began the Fbl6 work.

Prof. Jeanne Bell, Department of Pathology, Western General Hospital, kindly supplied the human cauda equina and sural nerve biopsy paraffin blocks, and frozen specimens of post-mortem human cauda equina.

Prof Jonathan Rees, Department of Dermatology, The Royal Infirmary of Edinburgh, provided the skin biopsy material.

I would also like to thank our collaborators, Dr. Vincent Timmerman's group in Belgium, Dr. Eric LeGuern's group in Paris, Dr. James Lupski's group in USA and Dr. Ezra Battaloglu's group in Turkey, and all of the CMT families concerned.

ABSTRACT

Charcot-Marie-Tooth (CMT) disease is one of the most common inherited neurological diseases with a prevalence of 1 in 2500. It is clinically and genetically heterogeneous with at least 22 loci and 11 genes now described with mutations resulting in the disease.

L-periaxin is a protein expressed in myelinating Schwann cells. It relocates from the adaxonal membrane in newly myelinating Schwann cells to the abaxonal membrane when myelination is complete. Periaxin-null mice develop a late-onset demyelinating peripheral neuropathy, suggesting that periaxin is important in maintaining compact myelin in a healthy Schwann cell.

We show that mutations in the human *PERIAXIN* gene are associated with a subtype of autosomal recessive CMT disease (Type 4F)/Dejerine-Sottas disease. Eight different mutations are now described in seven different families. We carried out immunohistochemistry on sural nerve biopsies from three of these patients, showing evidence of a stable truncated L-periaxin protein, missing its C-terminal domain in two patients (C715X and R1070X). This expands our knowledge of the function of L-periaxin. The PDZ domain at the N-terminus of L-periaxin allows homodimerisation of the protein, and the basic domain binds dystrophin-related protein 2 (DRP2), underpinning the DRP2-dystroglycan complex at the apical surface of the Schwann cell, and presumably forming a mechanical and functional link to the basement membrane. Even though the truncated proteins contain these domains the attendant demyelination suggests that they are not sufficient for L-periaxin's function.

The C-terminus of L-periaxin binds to the F-box protein Fbl6 which is shown to be in the Schwann cell cytoplasm. Fbl6 targets molecules for ubiquitination and degradation by the proteasome. The truncated forms of L-periaxin found in human patients found so far have lost this Fbl6 binding site.

The periaxin-null mouse is a mouse model of the human disease CMT4F. Morphological studies of peripheral nerve in these mice show that myelination and

axon number are normal in early life. One of the putative roles of L-periaxin is in myelin repair, and nerves in the periaxin-null mice can undergo remyelination, but with an abnormal control on the limit on myelin thickness. The periaxin-null mouse nerve fibres have thicker myelin sheaths than the wild-type controls, and this may be the forerunner of demyelination.

These studies suggest that studies of the cell biology of periaxin in the mouse and in human patients are likely to be synergistic in expanding our knowledge of Schwann cell biology and peripheral nerve disease.

INDEX

LIST OF FIGURES

LIST OF TABLES

ABBREVIATIONS

ALS	amyotrophic lateral sclerosis
APC	Adenomatous polyposis coli
ARCMT	autosomal recessive CMT
BSA	bovine serum albumin
CASPR	contactin associated protein
CHD	congenital hypomyelinating disease
CIPA	congenital insensitivity to pain with anhidrosis
CMT	Charcot-Marie-Tooth
CMV	cytomegalovirus
CNS	central nervous system
Cx32	connexin-32
DNA	deoxyribonucleic acid
DRG	dorsal root ganglia
DRP2	dystrophin related protein 2
DSS	Dejerine-Sottas
ECM	extracellular matrix
EGR2	early growth response 2
ES	embryonic stem
EST	expressed sequence tags
FD	familial dysautonomia
GDAP1	ganglioside induced differentiation associated protein 1
GFAP	glial fibrillary acidic protein
GJB1	gap junction associated protein 1
GST	glutathione S transferase
HBSS	Hanks balanced salt solution
HMG	high mobility group
HMN	hereditary motor neuropathy
HMSN	hereditary motor and sensory neuropathy
HNPP	hereditary neuropathy with liability to pressure palsies
HSAN	hereditary sensory and autonomic neuropathy
HSN	hereditary sensory neuropathy
IGHMBP2	Immunoglobulin μ-binding protein-2
IKBKAP	IκB kinase complex associated protein
KIF1Bβ	kinesin superfamily motor protein B
LCB1/2	long chain base 1/2
LRR	leucine rich repeat
MAG	myelin associated glycoprotein

MBP	myelin basic protein
MPZ	myelin protein zero gene
MTMR2	myotubularin related protein 2
NCAM	neural cell adhesion molecule
NDRG1	N-myc downstream regulated gene 1
NF155	neurofascin 155
NF-L/M/H	Neurofilament light/medium/heavy chain
NGF	nerve growth factor
NTRK1	neurotrophic tyrosine receptor kinase 1
OCT	optimal cutting temperature
PAC	plasmid artificial chromosome
PBS	phosphate buffered saline
PCR	polymerase chain reaction
PLP	proteolipid protein
PMP22	peripheral myelin protein 22
PNS	peripheral nervous system
P0	myelin protein zero protein
PRX	periaxin
SCE1	Schwann cell enhancer 1
SMARD	spinal muscular atrophy with respiratory distress
SOD1	superoxide dismutase 1
SPT	serine palmitoyl transferase
SPTLC1	Serine palmitoyltransferase long chain base subunit-1
TESPA	3-aminopropyltriethoxysilane

1. INTRODUCTION

To conduct impulses rapidly, nerves must either have a large diameter, or be insulated with a myelin sheath. Vertebrates use the latter option and for them myelin is an essential part of the central and peripheral nervous system. Acquired and inherited diseases affecting the myelination of the nervous system emphasise this importance.

In the peripheral nervous system (PNS) the Schwann cell forms the compact myelin sheath, whereas the oligodendrocyte performs this role in the central nervous system (CNS). The Schwann cell forms a one to one relationship with the axon, unlike the oligodendrocyte which can myelinate many different axons. Between each axo-glial segment lies the node of Ranvier where sodium channels are clustered. The action potential 'jumps' from one node to the next in a fast and efficient manner by saltatory conduction (saltare - to jump) (Figure 1).

1.1. THE DEVELOPMENT OF THE SCHWANN CELL

The Schwann cell is named after the German anatomist Theodor Schwann (1810-1882). Schwann cells develop from the neural crest and migrate along growing neurites (Le Douarin et al., 1991). In mature peripheral nerve they form two subtypes: nonmyelinating and myelinating Schwann cells, which are present in comparable numbers. There are two intermediates; the Schwann cell precursor, present at mouse embryonic day 12 and 13 and the immature Schwann cell, present from mouse embryonic day 15 until birth. At birth, Schwann cells start to differentiate into myelinating and nonmyelinating Schwann cells (Reviewed by Jessen and Mirsky (Jessen and Mirsky, 1999) (Figure 2)). Myelinating Schwann cells generate myelin sheaths that wrap large diameter axons, and nonmyelinating cells accommodate small diameter axons in shallow troughs along their surface.

Myelinating Schwann cells undergo extensive changes in gene expression and protein synthesis to allow them to synthesise large amounts of membrane and myelin specific proteins. This is made possible by the combined action of a set of transcription factors that are preferentially expressed in Schwann cells.

1.1.1. Transcription factors in Schwann cell differentiation

There are several families of transcription factors that are expressed in myelinating Schwann cells: homeodomain proteins, zinc finger proteins and HMG-domain proteins.

Pax3 is a paired homeodomain protein which is expressed during early development in the spinal cord and neural crest cells. There is a transient rise in Pax3 expression around the time of birth, it is then down-regulated in myelinating Schwann cells, but continues to be expressed in nonmyelinating Schwann cells. Pax3 may determine the choice between a myelinating and nonmyelinating Schwann cell phenotype (Wegner, 2000).

SCIP (also called Tst-1 or Oct 6) is another homeodomain protein expressed in Schwann cells. SCIP expression is dependent on an increase in intracellular cAMP levels, hence the name '**s**uppressed **c**-AMP-**i**nducible **P**OU protein.' This increase is conferred by axonal contact and occurs at the promyelinating stage. The protein is then down-regulated in most myelinating Schwann cells. Inactivation of both SCIP alleles in mice leads to transient arrest of Schwann cell development at this promyelinating stage, but when the cells have overcome this block, differentiation proceeds normally (Bermingham et al., 1996).

The Krox/Egr transcription factors are zinc finger proteins. The onset of Krox-20/Egr2 expression in the peripheral nervous system correlates with the appearance of embryonic Schwann cells (Topilko et al., 1994). Expression of Krox-20/Egr2 requires continual neuronal signalling from axonal contact, reaching maximal levels just before onset of myelination and remains unaltered in myelinating Schwann cells throughout life. In contrast, nonmyelinating Schwann cells express Krox-24/Egr1 (Topilko et al., 1997). Krox-20 upregulates the expression of many myelin proteins including myelin protein zero (P0), myelin basic protein (MBP), myelin associated glycoprotein (MAG), peripheral myelin protein 22 (PMP22) and periaxin (PRX) (Nagarajan et al., 2001). Other proteins, such as glial fibrillary acidic protein (GFAP) and neural cell-adhesion molecule (NCAM), normally present in immature Schwann cells and nonmyelinating cells, are down-regulated.

The Sox proteins contain a high-mobility-group (HMG) domain as their DNA-binding domain, similar to the one in male sex-determining factor SRY. Sox10 is expressed early in the neural crest and is then preferentially expressed in the late embryonic glial cell lineage and in mature Schwann cells and oligodendrocytes. Sox proteins are weak transcription factors on their own, but efficiently cooperate with co-expressed transcription factors. Sox10 strongly potentiates the activity of Pax3 and SCIP in transfection experiments (Kuhlbrodt et al., 1998). Thus, Sox10 may be involved not only in the commitment of cells to the myelinating glial lineage but also in maintenance of glial-specific gene expression.

1.1.2. The process of myelination

For successful myelination, Schwann cells must establish a 1:1 relationship with an axon, extend longitudinally until limited by a node of Ranvier, and form a myelin sheath by the spiralisation of the plasma membrane. Before birth, Schwann cells send cytoplasmic processes into bundles of axons, and progressively sort individual axons so that this 1:1 relationship is established, in a process called radial sorting (Webster, 1984). Axons destined to remain unmyelinated are ensheathed in groups by nonmyelinating Schwann cells. The transition of the Schwann cell, from a bipolar cell to a precisely ordered cylinder containing a compact myelin sheath, represents a complex architectural problem which has been solved in part by exploiting polarisation. Schwann cells deposit and organise a basal lamina at their basal surface away from the axon. The apical surface envelopes an adjacent axon with a layer of cytoplasm bounded by an extension of the plasma membrane. Then, these cells wrap concentric extensions of their membrane around the axon whilst remaining fixed to the basal lamina. After several rounds of spiralisation, cytoplasm is extruded by the apposition of the cytoplasmic surfaces of the membrane to allow compaction of the mature multi-lamellar sheath (Figure 3a). This compaction may be generated in part by interactions between the membrane proteins. The extracellular domain of P0 forms a tetrameric array that interlocks with similar arrangements in the opposing membranes, and the intracellular domain interacts in a homophilic manner. P0 may also be involved in a heterophilic interaction with PMP22 via the L2/HNK-1

epitopes of their glycosidic links (Bell and Haites, 1998). These arrangements allow closer juxtaposition of the membranes.

1.1.3. The role of extracellular matrix in myelination of peripheral nerve

The extracellular matrix (ECM) is critical for myelination of peripheral nerve. The basal lamina of the Schwann cell is formed during embryonic development and contains type IV collagens, laminin 2, fibronectin, N-syndecan, entactin and heparan sulphate proteoglycan (Bunge, 1993). ECM formation and myelination are tightly linked (Bunge, 1993). Immature Schwann cells do not have a basal lamina (Giannini and Dyck, 1990) and it is thought that contact with an axon regulates Schwann cell expression of laminin chain genes and directs synthesis of a basal lamina surrounding each Schwann cell-axon unit (Doyu et al., 1993).

In the absence of the assembly of ECM, myelination cannot proceed. Collagen synthesis is inhibited by exclusion of ascorbic acid and this prevents myelination in culture (Eldridge et al., 1989). Laminin is an essential component of the basal lamina as blocking β1-integrin, one of its receptors on the Schwann cell basal membrane, inhibits myelination (Fernandez-Valle et al., 1994). The *dy/dy* mouse, with low levels of expression of the laminin α2-chain gene (*Lama2*), has a discontinuous basal lamina around Schwann cells, a reduced number of myelinated axons and abnormal myelination. In *dy/dy* nerves, regenerating axons are found lying on the external surface of the Schwann cell in direct contact with the basal lamina (Uziyel et al., 2000). This suggests that, in the absence of the competent basal lamina, Schwann cells are not polarised and that polarised Schwann cells are required for normal myelination.

The ECM provides the structural and mechanical integrity to the PNS. In the central nervous system, there is no extracellular collagen and oligodendrocytes are not ensheathed in basal lamina. This allows much denser packing of nerve fibres, but at the cost of poor mechanical strength. Peripheral nerves are continually subjected to stretching and direct trauma, both in development and adulthood, and require higher tensile and mechanical strength (Podratz et al., 2001).

1.1.4. Schwann cell cytoplasm

Even in mature compact myelin, Schwann cell cytoplasm persists in channels called Schmidt-Lanterman incisures and in the adaxonal or periaxonal rim of the mature sheath (Bunge et al., 1989). These channels may serve as supply lines for the delivery of nutrients, or they may provide the submembrane scaffold for locating and orientating proteins within discreet areas of the myelin sheath (Figure 3b). The periaxonal rim of cytoplasm is contained in the paranodal loops, which are important in the formation of the node of Ranvier.

1.1.5. Formation of the Node of Ranvier

In myelinated fibres, sodium channels concentrate in the axonal membrane at nodes of Ranvier that are delimited by axoglial adhesion zones between each Schwann cell-axon unit. The tight wraps of Schwann cell myelin expand at their extremities to form cytoplasm-filled paranodal loops which adhere to the axonal membrane with septate-like junctions. These junctions contain contactin-associated protein (caspr) (alternatively known as paranodin) (Einheber et al., 1997; Menegoz et al., 1997), and contactin forming a *cis* complex in the paranodal axon membrane (Boyle et al., 2001). Caspr/paranodin interacts with the alternatively spliced isoform of the neuronal cell adhesion molecule neurofascin (NF155) in the Schwann cell membrane (Tait et al., 2000). The establishment of these tight contacts during development may help to cluster the sodium channels at the node of Ranvier (Rasband et al., 1999) (Figure 4). However, mouse mutants that are unable to synthesise myelin galactolipids and that display disrupted paranodal axoglial interactions still maintain nodal sodium channels (Dupree et al., 1999). Mice deficient in contactin also have disrupted junctions yet maintain sodium channel clustering (Boyle et al., 2001). Nevertheless, all of these mutants have severe neurological phenotypes, linked to substantially reduced conduction velocities.

Myelinated axons also have potassium channels which are sequested in the juxtaparanodal region. These Shaker or Kv potassium channels are believed to accelerate the rate of repolarisation of the axolemma. The *myelin deficient rat (md)*, and mice deficient in caspr/paranodin, contactin or galactocerebrosidase have

aberrant localisation of potassium channels, with displacement of the Kv channels into the paranodal region nearer to and sometimes overlapping with the sodium channels (Bhat et al., 2001; Boyle et al., 2001; Dupree et al., 1999). Thus the segregation of sodium and potassium channels is disrupted in these mutants that show demyelination. Disruption of the interaction between Schwann cells and the axon is one of the earliest correlates of axonal dysfunction in the demyelinating disease Guillain-Barre syndrome (Griffin et al., 1996). Lack of channel segregation may contribute to conduction block and spontaneous impulses seen in demyelinating diseases. Spontaneous impulse generation has been implicated in neuropathic pain in some demyelinating conditions (Gillespie et al., 2000).

Although much progress has been made in understanding the process of myelination and the interactions between Schwann cells and axons, we still lack knowledge of how myelin proteins interact to form, maintain and repair myelin. This is of critical importance in the understanding and development of future therapies for human demyelinating diseases both in the peripheral nervous system and ultimately the central nervous system.

1.2. PERIPHERAL NEUROPATHY

Peripheral neuropathy is a clinical syndrome where there is a disorder of function of the peripheral nerves. A typical patient has a progressive weakness and numbness of the hands and feet starting distally and progressing proximally. The pathology of the disorder of the peripheral nerves can be primarily demyelinating or axonal. The syndrome can be due to acquired or inherited causes, and if acquired may be reversible, especially if the pathology shows a picture of demyelination. The commonest cause of peripheral neuropathy in the developed world is secondary to diabetes mellitus, and the commonest cause of inherited peripheral neuropathy is Charcot-Marie-Tooth disease.

1.2.1. Inherited Human Peripheral Neuropathy

There has been extensive study of both axonal and demyelinating inherited forms of human peripheral neuropathy, over the last 10 years. In 1991, the molecular basis of

the first subtype was determined (Lupski et al., 1991), but this has now expanded to include many more molecular mutations. Clinical phenotype/genotype correlations in these patients and examination of the cell biology of the molecules involved are complementary to the understanding of myelination and demyelination. Many inherited human neuropathies come under the umbrella of Charcot-Marie-Tooth (CMT) disease, or hereditary motor and sensory neuropathy (HMSN). The naming of these diseases is controversial, with the clinical world keen to avoid using eponymous names for diseases, but scientists still use the historical names. The name of each type of neuropathy depends on the conviction of the groups that first describe them, and the list is becoming daily more complicated. I will name the diseases CMT diseases unless they are called a different name in most of the literature.

1.2.2. Charcot-Marie-Tooth Disease

In 1886, Drs Charcot, Marie and Tooth described patients with an inherited form of peroneal muscle atrophy – a disorder now known as Charcot-Marie-Tooth disease (CMT), or, more commonly by clinicians, hereditary motor and sensory neuropathy (HMSN).

CMT disease is common, with a prevalence of 1 in 2500 in the UK (Skre, 1974). The first symptoms usually begin in the first or second decade of life consisting of a progressive distal sensory and motor loss. Symptoms usually first occur in the legs, and progress to the hands leaving the patient with a sensory loss in a 'glove and stocking' distribution and an ascending motor weakness of the limbs. The distal muscle weakness may be obvious from an early age with an abnormal gait or clumsiness in running. Other typical features include weakness at the ankle, steppage gait, and the characteristic pes cavus deformity of the foot (Figure 5). Patients are moderately to severely disabled by these symptoms, although the disease is not usually life-threatening. Confirmation of the clinical diagnosis relies primarily on electrophysiology, and less on histopathology after sural nerve biopsy in this country, due to the permanent and sometimes painful sensory loss associated with this procedure.

In 1968, Dyck and Lambert (Dyck and Lambert, 1968) divided CMT disease into two types based on pathological and neurophysiological differences. They defined patients with slow nerve conduction velocities of normal amplitude indicating a primary demyelinating neuropathy as CMT disease type 1. Those with a primary axonal loss, with normal nerve conduction velocity but low amplitude were described as CMT type 2 patients. These differences indicated different aetiologies for the two classes of neuropathies, with myelin being initially affected in CMT1 and the axon directly affected in CMT2. However, some patients did not fit into this convenient classification, and they were said to have 'intermediate' forms of the disease.

However, since the advent of the molecular genetic revolution, CMT disease has been divided further according to the mutations in the genes involved. It has also challenged the initial subdivision, as families have been found who fulfil the CMT2 criteria, and yet have mutations in connexin-32, the gene defect leading to a subtype of CMT1 (Timmerman et al., 1996b). The clinical homogeneity, yet genetic heterogeneity of these subtypes suggests that they share a common physiological pathway to their phenotype, which is likely to be damage to the axon. This probably explains why patients with CMT can be asymptomatic for years, even with very reduced nerve conduction velocities; only when axons are damaged do symptoms appear (Krajewski et al., 2000; Sahenk, 1999).

Initially most research was into demyelinating forms of the disease and the autosomal dominant subtypes, through ease of classification. However, the number of autosomal recessive subtypes that have been identified is expanding. The first gene identified with mutations causing CMT2 was identified in 2000 – *NF-L* (Mersiyanova et al., 2000). To date, in traditional CMT diseases, mutations have been described in eleven genes, and CMT families have been linked to more loci, dividing up CMT disease into at least twenty-two subclasses. There is continuing controversy on how to subdivide the disease (Vance, 2000); however an attempt is made in Table 1. There is a view that efforts should be made to simplify the terminology for these inherited neuropathies by concentrating on the molecular diagnosis. One of the objections to continuing to call these diseases CMT diseases is

in defining the size of umbrella of CMT disease - when does an inherited peripheral neuropathy become a CMT disease? If CMT disease defines all inherited neuropathies then diseases such as the pure sensory and motor neuropathies (HSN and HMN) also are CMT diseases. Certainly, the natural home of these diseases is linked to the traditional CMT diseases, but they are often separated artificially in the literature.

The proteins encoded by these genes are involved in a variety of cellular functions, including cytoskeletal scaffolding (NF-L), the transport of small molecules within and across the myelin sheath (Cx32), signal transduction (MTMR2), cell arrest/proliferation and differentiation (PMP22, NDRG1, EGR2), myelin maintenance and formation (P0 and PRX) and axonal transport (KIF1Bβ), as discussed later.

The prevalence of all types of CMT disease is 20-40:100 000 with CMT2 accounting for about 20% of this (Ionasescu, 1995).

The commonest mutation associated with CMT disease is duplication of the gene *PMP22* which accounts for about 70% of demyelinating CMT disease (Nelis et al., 1996) and about 52% of unselected patients with hereditary neuropathies (Boerkoel et al., 2002). In this unselected subset of 153 patients, 7% had *Cx32* mutations, 3% myelin protein zero (*MPZ)* mutations, 3% *PMP22* mutations and about 1% had *EGR2*, *PRX* and *NF-L* mutations respectively. *MTMR2* mutations were not seen. Of note, 33% of these patients still did not have their CMT disease molecularly diagnosed, suggesting that there are more genes involved yet to be discovered. Also, one third of the point mutations seen represented de novo events suggesting that absence of a family history should not prevent molecular investigation for CMT disease (Boerkoel et al., 2002).

CMT disease is a genetically and clinically heterogeneous disease for which genotype-phenotype correlations are difficult to define. Both the phenotypic features and disease severity can either be consistent or differ widely within and amongst families (Senderek et al., 2001). This ambiguity in genotype-phenotype correlation probably reflects limitations in our knowledge and understanding of the effects of

genetic background and environment on the biological function of the affected proteins.

The genetics of CMT disease is a rapidly moving field and no less than six new subtypes of CMT disease were discovered on the basis of genetic mutations in the year 2001. No doubt, there are more to come. Understanding the molecular basis of CMT disease can therefore be expected to contribute significantly to the current limited understanding of the biology and pathophysiology of the peripheral nervous system.

1.3. DOMINANT DEMYELINATING CMT DISEASE

1.3.1. CMT1A

Peripheral myelin protein 22kD (PMP22)

The first of the CMT subtypes to be classified was CMT1A. Some families with autosomal dominant CMT showed linkage to part of chromosome 17, (17p11.2-p12) and these patients had duplication of the 1.5 MB area that included the normal *PMP22* gene (Lupski et al., 1991). These patients have increased expression of *PMP22* RNA (Yoshikawa et al., 1994) and transgenic mice over-expressing *Pmp22* develop a peripheral neuropathy resembling CMT1A (Huxley et al., 1996). Furthermore, a minority of CMT1A patients show point mutations in the *PMP22* gene, adding to evidence that this protein is involved. Trembler and Trembler-J mice, thought to be models of autosomal dominant CMT, were found to have mutations in *Pmp22* (Suter et al., 1992a; Suter et al., 1992b). Patients with hereditary neuropathy with liability to pressure palsies (HNPP), who have reversible pressure-induced segmental demyelination in the PNS, show lack of the same 1.5 MB DNA fragment and so have only one copy of the *PMP22* gene (Chance et al., 1993). This suggests that the 'dosage' of PMP22 protein expressed is important in the function of myelin sheaths.

PMP22 is a tetraspan transmembrane protein of unknown function, but the apparent dosage sensitivity suggests it is involved in a multimeric complex within myelin that requires exact macromolecular stoichiometry for proper functioning. PMP22 only

accounts for 2-5% of myelin protein, suggesting that it does not play a structural role (Reilly, 1998), however, it is necessary for both myelin formation and maintenance. PMP22 and P0 may complex together within the Schwann cell, suggesting that some *PMP22* mutations may cause disease by destabilising the P0 interactions necessary for the formation and stabilisation of compact myelin (D'Urso et al., 1999). Some mutant PMP22 molecules are not transported to the plasma membrane, and inhibit the trafficking of wild-type PMP22 to the plasma membrane (Naef and Suter, 1999). The retained wild-type and mutant PMP22 accumulate within the cell and appear to have a toxic effect on the Schwann cell (Notterpek et al., 1999). Therefore, most *PMP22* missense mutations cause disease by a combination of a dominant negative effect, inhibiting the transport of mutant and wild-type PMP22 to the plasma membrane and a toxic gain of function effect, resulting from the accumulation of PMP22 within the cell.

Proteolipid Protein (PLP), the major central nervous system myelin protein, also shows such dosage sensitivity. PLP and PMP22 show structural similarities, and duplications and deletions of *PLP* lead to Pelizaeus-Merzbacher disease, a central nervous system demyelinating condition (Pham-Dinh et al., 1991).

PMP22 mutations are the most common mutations found in CMT. Most CMT1A patients have the *PMP22* duplication and 70% of all CMT1 patients carry the duplication (Boerkoel et al., 2002; Nelis et al., 1996). Thus, *PMP22* duplication should be screened for first in a patient with suspected demyelinating CMT disease (Bell and Haites, 1998).

1.3.2. CMT1B

Myelin protein zero (P0) (from the myelin protein zero (*MPZ*) gene)

P0 is the major structural component of peripheral nerve myelin accounting for 50% of peripheral myelin protein. It contains a single membrane-spanning domain, a large glycosylated immunoglobulin-like extracellular domain and a smaller basic intracellular domain (Lemke et al., 1988). It is exclusively expressed by myelinating Schwann cells and is thought to be involved in linking together adjacent myelin

lamellae in compact myelin. The extracellular domain of P0 forms a tetrameric array that interlocks with similar arrangements in the opposing membranes, and the intracellular domain interacts in a homophilic manner. P0 may also be involved in a heterophilic interaction with PMP22 via the L2/HNK-1 epitopes of their glycosidic links (Bell and Haites, 1998).

P0-null mice have severely hypomyelinated axons, but also their myelin and axons degenerate with age. This suggests the role of P0 in the formation and maintenance of the PNS myelin sheath (Giese et al., 1992).

Mutations in the extracellular, intracellular and transmembrane domains of the proteins can all cause CMT1B (Warner et al., 1996b). Mutations disrupting the interactions within the tetramer or between tetramers produce disease by a dominant negative effect, whereas mutations retarding production of P0 produce disease by a loss of function effect (Warner et al., 1996a). However, some patients with *MPZ* mutations have axonopathic features and are diagnosed with CMT2 (Boerkoel et al., 2002).

1.3.3. CMT1D

Early growth response 2 transcription factor (EGR2)

The early growth response 2 gene (*EGR2*) is a Cys2His2 zinc finger transcription factor thought to affect the expression of late myelin genes. Mutations in the *EGR2* gene have been associated with CMT1, Dejerine-Sottas disease (DSS) and congenital hypomyelinating neuropathy (CHD) and these can be inherited in both a dominant and a recessive manner. Some *EGR2* mutations occur within the zinc finger DNA-binding domain. These mutations reduce DNA binding and therefore decrease transcriptional activity of downstream genes. A recessively inherited mutation, causing CHD, affects the inhibitory domain (R1) that binds the NAB transcriptional co-repressors. These repressors inhibit the transcriptional activity of multiple members of the immediate – early response gene family including EGR1 and EGR2. The R1 domain mutation prevents interaction of EGR2 with the NAB co-repressors and thereby increases transcriptional activity. Hence, dosage sensitivity may be

important with EGR2, as with PMP22 (Warner et al., 1999). Homozygous *Krox20* (*Egr2*) knockout mice display hypomyelination of the peripheral nervous system and Schwann cell arrest at an early stage of differentiation concurring with human cases of CHD with recessive *EGR2* mutations (Nelis et al., 1999a; Warner et al., 1998).

1.3.4. CMT1X

Connexin-32 (Cx32) or Gap junction protein 1 (GJB1)

Connexins are transmembrane proteins that assemble to form gap junctions, channels that facilitate the transfer of ions and small molecules across membranes. Cx32 is a tetraspan transmembrane protein which is located in the paranodal loops and the Schmidt-Lanterman incisures in noncompact myelin, and is thought to function as a channel for the transport of electrolytes and metabolites between the noncompact regions of the myelin sheath.

Mutations in this gene appear to be the most common cause of non-duplication CMT1 (Nelis et al., 1996) with mutations appearing throughout the domains of the protein (Warner et al., 1996b). *Cx32* mutations can cause a neuropathy with clinical and electrophysiological features of either a demyelinating or an axonal neuropathy. Male patients usually have a more severe and earlier onset neuropathy which is frequently demyelinating, whereas female patients generally have a later, milder disease often of an axonal type. The severity of disease among women may depend on the vagaries of X-chromosome inactivation as well as the nature of the mutation, genetic background and environment. The mutations in *Cx32* that have been studied result in either a loss of ability to form functional gap junction channels or an alteration in the gating properties of the channels (Abrams et al., 2000).

1.4. AXONAL NEUROPATHIES

1.4.1. CMT2A

Kinesin superfamily motor protein B gene (KIF1Bβ)

KIF1Bβ is a member of the kinesin superfamily of molecular motor proteins which function in aspects of axonal transport (Hirokawa, 1998). The molecules all have

similar motor domains but are otherwise divergent, presumably allowing the association with different cargo molecules. KIF1Bβ transports synaptic vesicle precursors. Knockout mice for this gene die within thirty minutes of birth, due to central apnoea, but mice heterozygous for the mutated allele develop a late-onset axonopathy similar to axonal forms of CMT disease. Synaptic vesicle proteins are specifically decreased in the peripheral axons of these mice (Zhao et al., 2001). A human family with CMT2A was found to have a mutation in the ATP binding site of KIF1Bβ, which segregated with their disease (Zhao et al., 2001). As mature axons are believed to lack protein synthesis machinery, proteins essential for neuronal survival must be transported down the axons by molecular motors. Thus, reduced levels of the motor protein may not sustain the requirements of the axons. The finding that neuropathies tend to affect distal muscles first can be partially explained by the idea that longer axons need higher levels of motor molecules.

1.4.2. CMT2B1

Lamin A/C nuclear envelope proteins (LMNA)

The gene encoding *LMNA*, which encodes lamin A/C nuclear-envelope proteins, is mutated in CMT2B1, an autosomal recessive form of axonal CMT disease (De Sandre-Giovannoli et al., 2002). The gene encodes four transcripts lamin A, AD10, C and C2 by differential splicing (Furukawa et al., 1994; Machiels et al., 1996). There is a homozygous point mutation, causing a R298C amino acid substitution segregating with the disease in three Algerian families. This mutation affects all four transcripts produced by *LMNA*. This amino acid substitution lies in the rod domain that is essential for protein-protein interactions. This domain is highly conserved through evolution. *Lmna* knockout mice, which produce none of the Lmna transcripts, show a phenotype indicative of a peripheral neuropathy and ultrastructural evidence of neuropathy with a markedly reduced axon density, an increase in axon diameter and the presence of non-myelinated axons (Sullivan et al., 1999). *LMNA* mutations are also associated with limb-girdle muscular dystrophy type 1B (MIM159001) (Muchir et al., 2000), autosomal dominant Emery-Dreifuss muscular dystrophy (MIM181350) (Bonne et al., 1999), dilated cardiomyopathy type

1A (MIM115200) (Fatkin et al., 1999) and autosomal dominant partial lipodystrophy (MIM1516600) (Shackleton et al., 2000). Thus mutations in this gene selectively affect nerve, skeletal muscle, cardiac muscle or adipocytes. Since LMNA is ubiquitously expressed, this suggests that there are distinct functional domains in lamin A/C essential for the maintenance and integrity of different cell lineages. These multiple functional domains may participate in chromatin organisation, anchorage of nuclear envelope proteins, arrangement of nuclear pore complexes and self-assembly (Nagano and Arahata, 2000). The nuclear lamins are part of the group of intermediate filament proteins along with NF-L and gigaxonin, mutations in which cause CMT2E and giant axonal neuropathy respectively.

1.4.3. CMT2E

Neurofilament-light gene (NF-L)

The neuronal cytoskeleton is composed of interconnected actin microfilaments, microtubules and intermediate filaments. Neurofilaments (diameter 10nm) are the major type of intermediate filaments in adult neurones. There are three neurofilament proteins - light (NF-L), medium (NF-M) and heavy (NF-H). These share a central coiled domain which is responsible for the assembly of 10nm filaments (Julien, 1999). The carboxy-terminals of the NF-H and NF-M subunits form side-arm projections at the periphery of the neurofilaments. It is thought that the phosphorylation of their KSP (Lys-Ser-Pro) repeats increases their negative charge and causes increased neurofilament spacing (Julien, 1999). NF-L appears to play the most important role in neurofilament assembly as it is the only neurofilament protein capable of organising filaments by itself (Carpenter and Ip, 1996). NF-L also regulates the expression of the other two types, as NF-L knockout mice only have 5% of the normal level of NF-M and NF-H expression. These NF-L null mice have diminished axon diameter and delayed regeneration of myelinated axons following crush injury of peripheral nerve but no CMT-like phenotype (Zhu et al., 1997).

A mutation in the *NF-L* gene was found in a Russian family with CMT2E in a domain of the protein responsible for neurofilament assembly (Mersiyanova et al., 2000). This mutation is predicted to disrupt neurofilament assembly, and alter the

expression and regulation of the other neurofilament proteins. A further mutation in this gene in a Belgian family has also been identified (De Jonghe et al., 2001). Neurofilament proteins are involved in the pathogenesis of other neurological disorders such as giant axonal neuropathy, amyotrophic lateral sclerosis, Parkinson's disease and Alzheimer's disease. The common feature in all these disorders is the accumulation of neurofilament aggregates during the disease process.

Axonal loss also occurs in demyelinating CMT disease and altered neurofilament phosphorylation has been observed in CMT1 (Watson et al., 1994). Additionally Trembler mice, with a missense PMP22 mutation, undergo axon demyelination, which results in decreased neurofilament phosphorylation, reduced axon diameter and slow axonal transport, yet the myelinated regions have normal parameters (de Waegh et al., 1992). This alludes to a final common pathway in the pathogenesis of CMT diseases, and re-emphasises the importance of axo-glial interactions.

1.5. AUTOSOMAL RECESSIVE DEMYELINATING CMT DISEASE

1.5.1. CMT4A

Ganglioside-induced differentiation-associated protein-1 (GDAP1)

This gene spans 13.9 kb of genomic DNA, with the coding sequences split into 6 exons. It gives rise to a 3.9 kb transcript and encodes 358 amino acids. The amino acid sequence of GDAP1 shows strong similarity to glutathione S-transferase enzymes that have a role in the detoxification of cells. Amino acid residues 26-119 show the βαβαββα topology of the glutathione binding site, and amino acid residues 210-287 show the α-helical domain II that may recognise xenobiotic substrates (Armstrong, 1997; Hayes and Pulford, 1995; Salinas and Wong, 1999). The carboxy-terminal region has two putative transmembrane domains. The protein is expressed ubiquitously but with apparent predominance in nervous system tissue. It is expressed in Schwann cells, axons and the central nervous system. The mouse homologue *Gdap1* was identified after ganglioside-induced differentiation of the mouse neuroblastoma cell line Neuro 2a (Liu et al., 1999). Mutations in this gene have been associated with both autosomal recessive demyelinating CMT and axonal

CMT neuropathy (CMT4A). The gene may be involved in a signal transduction pathway between the Schwann cell and axon, so when this is interrupted, may cause either axonal degeneration or demyelination in peripheral nerve. Mutated GDAP1 may prevent the correct catalysing S-conjugation of reduced GSH, resulting in progressive attrition of both axons and Schwann cells (Baxter et al., 2002; Cuesta et al., 2002).

1.5.2. CMT4B1

Myotubularin-related protein-2 (MTMR2)

MTMR2 belongs to a family of dual specificity phosphatases. These proteins are characterised by a protein tyrosine phosphatase/DSP signature and a SID domain. The latter domain interacts with proteins containing a SET domain, which are able to associate with chromatin, activating or repressing gene transcription. The mutations in this gene create nonsense mutations or premature termination of the protein, and so probably cause a loss of functional MTMR2 protein. This may result in constitutive phosphorylation of an unknown substrate, leading to Schwann cell proliferation with overgrowth of myelin (Bolino et al., 2000). CMT4B families are characterised clinically by focally folded myelin sheaths on nerve biopsy (Quattrone et al., 1996). Myotubularin, the first described member of this family, and MTMR2 both specifically dephosphorylate the D3 position of the inositol lipid, phosphatidylinositol 3-phosphate (PI(3)P) (Blondeau et al., 2000; Kim et al., 2002; Taylor et al., 2000). Therefore, they may be involved in the regulation of cellular PI(3)P levels. PI(3)P can serve as a targeting motif for membrane-trafficking and signalling proteins that contain lipid binding modules such as FYVE domains (Gaullier et al., 1998). Of interest, myotubularin mutations lead to the condition X-linked myotubular myopathy (Laporte et al., 2000).

1.5.3. CMT4D/HMSN-Lom

N-myc downstream-regulated gene 1 (NDRG1)

NDRG1 is ubiquitously expressed, and is thought to play a role in growth arrest and cell differentiation, possibly as a signalling protein between the cytoplasm and the

nucleus. There is a high level of expression of NDRG1 in the Schwann cell. A mutation in this gene, encoding a premature-termination codon, has been associated with CMT4D or HSMN-Lom. These patients all appear to descend from a single founder, who had this mutation (Kalaydjieva et al., 2000).

1.6. DEJERINE-SOTTAS DISEASE AND CONGENITAL HYPO-MYELINATING DISEASE

Dejerine-Sottas disease (DSS), Congenital Hypomyelinating Disease (CHD) and CMT disease are not distinct pathophysiological entities but form a continuous spectrum of peripheral myelinopathies. CHD is thought to be a congenital impairment in myelin formation whereas DSS involves aberrant myelination and subsequent remyelination. These diseases were initially thought to be autosomal recessive but clearly some are autosomal dominant, and the genes in which mutations are described are identical to those involved in CMT disease. The differences in clinical severity and phenotype of these diseases may be related to specific types or locations of mutations in the proteins with different subsequent effects on protein function. For example, a mutation causing a loss of function of the protein may give a milder phenotype (CMT disease) than one conferring a gain of function or dominant negative effect (DSS/CHD) (Warner et al., 1996a). However, the same mutation in different members of one family may produce a variety of different phenotypes (Senderek et al., 2001). This may be secondary to variation in genetic background.

Dejerine-Sottas disease is characterised by severe hypomyelination, markedly reduced nerve conduction velocities and an infantile onset (Lyon, 1969). Patients have DSS rather than CMT disease if they have three or more of the following characteristics: onset of walking after 14 months, complete absence of deep tendon reflexes, ataxia, and clinical enlargement of nerves or nerve conduction velocity of less than 10m /s (Ouvrier et al., 1987).

In the past, this syndrome was called CMT3, but with the discovery of mutations in the various genes causing other types of CMT disease, this categorisation has

virtually disappeared from use. The syndrome is genetically heterogeneous, occurring with mutations in *PMP22*, *MPZ*, *PRX* and *EGR2* (Boerkoel et al., 2001a).

Congenital hypomyelinating disease is envisaged as a defect in myelin formation, rather than a disorder of myelin maintenance and stability, because of the pathological picture and the non-progressive evolution of the disease. Clinically, abnormalities are present at birth or soon afterwards. The child is hypotonic, and areflexic, with distal muscle weakness and very slow nerve conduction velocities of less than 6-7m/s. Nerve biopsy from such children shows hypomyelination or amyelination of most fibres, variable basal laminae onion bulbs and no florid demyelination. There are no signs of active myelin breakdown (Harati and Butler, 1985). It has been described in patients with point mutations in *PMP22* (Fabrizi et al., 2001), *MPZ* (Warner et al., 1996a), *EGR2* (Warner et al., 1998), and *MTMR2* (Bolino et al., 2001).

1.7. HEREDITARY SENSORY NEUROPATHIES

1.7.1. Hereditary sensory neuropathy Type I

Serine palmitoyltransferase long chain base subunit-1 (SPTLC1)

Hereditary sensory neuropathy type 1 (HSN1) is the commonest inherited disease of peripheral sensory neurones. It is an autosomal dominant progressive degeneration of dorsal root ganglia and sensory neurones with onset in the second or third decades. There is marked distal sensory loss predominantly affecting the lower limbs. Loss of pain and temperature sensation leads to digital ulcerations and osteomyelitic bone destruction sometimes necessitating amputation. There may be motor and autonomic involvement. Morphometry demonstrates involvement of large fibres, but clinical findings are predominantly related to the loss of small unmyelinated fibres. Mutations in *SPTLC1* are associated with HSN1 (Bejaoui et al., 2001; Dawkins et al., 2001). This phenotype is also related to a second locus, 3q13-q22, suggesting locus heterogeneity for the phenotype (Kwon et al., 1995), though as there was also motor involvement and axonal loss these patients were assigned to CMT2B.

SPTLC1 has fifteen exons and its transcript is expressed in many tissues including rat dorsal root ganglia. It encodes a 473 amino acid protein designated 'Long Chain Base 1' (LCB1), subunit 1 of the serine palmitoyl transferase (SPT) enzyme. The SPT enzyme is a pyridoxal 5'-phosphate dependent enzyme which catalyses the first step of biosynthesis of sphingolipids, including ceramide and sphingomyelin. SPT consists of two subunits (LCB1 and LCB2) both of which are required for enzyme activity (Hanada et al., 1997). Ceramide produced by catabolism of sphingomyelin, or an increase in SPT activity is known to mediate apoptosis (Herget et al., 2000). An increase in glucosyl ceramide was seen in lymphoblast cell lines from HSN1 patients compared to those derived from healthy controls (Dawkins et al., 2001). These results suggest that haploinsufficiency, or a toxic gain of function per se, do not cause the phenotype of autosomal dominant HSN1, but instead it is due to augmentation of SPT activity. Increased ceramide production seems to mediate the massive neuronal cell death associated with neural tube closure during development of the spinal cord (Herget et al., 2000). It may be that *SPTLC1* mutations prevent ceramide levels returning to normal after this, resulting in gradual attrition of neurones over many years (Dawkins et al., 2001). The gene encoding the second subunit of SPT, *SPTLC2* on chromosome 14q is a candidate gene for other cases of HSN with no identified mutation.

1.7.2. Hereditary sensory neuropathy type III

IκB kinase complex associated protein (IKBKAP)

Familial dysautonomia (FD), Riley-Day syndrome or hereditary sensory neuropathy type III is an autosomal recessive disorder that affects the development and survival of sensory, sympathetic and some parasympathetic neurones. It is characterised by widespread sensory and variable autonomic dysfunction. There is increased sensitivity to pain and temperature, cardiovascular instability, recurrent pneumonia, inappropriate sweating, postural hypotension, vomiting crises and gastrointestinal dysfunction (Riley, 1949). The disease is fatal, with only 50% of patients reaching 30 years old. The pathology shows a striking, progressive depletion of unmyelinated

sensory and autonomic neurones, beginning early in development. Dorsal root and sympathetic ganglion neurone number is grossly reduced.

The disorder is primarily confined to those of Ashkenazi Jewish descent, with an incidence of 1 in 3600 live births, and a carrier frequency of the defective gene of 1 in 30 (Maayan et al., 1987). This ethnic bias is due to a founder effect with more than 99.5% of disease alleles sharing a common ancestral haplotype (Slaugenhaupt et al., 2001). Mutations occur in the IkB kinase complex-associated protein gene (*IKBKAP*) located at chromosome 9q31 (Anderson et al., 2001; Slaugenhaupt et al., 2001). The major haplotype mutation is located in the donor splice site of intron 20, which variably results in skipping of exon 20 in the mRNA of patients with FD resulting in a frameshift generating a truncated protein. This is particularly common in brain tissue and the phenotype variability of FD may be explained by the variable production of the mutant mRNA either in different tissues or at different times in development (Slaugenhaupt et al., 2001). The mutation associated with most minor haplotypes is a missense (R696P) mutation in exon 19, which disrupts a potential phosphorylation site (Anderson et al., 2001; Slaugenhaupt et al., 2001).

IKBKAP was thought to bind the IκB kinases and NF-κB and assemble these proteins into an active kinase complex (Cohen et al., 1998), hence its name. However, recent studies have challenged this, suggesting that it is part of a multiprotein complex playing a role in general transcriptional regulation (Krappmann et al., 2000).

1.7.3. Hereditary sensory neuropathy type IV (HSN-IV)

NTRK1

Mutations of the *NTRK1* (*TRKA*) gene coding for the neurotrophic tyrosine kinase receptor type 1 cause the autosomal recessive disease congenital insensitivity to pain with anhidrosis (CIPA), also called hereditary sensory and autonomic neuropathy Type 4 (HSAN4) or hereditary sensory neuropathy (HSNIV) (Indo et al., 1996). The disease is characterised by recurrent episodic fever, insensitivity to pain, anhidrosis, self-mutilating behaviour and mental retardation. The *TRKA* gene is located on

chromosome 1, consists of 17 exons and spans at least 23 kb. The gene encodes the receptor tyrosine kinase for nerve growth factor (NGF). Defects in NGF signal transduction at the TRKA receptor lead to failure to support the survival of sympathetic neurones and nociceptive neurones derived from the neural crest. Thirty-seven different TRKA mutations are now described, distributed in the extracellular domain involved in NGF binding, and in the intracellular signal-transduction domain (Indo, 2001). Nerve biopsy of these patients reveals loss of small myelinated fibres and a variable loss of unmyelinated C-fibres (Houlden et al., 2001). Mice lacking the gene for *TrkA* also show loss of responses to painful stimuli (Indo et al., 1996).

1.8. HEREDITARY MOTOR NEUROPATHIES

1.8.1. Distal hereditary motor neuronopathy type VI

Immunoglobulin μ-binding protein-2 (IGHMBP2)

Distal hereditary motor neuronopathy type VI (also known as spinal muscular atrophy with respiratory distress (SMARD)) is caused by mutations in the gene encoding immunoglobulin μ-binding protein-2 (IGHMBP2). This disease is characterised by dysfunction and progressive loss of α-motor neurones in the anterior horn of the spinal cord, leading to neurogenic muscular atrophy especially distally and life-threatening respiratory distress with evidence of unilateral or bilateral paralysis of the diaphragm. In mice, mutations in this gene cause the *nmd* phenotype, with progressive limb paralysis and death due to respiratory failure. IGHMBP2 consists of 993 amino acids and contains both DNA and RNA binding domains. The cellular function of the protein is unknown but it is involved in immunoglobulin class switching, pre-mRNA processing and in regulation of transcription (Grohmann et al., 2001).

1.8.2. Distal Hereditary Motor Neuronopathy VII (dHMN-VII)

This is an autosomal dominant disorder characterised by distal muscular atrophy and vocal cord paralysis. dHMN accounts for about 10% of the peroneal muscular atrophy syndrome (Harding and Thomas, 1980b). Motor and sensory nerve conduction velocities are normal, and electromyography shows features of

neurogenic atrophy, consistent with degeneration of the anterior horn cell of the spinal cord. As this disorder shows much overlap with CMT2C except for the lack of sensory involvement, it was suggested that these were allelic disorders (McEntagart et al., 2001), but they are now known to occupy different loci (Santoro et al., 2002).

1.9. INTERMEDIATE FORMS OF CMT DISEASE

Intermediate CMT disease is characterised by motor median nerve velocities of 25-45m/s within a family with the disease, hence forming an overlap between the accepted velocities for CMT1 and CMT2. Sural nerve biopsies show axonal degeneration and segmental demyelination and remyelination with onion bulb formation (Kennerson et al., 2001). Some affected families have very variable nerve conduction velocities, ranging from normal to severely reduced, where there are specific mutations in the *MPZ* gene (Thr124Met) (De Jonghe et al., 1999) or *NF-L* (Pro8Arg) (De Jonghe et al., 2001). Other autosomal dominant types have been linked to 19p12-p13.2 (Kennerson et al., 2001) and 10q24.1-q25.1 (Verhoeven et al., 2001) though the causal genes are not yet identified. CMT1X, due to Cx32 mutations, has a mixed demyelinating and axonal appearance on nerve biopsy, and affected males have variable nerve conduction velocities (Timmerman et al., 1996b). This is thought to be due to disruption of the connexin channel between myelin lamellae and axons, resulting in degeneration of both.

1.9.1. HMSN-Russe (HMSNR)

This is a severe sensorimotor neuropathy with prominent sensory loss, an intermediate reduction in nerve conduction velocity and severe disability, described in the same population of Romany families as HMSN-Lom. Sural nerve biopsies show a depletion of large myelinated nerve fibres, profuse regenerative activity and a uniformly reduced thickness of the myelin sheath relative to the axon diameter suggesting hypomyelination. *EGR2* is contained in this locus, but this has been excluded as the HMSNR gene (Rogers et al., 2000).

1.10. MISCELLANEOUS INHERITED NEUROPATHIES

1.10.1. Giant Axonal Neuropathy

Gigaxonin

Giant axonal neuropathy is a severe autosomal recessive sensorimotor neuropathy affecting both the peripheral nerves and the central nervous system. It is characterised by neurofilament accumulation, leading to segmental distension of the axons. Neurofilaments belong to the intermediate filament family and abnormal aggregation of multiple tissue specific intermediate filaments has been reported in this disease: vimentin in endothelial cells, Schwann cells and cultured skin fibroblasts, and glial fibrillary acidic protein in astrocytes. Keratin intermediate filaments are also altered, and most patients have characteristic curly or kinky hair (Ben Hamida et al., 1990). Families with giant axonal neuropathy have mutations in the *Gigaxonin* gene which has 11 exons (Bomont et al., 2000).

Gigaxonin is an ubiquitously expressed protein of 597 amino acids composed of an amino-terminal BTB (Broad-complex, Tramtrack and Bric a brac) domain followed by six kelch repeats, which are predicted to a adopt a β-propeller shape (Ito et al., 1994). Related proteins sharing a similar domain organisation have functions related to the cytoskeleton. One such protein, the human mayven protein, the orthologue of Drosophila kelch, interacts with actin through the kelch domain and may be a physical or functional link between the thin filaments and the intermediate filaments (Soltysik-Espanola et al., 1999). Another such protein, Keap1 protein, which is sequestered in the cytosol, inactivates the transcription factor Nrf2 (NF-E2 related factor 2) which modulates the expression of genes containing antioxidant responsive elements (Itoh et al., 1999). Thus neurofilament disorganisation and oxidative stress may have a role in this disease (Bomont et al., 2000).

1.10.2. Waardenburg Syndrome with peripheral neuropathy

SOX10

SOX10 is a transcription factor that is expressed early in the neural crest and then is preferentially expressed in the late embryonic glial cell lineage and in mature Schwann cells and oligodendrocytes. SOX10 also modulates other myelin-related transcription factors such as Oct6, PAX3 and EGR2, suggesting that it is important for myelin development and maintenance in the peripheral and central nervous system (Kuhlbrodt et al., 1998). The SOX family of transcription factors is defined by sequence similarity to the high mobility group DNA-binding motif (SRY box) present in the mammalian sex-determining gene, SRY. Heterozygous SOX10 mutations have been found in an animal model of Hirschsprung disease *Dominant megacolon (Dom)* (Southard-Smith et al., 1998), and in families with Waardenburg syndrome type 4, characterised by aganglionosis, pigmentation disorders and deafness (Pingault et al., 1998). Neither these patients nor *Dom* mice were reported to have dysmyelinating features. However, a Japanese patient was described in 1999 with a heterozygous mutation in SOX10. She had clinical features of Pelizaeus-Merzbacher disease, a central nervous system demyelinating disease, and a peripheral demyelinating neuropathy, in addition to features of Waardenburg syndrome. There was a 12 bp deletion in the coding region of SOX10 which disrupts the stop codon and extends the protein by 82 amino acids. This new sequence has similarities with the proline-rich domains of WT1 (Wilm's tumour) which can repress transcription. Thus, it was felt that this patient's unusual phenotype was due to a dominant-negative action by the mutated protein (Inoue et al., 1999).

A second patient was described in 2000 with a heterozygous mutation in SOX10 and a hypomyelinating peripheral neuropathy, chronic intestinal pseudoobstruction, dysautonomia and deafness. The mutation deletes one base in the last coding exon which results in a frameshift mutation generating a new carboxy-terminal tail and premature termination of the protein, with loss of the transactivation domain. A peripheral nerve biopsy showed micropolyfasciculation with each nerve fascicle subdivided into subfascicles. The myelin sheaths were thin or absent, but there was no sign of active myelin breakdown or attempts at remyelination, suggestive of a

congenital hypomyelination neuropathy. This patient's slow conduction velocities and clinical phenotype improved with age, again suggesting that this mutation impaired development rather than promoting degeneration (Pingault et al., 2000). The neurological phenotype of these patients may be explained by the altered synergy with downstream transcription factors (e.g. EGR2) or their downstream genes.

There is now considerable interest in the autosomal recessive types of Charcot-Marie-Tooth disease, which have been relatively less studied due to their lower incidence and the need for consanguineous families to obtain sufficient linkage information. The existence of autosomal recessive demyelinating peripheral neuropathies that are not linked to known loci has intensified the search for novel genes expressed in myelin-forming Schwann cells, and the *PERIAXIN (PRX)* gene is one such candidate.

1.11. PERIAXIN (Prx)

The *Periaxin* gene encodes a novel Schwann cell protein initially only studied in rodents. It was isolated in a screen based on detergent insolubility for cytoskeleton-related proteins in peripheral nerve (Gillespie et al., 1994). In rodents, the *Periaxin* gene encodes two proteins with PDZ domains, L-periaxin and S-periaxin, of 147 and 16kD respectively, that are expressed in myelinating Schwann cells (Dytrych et al., 1998). The two mRNA isoforms (4.7 kb and 5.2 kb respectively) are generated in approximately equal amounts. The PDZ domain is named after the three proteins in which it was first described: post-synaptic density protein-95 (**P**SD-95), drosophila **d**iscs large tumour suppressor gene (dlg) and the tight junction-associated protein **Z**O-1 (Kornau et al., 1995). This domain is often present in proteins that link plasma membrane proteins to the cytoskeleton (Sheng, 1996). S-periaxin is a truncated form of L-periaxin which arises by an alternative splicing event which involves the retention of intron 6. This intron introduces an in-frame stop codon that encodes a 21 amino acid C-terminus unique to S-periaxin. S-periaxin is present diffusely throughout the cytoplasm of the Schwann cell. The rat *Periaxin* gene is a 20.6 kb gene composed of seven exons (Gillespie et al., 1994) (Figure 6a). The mouse equivalent is found on mouse chromosome 7 (Gillespie et al., 1997).

L-periaxin consists of a basic domain near its N-terminus, (amino acids 118-196), a region of a series of repeats, (amino acids 430-730) and an acidic domain near its C-terminus (amino acids 1036-1163) (Dytrych et al., 1998) (Figure 6b). The repeat region of L-periaxin consists of a pentameric core (aliphatic non-polar: proline: glutamic acid or aspartic acid: aliphatic non-polar: variable) which is interrupted by a tripeptide spacer (leucine: proline: lysine). The function of this region is unclear, but it appears to be less flexible than the rest of the protein. It may act as a spacer separating the functional basic and acidic domains. Supporting this, structure prediction programmes suggest that L-periaxin has little secondary structure and a linear conformation (Gillespie et al., 1994).

The basic domain sequence contains a nuclear localisation signal responsible for nuclear targeting of the protein, which is developmentally regulated, as L-periaxin is found in the nucleus until E17.5 (Sherman and Brophy, 2000). During myelination, L-periaxin redistributes to the adaxonal membrane of the Schwann cell, and then to the abaxonal membrane, Schmidt-Lanterman incisures and paranodal membrane with maturation of the myelin sheath (Gillespie et al., 1994) (Figure 7). L-periaxin recapitulates this pattern following nerve crush injury (Scherer et al., 1995). This shift in L-periaxin localisation during myelination suggests that L-periaxin participates in membrane-protein interactions that are required to stabilise the mature myelin sheath. As a cytoskeleton-associated protein, L-periaxin may mediate such stabilisation through its PDZ domain, which is implicated in the assembly of signalling complexes at sites of cell-cell contact. Moreover, L-periaxin homodimerises through its PDZ domain, and binds dystroglycan-dystrophin-related-protein-2 (DRP2) through its basic domain, forming part of a complex linking the Schwann cell cytoskeleton to the extracellular matrix (Sherman et al., 2001). DRP2 binds β-dystroglycan, a transmembrane protein, linking to α-dystroglycan, which directly interacts with laminin in the basal lamina. Thus, a complex is built up at the abaxonal membrane of the Schwann cell, where periaxin homodimerises and serves as a scaffold upon which to assemble the DRP2/dystroglycan complex (Wrabetz and Feltri, 2001). This complex also contains Dp116, utrophin and actin (Figure 8). The basal lamina has an essential role in enabling the development of the Schwann cell and in stabilising the Schwann-cell-axon interaction (Carey et al., 1986; Eldridge et

al., 1989). In muscle, the dystrophin/dystroglycan complex is thought to buffer mechanical stress and it may be that the dystroglycan/DRP2/periaxin complex has a similar role in maintaining the myelin sheath. The clustering of the complex may not only convey a structural role by defining the basolateral membrane of the Schwann cell, but may also transduce signals that regulate myelin thickness and stability, similarly to the role of syntrophins, which also contain PDZ domains, in muscle (Roberts, 2001). It may provide a signalling mechanism from the basement membrane proteins to the Schwann cell interior by bringing other signalling molecules that associate with L-periaxin into close proximity. In periaxin-null mice, DRP2 is mislocalised and partially depleted indicating the importance of L-periaxin at underpinning the complex (Sherman et al., 2001).

Periaxin–null mice develop an apparently normally myelinated peripheral nervous system, so it appears that the presence of the periaxin proteins is not essential for myelination to occur. However, these mice progress to develop a late-onset peripheral demyelinating polyneuropathy (Gillespie et al., 2000). This suggests that periaxin may be required for the stabilisation of the myelin sheath and its maintenance. The process of myelin sheath repair may not entirely reiterate myelin sheath development, as the environment in the two situations is different. The myelin sheath in periaxin-null mice is unstable, leading to demyelination and reflex behaviours that are associated with the painful conditions caused by peripheral nerve damage. Older periaxin-null mice show extensive peripheral demyelination, with mechanical allodynia and thermal hyperalgesia, which is reversible with the intrathecal administration of a selective NMDA receptor antagonist. Pathology of the peripheral nerves shows hypermyelination, with sheath infolding initially. Later, most axons are naked or thinly myelinated, with redundant basal laminae and supernumerary Schwann cells forming 'onion bulb structures,' which are diagnostic of attempts to remyelinate demyelinated fibres (Gillespie et al., 2000). This pathology is reminiscent of human demyelinating CMT disease.

The phenotype of the periaxin-null mouse with its late-onset demyelinating peripheral neuropathy lent urgency to exploring its link with human disease. The mouse *Periaxin* gene is found on chromosome 7, which is syntenic with the long arm

of human chromosome 19 (Gillespie et al., 1997). Early in 2001, a large consanguineous Lebanese family was described with autosomal recessive CMT disease (CMT4F) linked to the locus 19q13.1-13.3 (Delague et al., 2000). In Chapter 3, I describe the cloning of the human *PRX* gene and the discovery of mutations in this gene in CMT4F and Dejerine-Sottas disease.

Although it is now clear that L-periaxin is essential to maintain healthy peripheral nerve myelin, the functional role of L-periaxin is unclear. Recently, it was discovered that a region at the C-terminus of L-periaxin binds to the F-box protein Fbl6, which is known to target its ubiquitinated binding partners to the proteasome via the SCF complex. This led to interest in the ubiquitination system.

1.12. UBIQUITINATION AS A METHOD OF PROTEIN REGULATION

Regulation of the abundance of cellular proteins is essential for cell survival and normal function. Newly synthesised polypeptides are generally unstable in the highly reactive cellular environment and tend to undergo spontaneous denaturation or chemical modifications through oxidation, isomerisation or glycation. To avoid the potentially dangerous effects of accumulation of unfolded or misfolded proteins, the cell expends much energy on mechanisms that act to prevent aggregation, or promote hydrolysis of abnormal proteins. A highly discriminative, energy dependent pathway operates in the cytoplasm to ensure removal of damaged proteins. This pathway, mediated by the protein ubiquitin, is a complex cascade of reactions involving multi-enzyme complexes whose action is temporally and tightly controlled and plays an important part in a broad range of cellular processes. In addition to destroying damaged proteins, the pathway targets many naturally short-lived polypeptides that are involved in the regulatory processes. The ubiquitin pathway of protein degradation is responsible for the turnover of key short-lived regulatory proteins that participate in processes as diverse as the cell cycle, cellular signalling in response to stress and extracellular signals, morphogenesis, the secretory pathway, DNA repair and organelle biosynthesis (Carrano and Pagano, 2001; Maniatis, 1999; Ulrich and Jentsch, 2000). Aberrations in such a complex system may be pathogenic in many diseases, both inherited and acquired. Protein regulation also occurs via an

unregulated vacuolar pathway that is mediated by lysosomes, endosomes and the endoplasmic reticulum.

1.12.1. The ubiquitination pathway

Hershko and Ciechanover discovered the ubiquitin/proteasome pathway in 1980 (Hershko et al., 1980) and it has since been shown to provide highly efficient control of the abundance of proteins involved in diverse cellular processes. The pathway comprises of a cascade of reactions: E1 enzymes initially activate ubiquitin in an energy dependent manner so that ubiquitin can bind a cysteine residue of the E1 enzyme in a thiolester linkage. Activated ubiquitin is next transferred to a cysteine residue of an ubiquitin conjugating enzyme (E2) which covalently transfers ubiquitin onto lysine residues or the N-terminal residue of target proteins (Breitschopf et al., 1998) or onto the last ubiquitin residue of a protein-bound multi-ubiquitin chain. E3 ubiquitin ligases recruit the target proteins for ubiquitination and these confer specificity to the pathway (Ciechanover, 1998; Hershko and Ciechanover, 1998). The structure of the system appears hierarchical: a single E1 activates ubiquitin, and can transfer it to several species of E2 enzymes, and each E2 acts with either one or several E3 enzymes (Ciechanover, 1998). The presence of ubiquitin residues on the substrate serves as a cue for its recognition by the 26S proteasome, which then removes the ubiquitin tag and degrades the target protein (Hershko and Ciechanover, 1998). Prior to its association with the proteasome, a class of enzymes, called ubiquitin-carboxy-terminal hydrolases, monitors the protein-ubiquitin conjugate and removes ubiquitin moieties from incorrectly targeted polypeptides. Ubiquitin is a 76 amino acid globular protein which may prevent it from proteolysis during the hydrolysis of its bound proteins allowing recycling of the molecules via the action of isopeptidases (Bebington et al., 2001) (Figure 9).

1.12.2. The proteasome

The 26S proteasome consists of the 20S core catalytic complex flanked on both sides by the 19S regulatory complexes. The 26S proteasome mainly recognises ubiquitin-tagged proteins. The complex is arranged as a stack of four rings, two α and two β rings, organised in the general structure of $\alpha\beta\beta\alpha$ (Groll et al., 1997). Both α and β

rings are composed of seven distinct subunits. The three catalytic sites, trypsin, chymotrypsin and post-glutamyl peptidyl hydrolytic-like sites, reside on the β subunits, arranged obliquely. The catalytically inactive α chains stabilise the ring structure of the β chains. Substrate recognition by the 26S proteasome is probably mediated by the interaction of specific subunits of the 19S complex with the poly-ubiquitin chain (Ciechanover, 1998).

1.12.3. The SCF complex

One member of the family of E3 ubiquitin ligases is the SCF complex. This complex consists of a core of four essential subunits: **S**kp1, a **c**ullin, the RING finger protein Rbx1/Roc1/Hrt1 and an **F**-box protein (Chen et al., 2000; Deshaies, 1999; Joazeiro and Weissman, 2000) (Figure 10). The Cullin protein acts as a scaffold for the complex, interacting with both a specific E2 protein and Skp1. The F-box protein acts as an adapter component linking the substrate for ubiquitination to the complex (Bai et al., 1996; Craig and Tyers, 1999). The F-box protein comprises a C-terminal motif, usually containing tryptophan-aspartic acid (WD40) repeats or leucine rich repeats (LRR) (Kobe and Deisenhofer, 1995), which interacts with the substrate which may be phosphorylated (Deshaies, 1999). The N-terminal F-box motif, named for its presence in cyclin F (Bai et al., 1996), is approximately fifty amino acids long and binds Skp1. The F-box protein confers substrate specificity, interacting with a number of target proteins but utilising the same core SCF complex for ubiquitination of the different substrates. The ability of the SCF backbone to bind multiple F-box proteins, each with specific substrate specificity, substantially increases the substrate repertoire.

Phosphorylation is a major mechanism used by cells to transduce signals rapidly. SCF complexes usually interact with phosphorylated substrates (Deshaies, 1999) suggesting they are ideal for dynamic processes that require abrupt change to be made irreversible via the degradation of key proteins. Hence SCF targets are key regulators in many pathways of signalling, transcription and the cell cycle (Kipreos and Pagano, 2000).

A large number of F-box proteins have been identified recently, though the substrates for many are unknown (Winston et al., 1999).

The subcellular localisation of F-box proteins has been studied using overexpressed tagged proteins, and F-box proteins have been found in both the cytoplasm and the nucleus. The localisation of the protein is not usually dependent on the F-box motif, and its binding to Skp1, as wild type and mutant F-box proteins are co-localised (Cenciarelli et al., 1999; Winston et al., 1999). Some F-box proteins are ubiquitous, whereas others are clearly tissue specific.

1.12.4. The Wnt signalling pathway

The Wnt pathway, regulating β-catenin levels, is one of the best characterised systems dependent on SCF-mediated ubiquitination and this depends on the action of the F-box β-TrCP. In mammals, β-catenin is involved in cell-cell adhesion and growth factor signal transduction. It is membrane-associated, through its interaction with E-cadherin and α-catenin, which form the adherens junction. It is also found in a cytoplasmic pool, where it is important for signalling (Gumbiner, 1995). The Wnt-1 ligand binds to the cell surface receptor Frizzled and initiates the Wnt signalling cascade. This leads to inhibition of glycogen synthase kinase (GSK3β) which fails to phosphorylate β-catenin. Thus, β-catenin is not recognised by the F-box protein β-TrCP, and so accumulates in the cytoplasm. Excess β-catenin translocates to the nucleus and functions as a co-activator for the transcription factor T cell factor/ lymphocyte enhancer binding factor (TCF/LEF-1) and modulates expression of its target genes (Huber et al., 1996). One such downstream gene is the oncogene c-myc (Pennisi, 1998).

In the absence of Wnt signalling, a complex of GSK3β, adenomatous polyposis coli (APC) and axin associates with and phosphorylates β-catenin at two specific serine residues (Ikeda et al., 1998). The F-box protein β-TrCP binds β-catenin taking it to the SCF complex for ubiquitination and proteasome degradation (Figure 11).

Enforced expression of β-catenin induces expression of its F-box protein β-TrCP, by stabilisation of β-TrCP mRNA (Spiegelman et al., 2000). As β-catenin is a substrate

of $SCF^{\beta\text{-}TrCP}$, there is an accelerated degradation of β-catenin, and the negative feedback loop provides an extra control mechanism. This is important as deregulation of APC, β-catenin and E-cadherin expression leads to increased transcriptional activity of TCF/LEF, and elevation of c-myc expression, resulting in tumour formation (Sadot et al., 2000).

Another substrate of the F-box protein β-TrCP is hedgehog, and mutations in desert hedgehog in humans are known to cause a peripheral neuropathy, as well as gonadal dysgenesis (Umehara et al., 2000). This suggests that Schwann cells use the ubiquitin pathway to regulate proteins involved in signalling.

1.12.5. Ubiquitination of L-periaxin and the regulation of its localisation

L-periaxin, similarly to β-catenin, appears to shuttle between the cytoplasm and the nucleus. L-periaxin has a nuclear localisation signal, at the N-terminus of the protein and in embryonic Schwann cells periaxin is located in the nucleus (Sherman and Brophy, 2000). After this time, L-periaxin is found to be membrane-associated, which is now known to be due to its interaction with the molecule dystrophin related protein-2 (DRP-2) in the DRP-2/dystroglycan complex (Sherman et al., 2001). The mechanism of control of periaxin localisation is unknown but we now know that L-periaxin interacts with the F-box protein Fbl6. Fbl6 interacts with the C-terminal acidic region of L-periaxin by yeast two hybrid assay. The interaction of L-periaxin with the C-terminal LRR region of Fbl6 has also been shown biochemically by in vitro pull down assays (Vasiliou in preparation). This interaction appears to target L-periaxin for ubiquitination as ubiquitinated forms of L-periaxin were immunoprecipitated from sciatic nerve explant cultures and detected by immunoblotting. The levels of L-periaxin in sciatic nerve explant cultures were stabilised on inhibition of the proteasome by epoxomicin, demonstrating the involvement of the proteasome in the turnover of L-periaxin (Vasiliou in preparation). Thus, the ubiquitin/proteasome pathway appears to be involved in the regulation of L-periaxin levels in the Schwann cell through its interaction with Fbl6. One may speculate that this controls the localisation of L-periaxin in the Schwann cell in a similar manner to β-TRCP and β-catenin. It is predicted that abnormalities

in the SCF^{Fbl6} pathway regulating L-periaxin levels in Schwann cells may cause other as yet identified forms of CMT disease.

1.13. NERVE CRUSH AND REGENERATION

We now know more about the interactions of L-periaxin at a molecular level, and the demyelinating effect of a lack of L-periaxin. However, we are still unclear as to why periaxin deficient mice can apparently assemble normal compact myelin in the development of the peripheral nervous system, indicating that the presence of periaxin is not prerequisite for development of a myelin sheath, but later develop a demyelinating peripheral neuropathy. This may suggest that periaxin is required for maintenance of the stability of the sheath, and perhaps in its ability to repair the myelin sheath in response to injury.

1.13.1. Nerve injury

Nerve injury is classified into five types. Sir Herbert Seddon (1943) first classified nerve injury as neurapraxia, axonotmesis and neurotmesis and Sir Sydney Sunderland (Sunderland, 1951) expanded this to include two more injury patterns. Neurapraxia (Sunderland first-degree injury) involves a local area of conduction block. Histologically there is segmental demyelination and a swift and complete recovery is expected. Axonotmesis (Sunderland second-degree injury) involves injury to the axon so that Wallerian degeneration occurs distal to the injury. Recovery occurs by axonal sprouting within the intact endoneural tubes of the Schwann cell basal lamina. The regenerated fibres are then remyelinated. Regeneration is directed to the appropriate distal receptors and complete recovery is expected. A Sunderland third-degree injury provides variable functional recovery, as it is associated with axonal injury and endoneural scarring, which impedes or misdirects axonal regeneration. A Sunderland fourth-degree injury describes a nerve in physical continuity, but with a functional scar block, across which regeneration is impossible. Neurotmesis (Sunderland fifth-degree injury) is a complete transection of the nerve, with no functional recovery.

There are several models of nerve injury in rodents. Nerve crush is a commonly used experimental model in the rat to allow investigations of peripheral nerve injury and regeneration. This has been evaluated and standardised by several groups. Bridge et al., (Bridge et al., 1994) were concerned that the different methods of crush might produce different injury patterns. They compared the time of crush – 15, 30 and 60 seconds, the number of crushes – single or double, and the type of instrument to produce the crush – jeweller's forceps and serrated haemostat. There were no significant differences between any of the experimental groups, either in histology, behaviour, neurophysiology or recovery time. In rats at two weeks, the predominant histological picture was that of Wallerian degeneration with some regeneration, increased endoneural space and capillary thickening. Scarring within the endoneurium was not seen. By week eight, almost complete recovery occurred, though fibre size had not yet returned to normal. Functional recovery occurred by week four, as assessed by walking track analysis. Electrophysiological testing returned to normal by week eight. This study showed that despite the method used to induce nerve crush, the result was very similar, producing a second-degree injury (axonotmesis).

Brown and Hardman (Brown and Hardman, 1987) studied the accuracy of reinnervation of motoneurones following crush injury in the rat sciatic nerve using retrograde tracing techniques. They noted very few errors of projection, with only 3% of axons being misplaced. Hence, third-degree injury seems rare in this model.

Nawwar et al., (Nawwar et al., 1995) attempted to calibrate their nerve crush forceps using transducers, but achieved no better results than using a jeweller's forceps (Bridge et al., 1994).

Axonotmesis has also been achieved using cryoprobe lesions. Again, comparison of complete cryoprobe injury and crush injury has not shown any difference in the histology, behavioural tests or recovery of treated animals. However, cryoprobe treatment was less likely to produce a complete full thickness lesion compared to the crush treatment (Kerns et al., 1991).

Thus a nerve crush model resulting in axonotmesis (Sunderland second degree injury) provides an opportunity of studying remyelination of regenerated nerve fibres. Experiments designed to evaluate the ability of periaxin-null mice to remyelinate crushed nerve fibres are described in Chapter 4

FIGURE 1 - PROPAGATION OF THE ACTION POTENTIAL

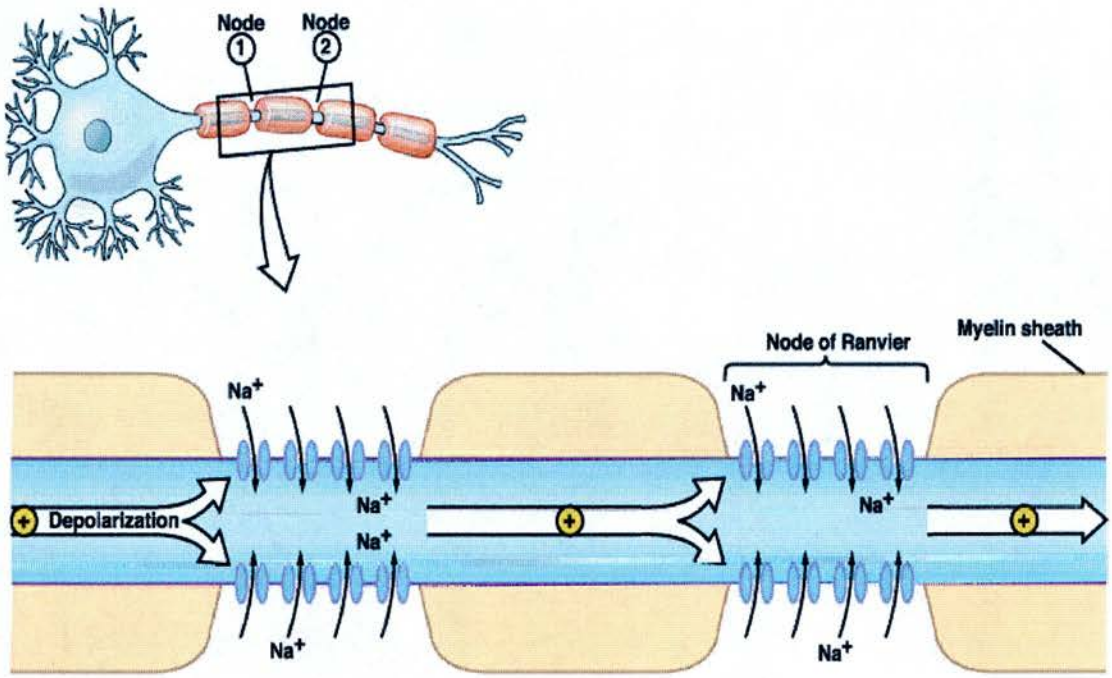

Diagram of propagation of the action potential in a myelinated nerve by saltatory conduction. Sodium channels are clustered at the Nodes of Ranvier and sodium inflow here propagates the depolarisation and allows fast and efficient transmission. Thus, the action potential appears to 'jump' from one node to the next.

FIGURE 2 - DEVELOPMENT OF THE SCHWANN CELL

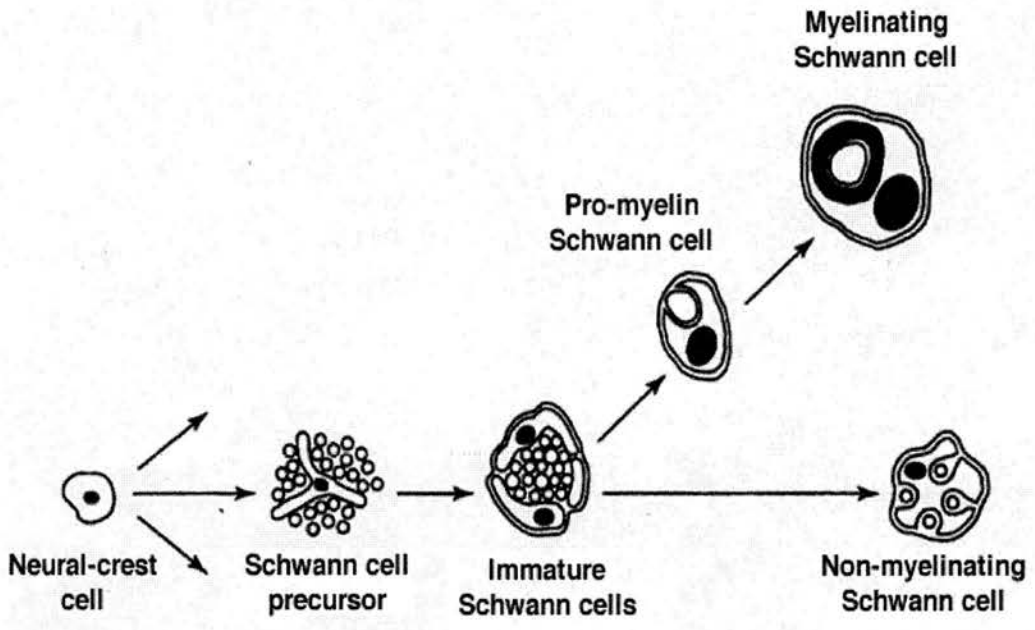

Early migrating neural crest cells give rise to Schwann cell precursors, which subsequently form immature Schwann cells. These are able to differentiate into either myelin-forming or nonmyelinating mature Schwann cells (After Jessen and Mirsky, 1999).

FIGURE 3 - THE MYELINATING SCHWANN CELL

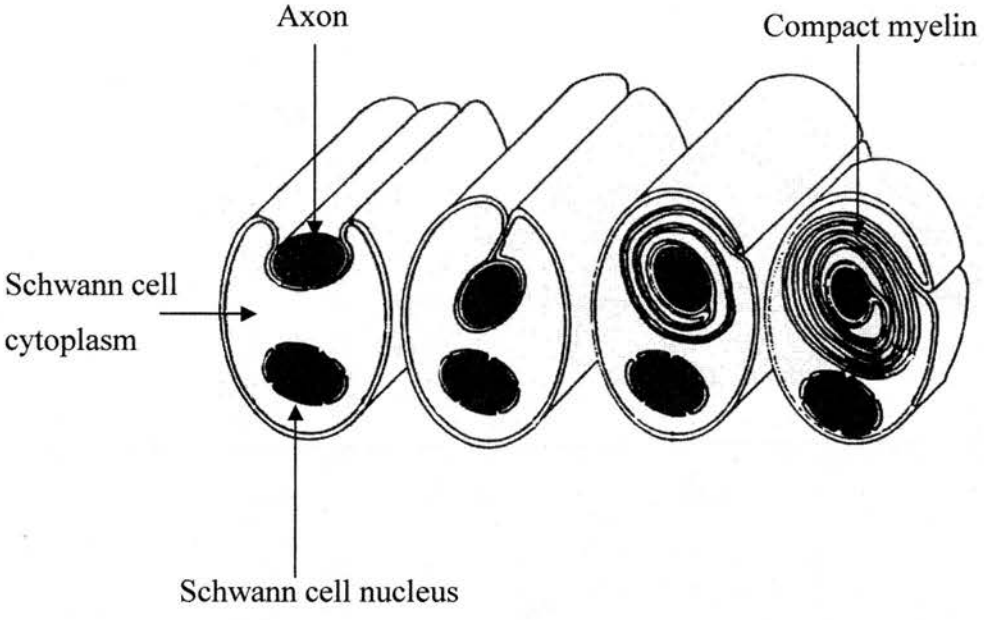

a - A myelinating Schwann cell comes in contact with an axon, envelopes it, and then forms compact myelin by spiralisation of the plasma membrane.

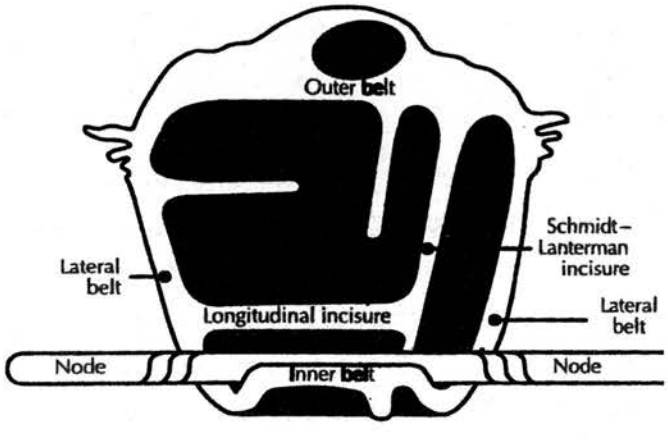

b- Diagrammatic representation of an unwrapped myelinating Schwann cell showing non-compacted cytoplasmic channels (paranodal loops or lateral belts and Schmidt-Lanterman incisures) coursing through compact myelin (black).

FIGURE 4 - THE NODE OF RANVIER

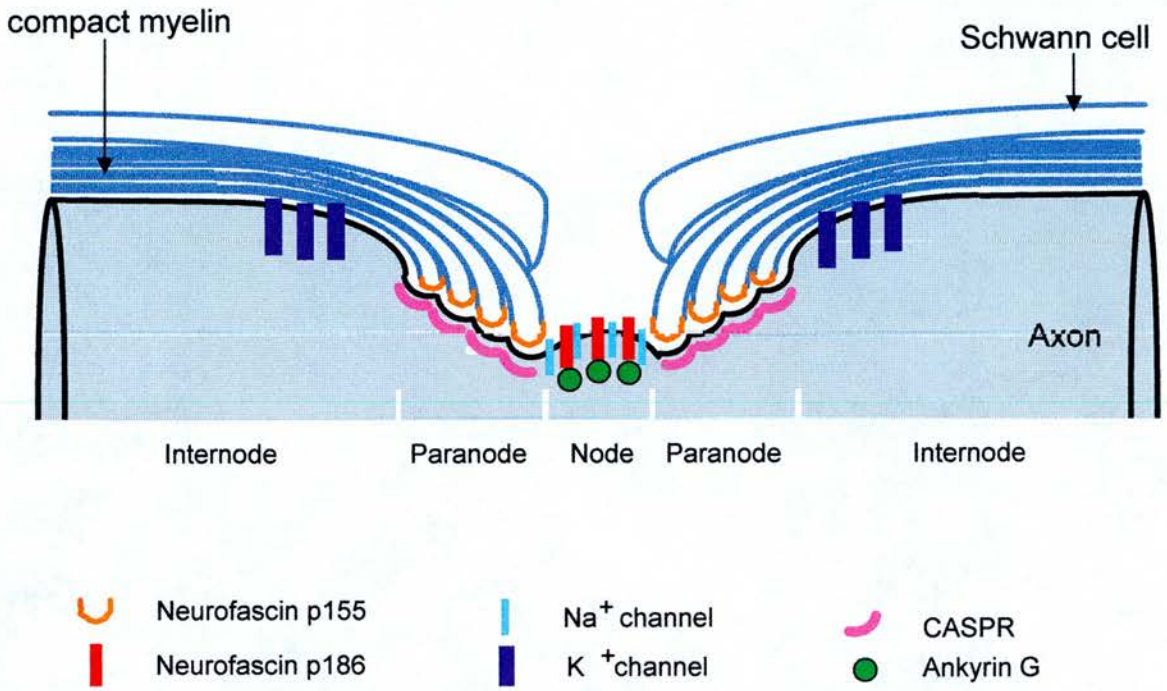

Diagram of the Node of Ranvier to show the localisation of molecules at the node and paranode. (after Tait)

FIGURE 5 – PATIENTS WITH CMT DISEASE

a: Photograph of a patient's hand with CMT disease. There is prominent loss of muscle bulk in the small muscles of the hand.

b: Photograph of a patient's legs with CMT disease. There is severe atrophy of the muscles distally compared to proximally, and the patient has pes cavus.

(Photographs supplied by Dr Colin Mumford)

FIGURE 6 – RODENT *PERIAXIN* GENE AND PROTEIN

a.

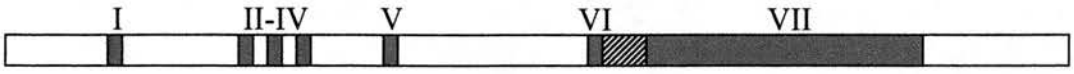

a: Structure of the murine *Periaxin* gene.

Exons are numbered and indicated by blue boxes. Introns are shown as white boxes between the exons, except for intron 6, which is depicted as a striped box.

b.

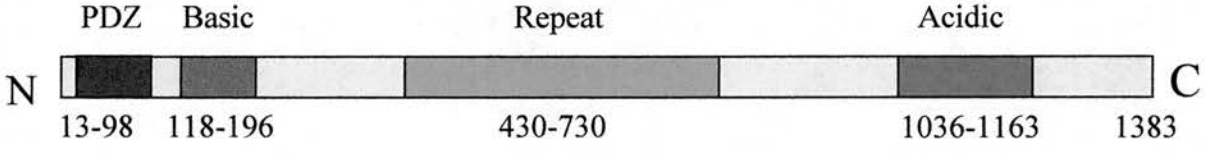

b: The domain structure of rat periaxin.

The repeat-rich region separates a strongly basic N-terminal segment from the acidic C-terminus.

FIGURE 7 - THE LOCALISATION OF PERIAXIN CHANGES DURING DEVELOPMENT

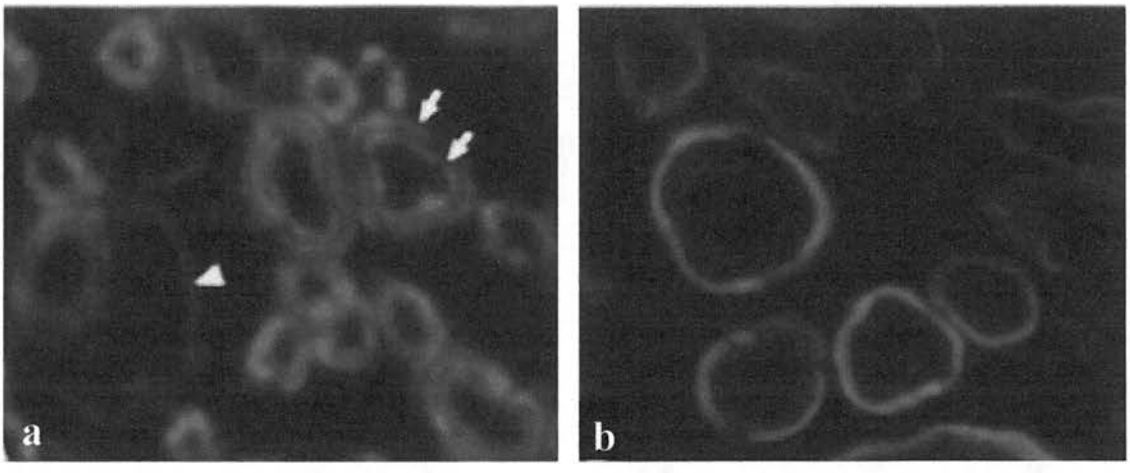

a: At post-natal day 7, periaxin is localised at both the adaxonal and the abaxonal membranes of the Schwann cell (arrows).

b: At post-natal day 42, periaxin is localised at the abaxonal membrane.

(from Dytrych et al., 1998)

FIGURE 8 - THE PERIAXIN / DRP2 / DYSTROGLYCAN COMPLEX AT THE SCHWANN CELL MEMBRANE

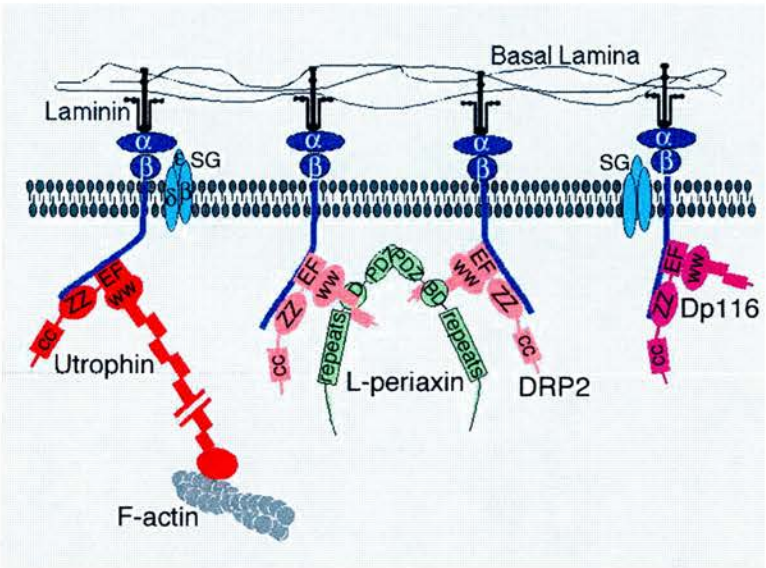

L-periaxin homodimerises, and binds to the spectrin-like repeats of DRP2 through its basic domain. DRP2 binds to the transmembrane protein β-dystroglycan (β), which binds α-dystroglycan (α) and links into the laminin in the basal lamina. β-dystroglycan also binds Dp116 and utrophin. SG - Sarcoglycans. (after Sherman et al., 2001)

FIGURE 9 - THE UBIQUITINATION DEGRADATION PATHWAY

1) Ubiquitin (Ub) is activated by the formation of a thiolester bond with an E1 enzyme, that requires ATP.

2) Ubiquitin is subsequently ligated to an E2 conjugating enzyme, in an energy independent manner releasing E1.

3) The E3 ubiquitin ligases mediate the transfer of ubiquitin residues from E2 to the substrate protein.

4) Ubiquitin C-terminal hydrolases (Uch) and ubiquitin specific proteases (UBP) remove ubiquitin molecules from erroneously tagged proteins.

5) Substrates for degradation are targeted to the proteasome to be destroyed in an energy dependent manner. The Ubiquitin tag is removed by proteases of the 19S subunit and recycled.

6) The 20S core of the 26S proteasome cleaves the substrate into small peptide fragments or individual amino acids that are reused for protein synthesis.

(after Vasiliou)

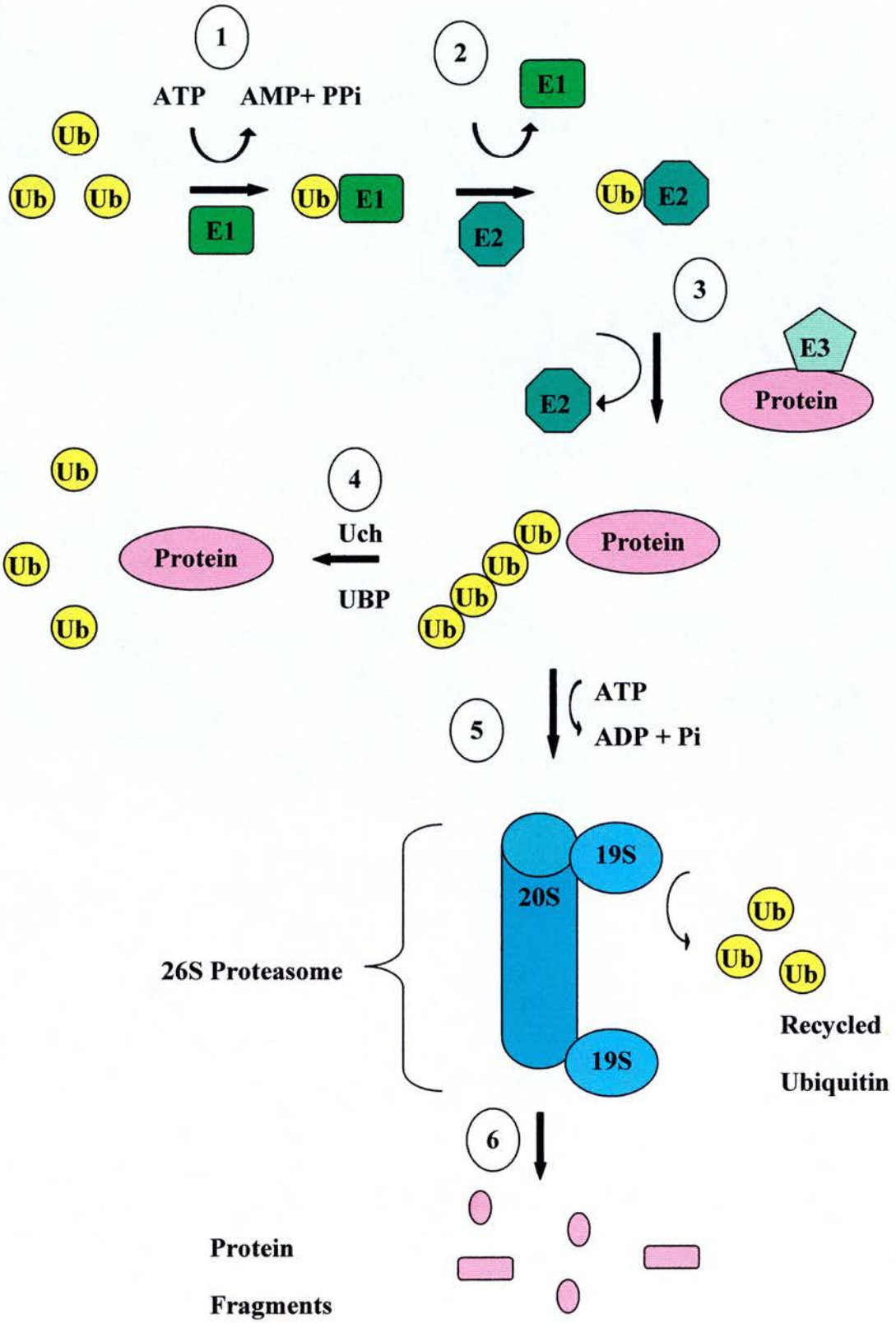
1
ATP
AMP+ PPi
Ub
Ub
Ub
E1
Ub
E1
2
E1
E2
Ub
E2
3
E2
E3
Protein
Ub
Ub
Ub
Protein
4
Uch
UBP
Ub
Ub
Ub
Ub
Protein
5
ATP
ADP + Pi
26S Proteasome
19S
20S
19S
Ub
Ub
Ub
Recycled
Ubiquitin
6
Protein
Fragments

FIGURE 10 - E3 UBIQUITIN LIGASE - THE SCF COMPLEX

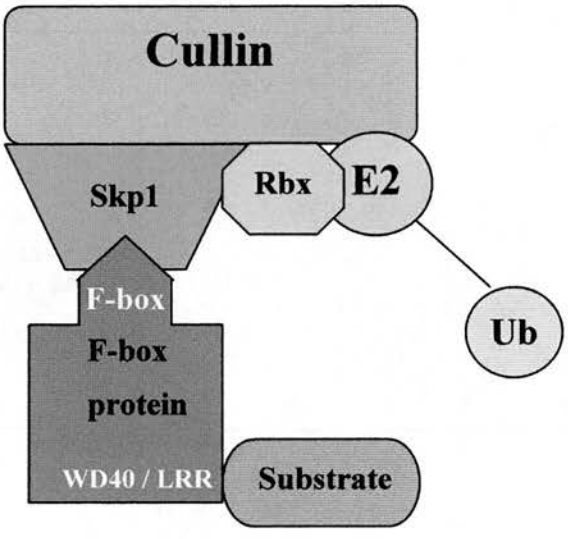

The core consists of Cullin 1, a RING-finger protein Rbx and Skp1. The substrate is recruited by an adaptor protein (F-box protein) that binds to Skp1 via its F-box domain and the substrate to be ubiquitinated via its WD40 or LRR domain.

(adapted from Vasiliou)

FIGURE 11 - REGULATION OF β-CATENIN

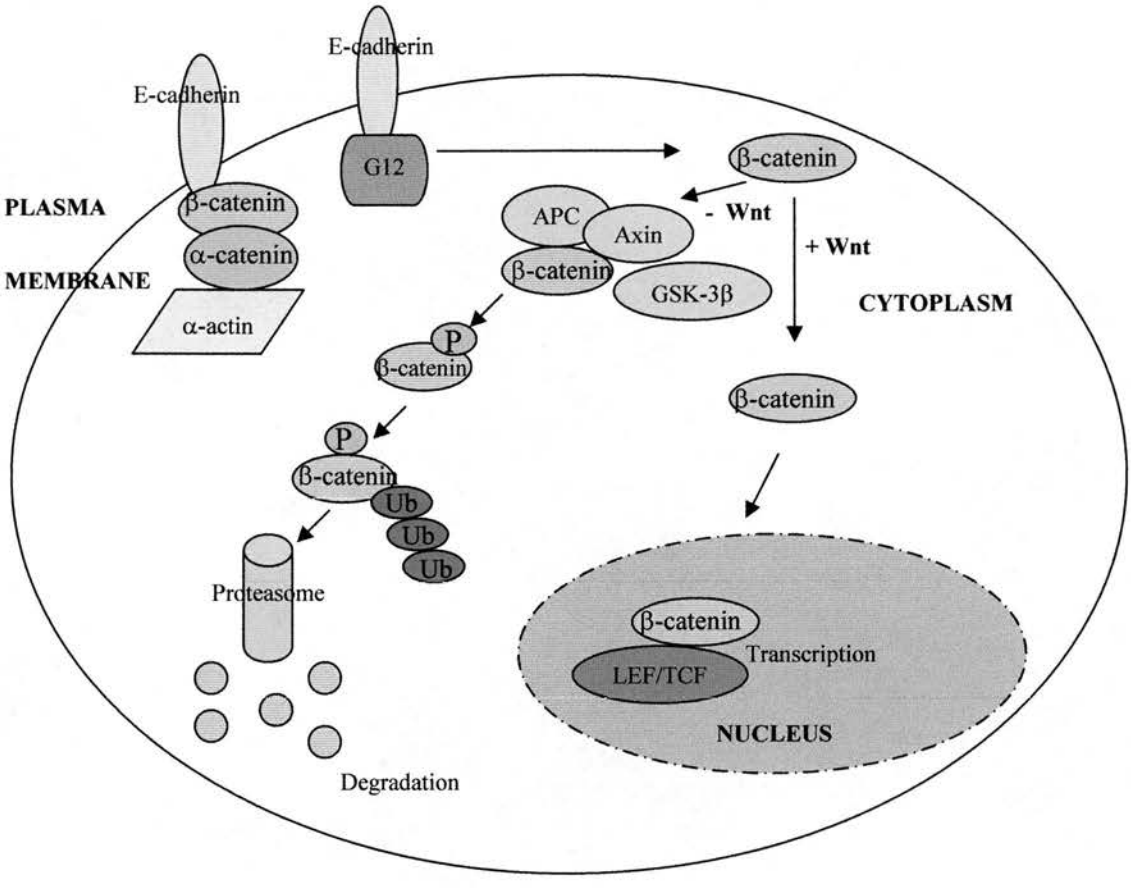

β-catenin links the cytoplasmic region of E-cadherin to α-catenin and the actin cytoskeleton in the adherens junction. Displacement of β-catenin by G12 results in a pool of free cytoplasmic protein. Upon Wnt signalling, cytoplasmic β-catenin translocates to the nucleus where it acts as a transcription factor. In the absence of Wnt, the protein is targeted for destruction in the ubiquitin/proteasomal pathway.

(after Vasiliou)

Table 1: CMT genes and disease types

MIM numbers refer to the reference numbers assigned to the disease or the gene in the online database 'Online Mendelian Inheritance in Man' (www3.ncbi.nlm.nih.gov/omim/).

Subclass	Description	Molecular division	References
CMT1 - demyelinating neuropathies			
CMT1A (MIM118220)	Autosomal Dominant	*PMP22*duplication *PMP22* point mutations (17p11.2) (MIM601097)	(Lupski et al., 1991; Patel et al., 1992; Roa et al., 1993b; Timmerman et al., 1992)
CMT1B (MIM118200)	Autosomal Dominant	*MPZ* (1q22-23) (MIM159440)	(Hayasaka et al., 1993)
CMT1C (MIM601098)	Autosomal Dominant	16p13.1-p12.3	(Street et al., 2002)
CMT1D	Autosomal Dominant	*EGR2* (10q21.1-q22.1) (MIM129010)	(Nelis et al., 1999b; Warner et al., 1998; Warner et al., 1999)
CMT1X	X-linked	*Cx-32/GJB1* (Xq13.1) (MIM304040)	(Bergoffen et al., 1993)
CMT2 - axonopathies			
CMT2A (MIM118210)	Autosomal dominant Prominent sensory loss	*KIF1Bβ* 1p35-p36 (MIM605995)	(Ben Othmane et al., 1993b; Zhao et al., 2001)
CMT2B (MIM600882)	Autosomal dominant Prominent sensory loss Similar to HSN-1 but not allelic	3q13-q22	(De Jonghe et al., 1997; Kwon et al., 1995)
CMT2B1 (MIM605588)	Autosomal recessive	*LMNA* (1q21.2-q21.3) (MIM150330)	(Bouhouche et al., 1999; De Sandre-Giovannoli et al., 2002)
CMT2B2 (MIM605589)	Autosomal recessive	19q13.3	(Leal et al., 2001)
(CMT4C2)	Autosomal recessive Pyramidal features	8q21.3	(Barhoumi et al., 2001)
CMT2C (MIM606071)	Autosomal dominant Diaphragm and vocal chord paralysis	Unknown	(Santoro et al., 2002)
CMT2D (MIM601472)	Autosomal dominant Prominent hand weakness May be same as HMNV	7p14	(Ionasescu et al., 1996)
CMT2E (MIM162280)	Autosomal dominant	*NF-L* (8p21) (MIM162280)	(De Jonghe et al., 2001; Mersiyanova et al., 2000)
CMT2P	Autosomal dominant Proximal atrophy High creatine kinase	3p13.1	(Takashima et al., 1999)
CMT2F (MIM606595)		7q11-q21	(Ismailov et al., 2001)

CMT4 Autosomal Recessive Demyelinating neuropathies			
CMT4A (MIM214400)	Basal lamina onion bulbs	*GDAP1* (8q13-21.1) (MIM606598)	(Baxter et al., 2002; Ben Othmane et al., 1993a; Cuesta et al., 2002)
CMT4B1 (MIM601382)	Focally folded myelin sheaths	*MTMR2* (11q22) (MIM603557)	(Bolino et al., 2000; Quattrone et al., 1996)
CMT4B2 (MIM604563)	Focally folded myelin sheaths	11p15	(Othmane et al., 1999)
CMT4C (MIM601596)	Few onion bulbs	5q23-q33	(LeGuern et al., 1996)
CMT4D/HMSN-Lom (MIM601455)	Onion bulbs Deafness	*NDRG1* 8q24 (MIM605262)	(Kalaydjieva et al., 2000; Kalaydjieva et al., 1996)
CMT4E (MIM605253)	Onion bulbs	*EGR2* 10q21-q22 (MIM129010)	(Warner et al., 1998)
CMT4F (MIM145900)	Onion bulbs	*PRX* 19q13.1-13.3 (MIM605725)	(Boerkoel et al., 2001b; Delague et al., 2000; Guilbot et al., 2001)
Intermediate neuropathies			
DI-CMT (MIM606482)	Autosomal dominant	19p12-p13.2	(Kennerson et al., 2001)
Intermediate CMT (MIM606483)	Autosomal dominant	10q24.1-q25.1	(Verhoeven et al., 2001)
HMSN-R (MIM605285)	Autosomal recessive	10q22-q23	(Rogers et al., 2000)
Dejerine-Sottas Disease (MIM145900)			
CMT3A	Autosomal dominant	*PMP22* point mutations	(Roa et al., 1993a)
CMT3B	Autosomal dominant	*MPZ*	(Hayasaka et al., 1993; Warner et al., 1996a)
CMT3D	Autosomal dominant	*EGR2*	(Timmerman et al., 1999)
CMT4F	Autosomal recessive	*PRX*	(Boerkoel et al., 2001b)
Congenital hypomyelination (MIM605253)			
		PMP22 point mutations	(Ceuterick-de Groote et al., 2001; Fabrizi et al., 2001; Simonati et al., 1999)
		MPZ	(Mandich et al., 1999; Warner et al., 1996a)
		EGR2	(Warner et al., 1998)
		MTMR2	(Bolino et al., 2001)
Hereditary sensory neuropathy			
HSNI (MIM162400)	Autosomal dominant ulcero-mutilating features	*SPTLC1* (9q22.1-9q22.3) (MIM605712) ?	(Bejaoui et al., 2001; Dawkins et al., 2001) (Auer-Grumbach et al., 2000b; Bellone et al., 2002)
HSNIII/Riley-Day/HSAN3	Autosomal recessive	*IKBKAP* (9q31) (MIM603722)	(Slaugenhaupt et al., 2001)

(MIM223900)			
HSNIV/CIPA/HSAN4 (MIM256800)	Autosomal recessive	*NTRK1/TRKA* 1q22 (MIM191315)	(Bodzioch et al., 2001; Houlden et al., 2001; Indo et al., 1996; Shatzky et al., 2000)
HSAN6 (MIM310470)		X	(Jestico et al., 1985)
Distal hereditary motor neuronopathy			
dHMN-II (MIM158590)	Adult onset distal wasting and weakness	12q24.3	(Timmerman et al., 1996a)
dHMN-V (MIM600794 and MIM601472)	Autosomal dominant prominent hand weakness May be same as CMT2D	7p14	(Christodoulou et al., 1995)
dHMN-VI (Spinal muscular atrophy with respiratory distress) (MIM604320)	Autosomal recessive	*IGHMBP2* 11q13.2-q13.4 (MIM600502)	(Grohmann et al., 2001)
dHMN-VII (MIM158580)	Autosomal dominant with vocal chord paralysis	2q14	(McEntagart et al., 2001)
Others			
CMT1/Pelizaeus-Merzbacher	Autosomal dominant	*SOX10* 22q13 (MIM602229)	(Inoue et al., 1999; Pingault et al., 2000)
Giant axonal neuropathy (MIM256850)	Autosomal recessive	*GAN* (16q24.1) (MIM605379)	(Bomont et al., 2000)

2. MATERIALS AND METHODS

2.1. CLONING THE HUMAN *PERIAXIN* GENE

Several different methods were used to obtain the human *PERIAXIN* sequence.

2.1.1. Polymerase chain reaction (PCR)

Reverse transcription polymerase chain reaction (RT-PCR) was carried out on RNA extracted from human sciatic nerve, using primers matching rat *Periaxin* sequence. 150 ng of random primers (hexamers and nonomers of random sequence) were added to 4 μg of sciatic nerve RNA in DEPC water and incubated at 70 °C for ten min to denature. The sample was left for two min on ice to anneal. Then 4 μl of 1st strand buffer, 2 μl 0.1M DTT, 1 μl 10 mM dNTPs and 1 μl superscript Reverse Transcriptase were added, incubated at 25 °C for ten min and then at 42 °C for forty five min. The sample was heated at 75 °C for fifteen min and put on ice. 1 μl of this was used as a template for each PCR reaction. The PCR mix consisted of 5 μl of each 5 μM primer solution, 5 μl of 2 μM dntp solution, 5 μl of 10x buffer, 1 μl of template, and 0.5 μl of PFU enzyme made up to 50 μl with water.

Similarly, PCR was used with genomic DNA as a template using rat or human specific *Periaxin* primers, as listed in Table 2.

2.1.2. Plasmid Artificial Chromosomes

We obtained a human Plasmid Artificial Chromosome (PAC) library from the Human Genome Mapping Project in Cambridge, and screened this with a probe consisting of the complete rat periaxin cDNA to select PAC clones that contained human *PERIAXIN*. Two PAC clones were obtained – PAC68 and PAC71. Working with these PAC clones was difficult due to the poor yield from plasmid preparations, as they have a copy number of one. Thus, large cultures of bacteria are required to obtain a small amount of PAC, and there is proportionally more contamination with protein and genomic DNA unless steps are taken to account for this.

2.1.3. PAC preparation (A variation of the Qiagen Midi-prep method)

A glycerol stock of PAC was grown in 250-500 ml of Luria Broth and 25 μg/ml Kanamycin for 18 hours. This was spun down at 6000 rpm at 4 °C for fifteen min. The pellet was resuspended in 10 ml of P1 (50 mM TrisCl pH 8, 10 mM EDTA and 100 μg/ml RNase A). Solution P2 (10 ml) was added (200 mM sodium hydroxide and 1 % SDS w/v), mixed gently and left at room temperature for five min. Solution P3 (10 ml) was added (3 M potassium acetate pH 5.5), mixed gently and left on ice for thirty min. This was spun down at 15000 rpm at 4 °C for thirty min, the supernatant decanted into clean tubes and spun again at 15000 rpm at 4 °C for fifteen min. The supernatant was then precipitated with isopropanol (0.75 volumes), and spun at 15000 rpm at 4 °C for thirty min, to decrease the volume before putting it through the column. The pellet was resuspended in 10 ml of QBT (750 mM NaCl, 50 mM MOPS pH 7, 15 % isopropanol v/v, 0.15 % triton X-100 v/v) and passed through a midi column primed with the same buffer. The column was washed twice with 10 ml of QC wash buffer (1 M NaCl, 50 mM MOPS pH 7, 15 % isopropanol v/v) and then the DNA was eluted from the column with 6 ml of QF buffer (1.25 M NaCl, 50 mM TrisCl pH 8.5, 15 % isopropanol v/v) warmed to 50 °C. The DNA was again precipitated with 0.75 volumes of isopropanol, and spun at 13000 rpm for thirty min at 4 °C. The pellet was washed with ice cold 70% ethanol and spun for five min. The pellet was left to dry for ten min and then resuspended in TE (0.01 M Tris/HCl pH 8.0, 5 mM EDTA pH 8.0) containing Rnase cocktail (Ambion) by leaving overnight at 4 °C. Pipetting the solution up and down was avoided as this can shear large pieces of DNA. The amount and quality of the DNA was checked using absorbance at 260 nm and by running a sample out on an agarose gel.

2.1.4. Instability of PAC clones

PAC clones can sometimes be unstable, and over time PCR and Southern blots using PAC71 as a template ceased working, suggesting that the *PERIAXIN* gene was lost from this PAC clone. Fortunately, PAC68 was stable. I determined the sequence of exons II, III and IV, and intervening introns 2 and 3 by PCR directly from the PAC68 using rat-specific primers (Table 2).

2.1.5. Digestion of PAC 68 clone and detection of fragments by Southern blot

The PAC was digested with frequent cutting restriction enzymes to generate smaller fragments. These were electrophoresed on a pulsed field gel for high resolution of the fragments. An 0.8 % agarose TBE gel was run in cooled (13 °C) 0.5 x TBE buffer at 6 Volts/cm for 18 hours with the pulse setting at 0.1 – 10 and then stained with ethidium bromide. This was transferred to a nylon membrane and hybridised with the whole length rat periaxin cDNA probe by Southern blot.

2.1.6. The hybridisation probe

The whole length rat periaxin cDNA probe was obtained by digestion of the 4.6 kb fragment from its plasmid pSPORT (Stratagene) with *Sal*I/*Not*I.

2.1.7. Southern blotting of PAC DNA

The DNA was transferred to a nitro-cellulose membrane (Schleicher and Schuell) under a pressure of 45 mbar. The gel was first covered with denaturing solution for twenty min, then with neutralising solution (87.7 g NaCl, 121.1 g Tris, 2 ml 0.5 M EDTA, 800 ml H_20 pH 7.2) for twenty min and finally with 20x SSC (3 M sodium chloride, 0.3 M trisodium citrate) for one hour. The membrane was dried overnight at 80 °C.

2.1.8. Radioactive labelling of hybridisation probe

The probe (30 ng) was labelled using the random prime DNA labelling kit (Gibco BRL). The DNA was boiled in distilled water (23 µl total volume) for three min to denature it and put onto ice. Following a brief spin nucleotide mix (6 µl) and random primer mix (15 µl) were added. The probe was then incubated with 1.85 Mbeq ^{32}P labelled phosphate (ICN) and 3 U Klenow fragment enzyme at 25 °C for one hour. The reaction was terminated with 5 µl of STOP solution and 100 µl of 10 mg/ml sheared salmon sperm DNA.

2.1.9. Hybridisation process

The membrane was soaked briefly in distilled water and placed into a 50 ml Falcon tube with 5 ml of Quik-Hyb solution (Qiagen) and allowed to warm to 65 °C for thirty min. The probe was boiled at 98 °C for ten min and allowed to hybridise to the filter at 65 °C for two hours. Then the filter was washed twice with low stringency buffer (2 x SSC (0.3 M sodium chloride, 0.03 M sodium citrate) / 0.1 % SDS) for ten min each time, at room temperature. It was subsequently washed twice with high stringency buffer (0.2 x SSC (0.03 M sodium chloride, 3 mM sodium citrate) / 0.1 % SDS) for thirty min each time at 65 °C. The filter was dried at room temperature and wrapped in Saran film. Autoradiography was carried out over 48 hours.

2.2. DETECTION OF *PERIAXIN* MUTATIONS

2.2.1. Detecting the mutation R196X

The Paris group amplified exon VII of *PERIAXIN* in ten overlapping fragments. The PCR products were purified using QiaQuick PCR Purification kit (Qiagen) and sequenced by BigDye terminator chemistry (Perkin-Elmer) on an ABI377 (Perkin-Elmer). The PCR product of the first fragment of exon VII was digested with the enzyme *Rsa*I (three hours at 42 °C) followed by analysis on a 2 % agarose gel.

2.2.2. Detecting PERIAXIN protein, or its truncated form by immunofluorescence

Nerve biopsies taken from humans are usually fixed in formalin and then embedded in paraffin blocks. This preserves the tissue structure well but the formalin fixation can mask antigens, disrupting antibody binding. There are five periaxin antibodies which label periaxin antigen well on frozen mouse or rat peripheral nerve sections (Table 3), but these have never previously been used on human sections, or on paraffin sections.

2.2.3. Human C-terminal periaxin antibody

As the rabbit and sheep C-terminal periaxin antibodies do not recognise human Periaxin, we raised a human-specific C-terminal antibody to the peptide sequence

KARSGSGDQEEGGLRVRLPS in rabbits. To enhance its antigenicity, the peptide was coupled to Keyhole Limpet haemocyanin by an N-terminal Cysteine residue. The peptide was synthesised by Invitrogen. The supplied dehydrated salt was dissolved in MilliQ water to a concentration of 1 mg/ml and 2 ml aliquots were stored at -40°C. Prior to injection, each 2 ml aliquot was mixed with 3 ml of Freund's complete adjuvant (Sigma) and mixed by vigorous shaking overnight. This mix was spun briefly and three 1.5 ml aliquots were prepared in 3 ml syringes (Becton Dickinson). Each aliquot was injected into a male New Zealand White rabbit. Two boost injections were given three and five weeks later when the aliquots were prepared in 3 ml of Freund's incomplete adjuvant (Sigma). The rabbits were bled ten days after the first boost to test for antibody production and then bled out at seven weeks. Professor P.J.Brophy carried out all injections and cardiac exsanguination at the CTVM Facilities, Easter Bush, Edinburgh.

2.2.4. Western blotting

Proteins were resolved according to size on a SDS-PAGE gel and transferred to a nitro-cellulose membrane (0.45 μm, Schleicher and Schuell) in a buffer containing 25 mM Tris-HCl, 250 mM glycine and 20 % methanol. The transfer was carried out in a Hoefer Mighty Small Transphor Unit (Pharmacia Biotech) cooled apparatus for two hours at 0.48 amps. The nitro-cellulose filter was then blocked in 5 % dried skimmed milk, 0.1 % Tween-20 in PBS (Appendix A) overnight. It was rinsed with 0.2 % gelatin, 0.1 % Tween-20 in PBS and incubated with the primary antibody diluted in the same buffer, for one hour on a shaker. The filter was washed three times for ten min in 0.2 % gelatin, 0.1 % Tween-20 in PBS and incubated with the secondary antibody, which is HRP-labelled, diluted in the same buffer for one hour on a shaker. Excess secondary antibody was then washed off with three ten minute washes in 0.1 % Tween-20 in PBS. The peroxidase was detected using the enhanced chemiluminescence (ECL) method (Amersham) or by adding 3,3 diaminobenzidine (DAB) solution (0.05 % DAB in 50 mM TRIS pH 8.0) and 0.02 % hydrogen peroxide. If DAB was used for developing the blots, then 0.1 % Triton X-100 was used in place of Tween-20 in all of the solutions.

2.2.5. Assessment of rabbit anti-serum by Western blotting

Test bleeds (3 ml) were collected from the rabbits in 5 ml Bijoux tubes and allowed to clot at 4 °C overnight. The serum was taken into 1.5 ml microfuge tubes and spun at 13000 rpm for two min to remove the clotted blood. Aliquots were stored at -40 °C. To assess the specificity of the anti-serum, a Western blot was performed using human cauda equina post-mortem material boiled in 2 % SDS solution and run out on an 8 % SDS-PAGE gel. The final bleed of the human C-terminal antibody (2186) was used at a dilution of 1:1000, and the secondary antibody, donkey anti-rabbit IgG-HRP (Diagnostics Scotland), at a dilution of 1:500, when developing with DAB solution, and 1:4000 and 1:2000 respectively for developing with the ECL technique. Affinity purified anti-serum was tested in the same manner, used at a dilution of 1:200 (DAB).

2.2.6. Affinity Purification of anti-serum

The anti-serum was affinity purified using an α-aminohexyl sepharose 4B column, conjugated to non-KLH coupled peptide. α-aminohexyl sepharose 4B (1 ml) was pipetted into a 15 ml Falcon tube, spun briefly to remove the excess ethanol and washed four times with 3 ml of PBS (Appendix A). It was then resuspended in 2 ml of PBS and 5 mg of MBS (m-maleimidobenzoyl-N-hydroxysulfosuccinimide ester) added, dissolved in 200 µl of dimethylformamide. The tube was placed on a rotating wheel at room temperature for two hours and then spun down and washed four times with 3 ml of PBS. The final spin (five min) was to pack the gel. Non-KLH coupled peptide (10 mg) was dissolved in 800 µl of 10 mM hydrochloric acid and the pH adjusted to 6.0 with 100 mM sodium hydroxide. The gel was incubated with this peptide solution on a windmill at room temperature overnight.

The peptide/sepharose conjugate was washed with two volumes of 1 M Tris-HCl pH 7.5, then with two volumes of 50 mM citric acid, pH 2.5 and lastly with three washes of two volumes of PBS. Anti-serum (5 ml) was added to the column and allowed to mix on a windmill at 4 °C overnight.

The slurry was then loaded into a 10 cm x 1 cm column (Biorad) and allowed to settle. The column was washed with 5 ml 20 mM sodium citrate until the absorbance at 280 nm was zero. Citric acid (50 mM pH 2.5) (6 ml) was added to elute the antibody and 0.5 ml fractions collected into microfuge tubes containing 0.35 ml 1 M HEPES pH 7.5. The yield was determined by reading the absorbance at 280 nm of the collected fractions. To clear the column, it was washed with elution buffer to remove all antibody, then washed with 20 mM sodium citrate pH 7.7 and four times with PBS. It was stored in PBS with 0.01 % sodium azide at 4 °C.

2.2.7. Immunohistochemistry

2.2.7.1. Paraffin sections

Sections (5 μm) of formalin-fixed sural nerve biopsies embedded in paraffin were collected on 3-aminopropyltriethoxysilane (TESPA)-subbed slides. The paraffin was removed by immersing in two changes of xylene over thirty min, and the tissue was rehydrated through alcohol (100 % for five min, then 95 %, 70 %, 50 % 30 % for thirty seconds each) to water (two 1 minute changes). The sections were then washed in 0.85 % NaCl for five min and microwaved at 700 W in 0.1 M citrate buffer (pH 6) for ten min. They were allowed to cool in the same buffer for twenty min and then fixed in 4 % paraformaldehyde for ten min (Cattoretti et al., 1992). The sections were washed in two changes of PBS (Appendix A) over ten min.

Double-label immunofluorescence was carried out. Sections were blocked for one hour at room temperature in a solution of 5 % (v/v) fish gelatin, 0.1 % (v/v) Triton X-100 in PBS. Blocked sections were incubated overnight with primary antibody diluted in the same solution, under humid conditions at room temperature. Slides were then washed three times in PBS containing 0.1 % (v/v) triton X-100 over one hour and then incubated with the appropriate dilution of FITC or TRITC-conjugated secondary antibodies in the blocking solution for ninety min. The slides were washed three times in PBS over forty-five min, mounted with Vectashield (Vector Labs), and examined under a fluorescence microscope. Dilutions and sources of antibodies used are shown in Table 4.

2.2.7.2. Frozen sections

Frozen sections of tissue (5 μm) were collected similarly on 3-aminopropyltriethoxysilane-subbed slides. The OCT (optimal cutting temperature) in which the samples were embedded was washed away with PBS (Appendix A) and the sections were fixed in 4 % paraformaldehyde for five min. Then, the sections were blocked and treated in the same way as in Section 2.2.7.1.

2.2.8. Sural nerve pathology

Semi-thin sections (1 μm) were cut from osmicated resin-embedded nerve, stained with toluidine blue and viewed under the light microscope. Ultrathin sections were cut from the same blocks, stained with uranyl acetate and lead citrate and examined on a Phillips BioTwin electron microscope.

2.3. OVER-EXPRESSION VECTOR

The periaxin overexpression vector consists of mouse L-Periaxin cDNA under the control of the MBP promoter and Schwann cell enhancer 1 (SCE1). The vector, clone 8, contains 9 kb of MBP promoter plus the SCE1. The SCE1 enhancer is a 600 bp fragment that will function regardless of orientation and position upstream or downstream of the gene (Forghani et al., 2001). Mouse L-periaxin cDNA (4.6 kb) was excised from the plasmid pIBI30 with *EcoR*I and *BamH*I enzymes in buffer React3. This was cloned into plasmid pSP72 (Promega) at the *EcoR*I/*BamH*I sites, and excised with *Cla*I/*Sal*I restriction digest in buffer H. This fragment was then subcloned into the *Cla*I/*Sal*I sites of the clone 8 vector.

Clone 8 vector

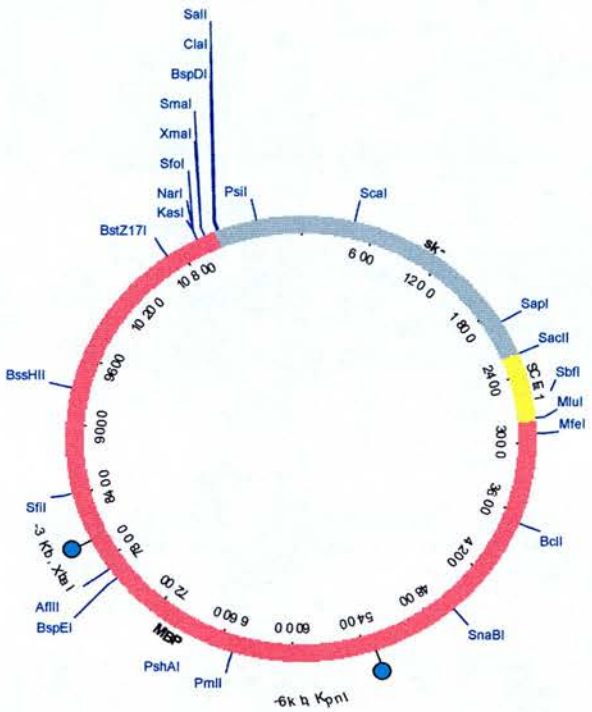

2.3.1. Preparation of DNA for injections

The transgene (13.6 kb) was excised with a *BamH1/Sst*II double digest in React2 buffer overnight at 37 °C (50 µg). The digest was run out on a 0.8 % low melting point agarose gel in Tris-acetate buffer ((TAE) 0.04 M Tris-acetate, 1 mM EDTA) at 4°C and the linearised transgene cut out with minimal agarose. This was weighed, 0.04 volumes of 25 x agarase buffer (Boehringer) added (i.e. 2 µl for 50 mg), and incubated at 65°C for fifteen min. The sample was incubated at 45 °C for ten min to cool down, 0.8 units of agarase enzyme per 100 mg agarose were added, and left for two hours at 45 °C. Following agarase treatment, the DNA sample was diluted in 10 ml of low salt buffer and purified using Elu-tip D-column set (Schleicher and Schnell) NA01010 according to the manufacturers instructions. The DNA was eluted from the Elutip column into a pre-cleaned microfuge tube (rinsed with filter-sterile water), and ethanol precipitated. The pellet was washed with 500 µl of 70% ethanol, spun for five min at room temperature and allowed to dry. This was taken up in 50µl Millipore-filtered injection buffer (10 mM Tris-HCl pH 7.5, 0.1 mM EDTA pH 8.0)

and a sample was run out against high DNA mass ladder on an agarose gel to check size and amount. Approximately 2 μg of DNA was dialysed against 1 litre of injection buffer at 4 °C for 48 hours, with three changes of buffer over this time. The concentration was checked against a DNA high mass ladder by running a sample on an agarose gel, diluted with filtered injection buffer to 2.5 ng/μl, and stored in 20 μl aliquots at –70 °C ready for injection.

2.4. CONDITIONAL CONSTRUCT

We made a conditional construct which, using homologous recombination, inserts loxP sites either side of exon V of murine *Periaxin*. When this fragment of DNA between the loxP sites is removed by Cre recombinase activity, the translation frame is altered in exon VI introducing a downstream stop codon. A protein of thirteen amino acids (nine from exon IV and four from exon VI) could be translated, but this would most probably be unstable.

Conditional construct

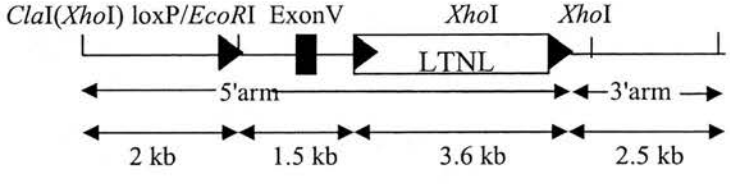

The full-length genomic mouse *Periaxin* DNA sequence was put together by Lee Dytrych and Stewart Gillespie (Dytrych et al., 1998).

2.4.1. The 5' arm of the construct

The 5' arm of the construct was put together from two fragments digested from the full-length *Periaxin* clones. The *Xho*I/*Kpn*I fragment of the 5' arm was subcloned into bluescript vector (Stratagene). The *Kpn*I/*Xho*I fragment was subcloned into pGEM7 (Promega). Then, the first fragment was digested from its position in

bluescript with *Cla*I/*Kpn*I and subcloned into pGEM7 containing the *Kpn*I/*Xho*I fragment.

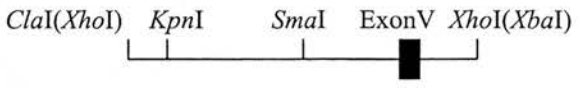

The next step was to insert the single loxP site in the *Sma*I site of the 5' arm. These oligonucleotides were designed to contain the loxP site with ends designed to ligate into a *Sma*I site and a 3' *EcoR*1 site (GAATTC) for screening purposes. The forward and reverse oligonucleotide sequences were obtained from Oswel and high performance liquid chromatography (HPLC) purified.

Forward

5'CCCATAACTTCGTATAATGTATGCTATACGAAGTTAT**GAATTC**GGG3'

Reverse

5'CCC**GAATTC**ATAACTTCGTATAGCATACATTATACGAAGTTATGGG3'

These oligonucleotide sequences were annealed together by taking 30 pmoles of each and, in the presence of NEB buffer 2 (New England Biolabs), they were incubated on a PCR machine at 98 °C for 5 min, and then at -1°C per cycle until reaching 25 °C. These annealed oligonucleotides were then ligated into the *Sma*I site of the 5'arm. The most efficient ligation occurred at the molar ratio of 10:1 of oligonucleotides: vector.

The subclones were screened for the presence of a new *EcoR*I site and the absence of a *Sma*I site by enzymatic digestion, and five of these were sequenced using the intron 4 reverse primer MP2 (GAGGCACCTTAAGCCATGCG) to ensure that the cassette was in the correct orientation. Three out of five of these clones were in the correct orientation.

2.4.2. The 3' arm

A 2.5 kb fragment was digested from the subclone 5.5 with *Xho*I and subcloned into the *Sal*I site of pSP72 (Promega).

2.4.3. Putting the 5' and 3' arms together

The 5' arm containing loxP in the *Sma*I site was digested with *Cla*I and *Xba*I and subcloned into the pSP72 vector (Promega) containing the 3' arm.

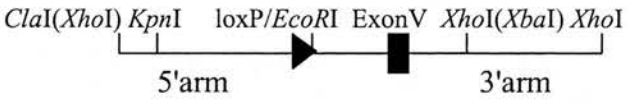

The last step was to put the cassette containing herpes simplex thymidine kinase (T) and neomycin resistance (N) flanked by loxP sites (L), (LTNL), into the *Xba*I site at the end of the 5' arm. This cassette was digested from its vector with high concentration *Xba*I enzyme in React2 buffer (Gibco). The pSP72 (Promega) vector containing both 5' and 3' arms was also digested with *Xba*I in the same way, then phenol/chloroform extracted, and ethanol precipitated in the presence of 3 M sodium acetate. This was taken up in 17 µl of water, 2 µl of 10 x buffer and 1 µl of calf intestinal alkaline phosphatase and incubated at 37 °C for thirty min to dephosphorylate the ends of this vector and reduce the likelihood of simple recircularisation. Each digest was run out on a 0.8 % agarose TAE gel (0.04 M Tris-acetate, 1 mM EDTA) and the 9 kb linear fragment of the vector, and the 3.6 kb LTNL cassette were purified from the gel using the Qiaex method (Qiagen). These fragments were then ligated overnight at 4 °C in the presence of T4 DNA ligase, and its buffer (MBI Fermentas). The subclones were screened by an *Xba*I digest to show release of a 3.6 kb fragment. The orientation of the cassette was determined by digesting with *BamH*I in React3 buffer as the LNTL has a *BamH*I site 0.4 kb from its 3' end. The correct orientation gave fragments of 6.3 and 5.3 kb, and the incorrect of 3.5 and 8.1 kb. Six out of twelve of them were in the correct orientation.

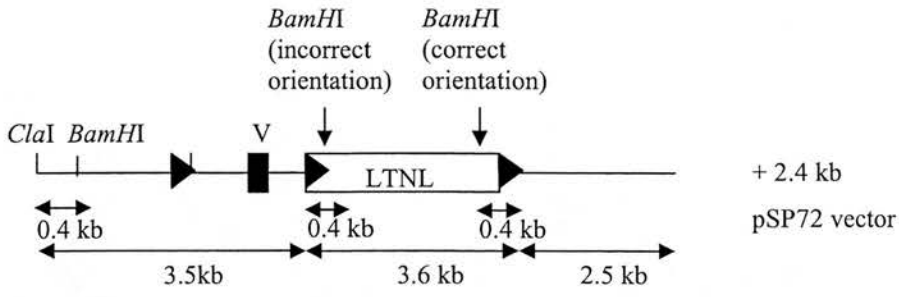

Large quantities of the completed construct were obtained using the maxiprep (Qiagen) kit using the low copy method, as the vector was large (12 kb).

2.4.4. Testing the loxP sites

To ensure that the loxP sites were correct and that Cre recombinase could stimulate recombination between them, I transformed competent Cre-expressing BCC132 cells with the conditional construct. The conditional construct (0.2 μg) was added to competent BCC132 cells and incubated at 42 °C for ninety seconds. SOC medium (800 μl) (Appendix A) was added and this was incubated at 30 °C for one hour to allow Cre expression. Then, the cells were incubated at 37 °C to allow growth and plated out on L-AMP (L-agar/ 100 μg/ml ampicillin) plates. Plasmid DNA was recovered from the colonies and screened for recombination events. Restriction digestion with *Cla*I and a double digest with *Cla*I/*Eco*RI confirmed that all three possible recombination events had occurred.

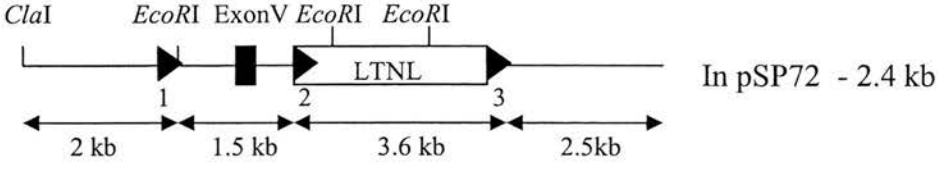

	*Cla*I digest	*Cla*I/*EcoR*I digest
No recombination	12 kb	2, 1.6, 1.7, and 6.7 kb
Recombined between loxP sites 1+3	6.9 kb	6.9 kb
Recombined between loxP sites 2+3	8.4 kb	2 and 6.4 kb
Recombined between loxP sites 1+2	10.5 kb	2.1, 1.7, and 6.7 kb

Out of five clones selected, there were none in which no recombination occurred. One recombined between loxP sites 1 and 3, and two between sites 2 and 3 and two between sites 1 and 2. Therefore, all loxP sites are functioning as expected.

The vector (300 μg) was then linearised with the enzyme *Cla*I (in the presence of bovine serum albumin, and buffer NEB4 (New England Biolabs)) overnight at 37 °C. A sample was run out on a 0.8 % agarose TAE (0.04 M Tris-acetate, 1 mM EDTA) gel to check that it was fully linearised. Then the remaining DNA was extracted with phenol-chloroform and 2.2 volumes of absolute ethanol were added. This was then taken to the Centre of Genome Research for electroporation into embryonic stem (ES) cells.

After electroporation, they cultured the ES cells in Geneticin (G418) which selects for those clones containing the construct at any site, as it contains the sequence for neomycin resistance. The DNA was extracted from these positive clones and screened with the 5' and 3' probes to ensure that the construct had undergone homologous recombination and was incorporated into the correct site. The 5' probe, generated by PCR using the primers LMD2/MP1 (see Table 5), is a 334 bp sequence containing sequence from exons II to IV lying outwith the construct, and adjacent intron sequence. When wild-type genomic DNA is digested with the restriction enzyme *EcoR*I, this probe hybridises to a 10.5 kb fragment on a Southern blot as opposed to a 6 kb fragment in the targeted genomic DNA (Figure 12a). The 3' probe (LMD13/MP5) is a 400 bp sequence containing exon VI sequence 5' to the *Sma*I site,

plus some intron 5 sequence. When wild-type genomic DNA is digested with the restriction enzyme *Sma*I, this probe hybridises to an 8.5 kb fragment on a Southern blot as opposed to a 9.2 kb fragment in the targeted genomic DNA (Figure 12a).

A plasmid containing Cre recombinase was electroporated into these clones able to grow in G418 and that showed the correct pattern on Southern blots with the 5' and 3' probes. The Cre was transiently expressed allowing the recombination events to occur between the loxP sites. Those clones with recombination between loxP sites 1 and 2 were selected out with gancyclovir, as these cells contain the thymidine kinase gene that converts this to a toxin. The other two recombination events generate a knock-out of the *Periaxin* gene (loxP sites 1 and 3) or the floxed exon V of *Periaxin* (loxP sites 2 and 3). When 'knock-out' DNA is digested with the restriction enzyme *Eco*RI, the 5' probe hybridises to a 9 kb fragment on a Southern blot as opposed to a 6 kb fragment in the floxed *Periaxin* DNA (Figure 12b). When 'knock-out' DNA is digested with the restriction enzyme *Sma*I, the 3' probe hybridises to an 18.5 kb fragment on a Southern blot as opposed to a 20 kb fragment in the floxed *Periaxin* DNA (Figure 12b).

2.5. SCIATIC NERVE CRUSH

University of Edinburgh Care of Animals regulations were observed throughout these experiments.

Six-week-old mice were anaesthetised with midazolam (3 μg/g), fentanyl (0.5 μg/g) and fluanisone (16 μg/g), and an incision made to expose the right sciatic nerve. At the sciatic notch, the nerve was crushed for ten seconds, three times, with jeweller's forceps (T5254 Agar Scientific). The wound was closed with a clip. After two or six weeks, the mice were anaesthetised with halothane, and then perfused with 2.5 % glutaraldehyde and 2 % paraformaldehyde in 0.1 M sodium cacodylate buffer (pH 7.3). The sciatic nerves were removed. The proximal end was cut at the site of crush, at the sciatic notch, or equivalent level on the contra-lateral leg, and muscle was left on the distal end of the nerve, to allow easy orientation after fixation. The nerves were fixed for two hours in the same fixative, post-fixed in osmium tetroxide and embedded in araldite.

Transverse semi-thin sections of one micron were cut immediately distal to the crush site, and stained with Toluidine blue. The myelin thickness of fibres regenerated after crush depends not only on the ability of the Schwann cell to remyelinate but also on the efficiency of axonal sprouting and elongation, and so great care was taken to perform measurements at the same distance from the crush site.

The total cross-sectional area of nerve was measured using the IP Lab Spectrum software. Measurements of myelinated axon number, density, diameter and myelin thickness were then performed on 30 % of the area of each nerve chosen randomly, using the IP Lab Spectrum software (Figure 13). Random areas of the nerve were selected by superimposing a numbered grid and using a random number table to select squares. Analysis of significance was carried out using the t-test for normally distributed data and the Kolmogorov-Smirnov test for non-parametric data. Regression lines were compared using ANOVA. Each experimental group consisted of between three and five mice.

2.6. FBL6 ANTIBODIES

Sylvia Vasiliou constructed a GST fusion protein containing amino acids 49-115 of Fbl6 previously and this was used as an antigen to produce an antibody, as described in Section 2.2.3.

2.6.1. Purification of GST-fusion protein

The GST-fusion clone of Fbl6 in codon-plus bacteria was grown in 2 x 500 ml of L-broth culture containing 100 μg/ml ampicillin at 37 °C until reaching an optical density at 600 nm (OD_{600}) of 0.5-0.6, and then induced with 1 mM IPTG for three hours at 37°C. The cultures were spun at 4000 rpm at 4 °C for ten min and the pellet resuspended in 12.5 ml of buffer (50 mM Tris pH 8.0, 50 mM NaCl, 2 mM DTT, 1 mM PMSF, 1 mM benzamidine and one protease inhibitor tablet (Boehringer-Mannheim)). This was then sonicated for 6 x ten seconds and spun for twenty min at 14000 rpm at 4°C. Glutathione sepharose 4B (Pharmacia) was washed with PBS (Appendix A) three times and the supernatant added, and incubated on a rotating wheel at room temperature for one hour and then at 4 °C for one hour. The matrix

was loaded into a column (Biorad) and washed with PBS. The fusion protein was eluted with 10 mM glutathione in 50 mM Tris pH 8.0.

The protein yield was estimated by reading the absorbance at 280 nm and checked on a SDS-PAGE gel compared to BSA standards.

2.6.2. Affinity Purification of Fbl6 antibody (2194)

As the antibody was raised to a GST fusion protein, with a pI of 8.69, affi-gel 10 (for neutral or basic proteins) was used as a matrix. GST-fusion protein (fused to amino acids 49-115 of Fbl6) (5 mg) was concentrated into 2 ml and dialysed against 2 litres of 20 mM Hepes pH 7.5 overnight at 4 °C to remove GST molecules and Tris molecules as the latter bind to the amino groups of affi-gel. Packed affi-gel 10 (1 ml) was pipetted into a 15 ml Falcon tube, spun briefly to remove the excess ethanol and washed four times with 6 ml of PBS (Appendix A). A final spin (five min) was performed to pack the gel and the 5 mg of GST fusion protein was added and mixed on a windmill at 4 °C overnight.

The GST fusion protein/affi-gel conjugate was washed with two volumes of 1 M Hepes pH 7.5, then with two volumes of 50 mM citric acid, pH 2.5 and lastly with three washes of two volumes of PBS. Ethanolamine (1 M, pH 8.0) was added for one hour at room temperature to block free amino sites on the gel. Excess was washed away with PBS. Anti-serum (5 ml) was added to the tube and allowed to mix on a windmill at 4 °C overnight.

The slurry was then loaded into a 10 cm x 1 cm column (Biorad) and allowed to settle. The column was washed with 5 ml 20 mM sodium citrate until the absorbance at 280 nm was zero. Citric acid (50 mM pH 2.5) (6 ml) was added to elute the antibody and 0.5 ml fractions collected into microfuge tubes containing 0.35 ml 1 M Hepes pH 7.5. The yield was determined by reading the absorbance at 280 nm of the collected fractions. To clear the column, it was washed with elution buffer to remove all antibody, then washed with 20 mM sodium citrate pH 7.7 and four times with PBS. It was stored in PBS with 0.01 % sodium azide at 4 °C.

2.6.3. Using Fbl6 antibody 2194

The antibody (2194) was used at 1:2000 in western blots with ECL development and 1: 200 on immunohistochemistry. The affinity-purified antibody was used at 1:500 on western blots with ECL development and 1:10 on immunohistochemistry.

Immunohistochemistry was done on frozen Sections and teased fibres from mouse sciatic nerve perfused intracardially with 4 % paraformaldehyde in 0.1 M sodium phosphate buffer pH 7.5, and fixed in the same solution for one hour. The tissue was then washed in three changes of 0.1 M sodium phosphate buffer for one hour. Sciatic nerve to be frozen was then cryoprotected by taking it through sucrose solutions (5 %, 10 % for an hour each, then 25 % overnight at 4 °C). It was then embedded in Optimal Cutting Temperature (OCT) matrix by freezing in isopentane cooled to -70 °C with liquid nitrogen. It was stored at -70 °C and cut into 5 μm Sections onto TESPA coated slides (Section 2.2.7) using a cryostat. Immunohistochemistry was carried out as described in Section 2.2.7. Staining with the mouse antibody S100 (Affiniti 1259) (used at 1:400) requires pre-treatment of tissue in methanol for ten min at -20 °C.

Sciatic nerve taken for teasing fibres was post-fixed in the perfusant as described above for one hour and washed three times in 0.1 M sodium phosphate buffer over one hour. Then, it was transferred to a small dish with PBS (Appendix A) and the perineurium removed under a dissection microscope. Individual nerve fibres were teased out onto TESPA slides with acupuncture needles and allowed to dry. Prior to use for immunohistochemistry, the slides were immersed in acetone for ten min at -20 °C and allowed to dry at room temperature. Immunohistochemistry was then carried out as described in Section 2.2.7. Staining with the mouse antibody S100 (Affiniti 1259) (used at 1:400) again requires pre-treatment of tissue in methanol for ten min at -20°C. The 170pep1 (repeat region) periaxin antibody was used at 1:4000 as before.

2.7. BUILDING FLAG-TAGGED Fbl6 CONSTRUCTS

Stewart Gillespie had previously constructed the full-length Fbl6 clone in plasmids pCMV5 and pGEM11 (Promega).

2.7.1. N-terminal Flag-tagged Fbl6

The 5' end of Fbl6 was made by PCR so that it did not contain the start codon. PCR primers F9 containing a 5' *BamH*I site and reverse primer R10 (Table 6) were used to amplify a 1 kb fragment, missing the start codon, which was digested with *BamHI*/*Hind*III in buffer React2 (Gibco) and the 650 bp fragment subcloned into plasmid pCMV-Tag2b (Stratagene) at these sites. Then, the rest of Fbl6 (950 bp) was digested from the full-length Fbl6 in pGEM11 with *Hind*III/*Sal*I (React3), and subcloned into the same plasmid pCMV-Tag2b. This plasmid contains an in-frame N-terminal FLAG with an upstream start codon and Kozak sequence. The constructed plasmid was sequenced to check it.

2.7.2. C-terminal Flag-tagged Fbl6

The 3' end of Fbl6 was made by PCR so that it did not contain the stop codon. PCR primers F2 and reverse primer F8 (the latter containing a *Sal*I site in place of the stop codon) (Table 6), were used to amplify a 960 bp fragment, missing the stop codon, which was digested with *Hind*III/*Sal*I in buffer H and subcloned into plasmid pCMV-Tag4a (Stratagene) at these sites. Then the remaining part of Fbl6 was digested from its place in plasmid pGEM11 with *EcoR*I/*Hind*III, and subcloned into the same plasmid pCMV-Tag4a, which contains an in-frame C-terminal FLAG with a downstream stop codon. The constructed plasmid was sequenced to check it.

2.8. TRANSFECTION EXPERIMENTS

2.8.1. Making Cos-7 cells permanently transfected with periaxin

Cos-7 cells were grown in 10 % fetal calf serum (complement inactivated), 2 mM glutamine, 1 u/ml penicillin, 0.1 mg/ml streptomycin in Dulbecco's Eagle Medium (DMEM) (all from Sigma) (referred to as complete medium). Cos-7 cells were made to permanently express periaxin. A plasmid containing full-length L-periaxin and

geneticin (G418) resistance was transfected into low passage Cos-7 cells and the successful transfectants selected for with geneticin (0.4 mg/ml). These cells were then split and grown up so that clonal expansions were obtained.

2.8.2. Transfections

Cos-7 cells were transfected using Fugene 6 (Roche). The cells were split the day before transfection and plated out in 35 mm dishes (Iwaki) so that they were 80-90 % confluent on the day of transfection. Fugene 6 (3µl) was added to 100 µl of Optimen medium (Gibco) and this was added to 2 µg DNA to be transfected. This was left for fifteen min for the cationic complexes to form. Fresh medium (2 ml) was added to the Cos-7 cells and then the Fugene/DNA solution was added to each dish and gently mixed. The cells were harvested twenty-four hours later.

For lactacystin treatment, the cells were incubated in medium with 30 µM lactacystin sixteen hours after transfection for a further eight hours, and then harvested.

2.8.3. Western blotting with transfected cells

The transfected cells were washed in Hanks balanced salts solution (HBSS) (Sigma) and the scraped from the plate in the presence of HBSS and proteinase inhibitors (leupeptin 10 µg/ml, TLCK 0.5 mM, benzamidine 1 mM, antipain 10 µg/ml, PMSF 1 mM - all from Sigma). The cells were pelleted by centrifugation at 13000 rpm 4 °C for two min and taken up in 100 µl-200 µl 2 % SDS and boiled for ten min. The sample was spun down again for ten min at 13000 rpm and the supernatant removed and stored at -20 °C. An estimation of protein concentration in these samples was obtained using the BCA kit (Pierce).

2.8.4. Immunohistochemistry on transfected cells

Circular coverslips (13 mm) were washed for one minute in 1 M HCl and this rinsed away with MQ water. They were then stored in high quality 70 % ethanol made with MQ water. When ready to use, the coverslips were placed in culture dishes and the ethanol washed away with sterile MQ water. Poly-D-Lysine solution (0.1 mg/ml) (Sigma) was placed onto each coverslip and left for thirty min at room temperature.

The coverslips were then washed twice with sterile MQ water, and then the dishes used to grow and transfect cells.

For immunohistochemistry, the medium was aspirated away and the cells fixed in 4 % paraformaldehyde (Sigma) for twenty min. They were washed in PBS (Appendix A) three times and placed into a moist chamber. Blocking solution (5 % fish gelatin/0.1 % triton/ PBS) was added for twenty min. Primary antibodies (170pep1 periaxin antibody 1:1000 and FLAG antibody M2 Sigma 1:100) were added for one hour, diluted in the same blocking solution. Excess was washed away with 0.1 % triton in PBS. The fluorescently labelled secondary antibodies (goat anti-rabbit Cappell FITC 1:200 and goat anti-mouse Southern Biotech TRITC 1:200) were added for forty-five min. Excess was washed away with PBS. The coverslips were mounted on a slide with a drop of Vectashield (Vector Labs) and examined under a fluorescent microscope.

2.9. Appendix A

10 x PBS (Maniatis)

40 g NaCl

1 g KCl

7.2 g Na_2HPO4

1.2 g KH_2PO4

in 500 ml pH to 7.4

SOB medium

95 ml MQ

2 g Bactotryptone

0.5 g Bactoyeast extract

0.05g NaCl

Add 1 ml 250 mM KCl, pH to 7.0 and make up to 100 ml.

Autoclave.

Add 0.5 ml 2 M $MgCl_2$ just before use.

To convert to SOC medium:

To 10 ml SOB, add:

50 µl 2 M $MgCl_2$

200 µl 1 M glucose

FIGURE 12 – SCREENING FOR THE FIRST STEP FOR THE CONDITIONAL PERIAXIN MOUSE

a: Diagram of the targeted DNA as the first step in the formation of a conditional knock-out of *Periaxin*, with comparison to the wild-type. The clones growing in the presence of Neomycin are screened with the 5' and 3' probes and selected according to the correct size of fragment as indicated.

b: Diagram of the desired floxed situation, produced after transient expression of Cre recombinase, with comparison to the periaxin knock-out situation. The clones growing in the presence of gancyclovir are screened with the 5' and 3' probes and selected according to the correct size of fragment as indicated.

a:

First targeted sequence

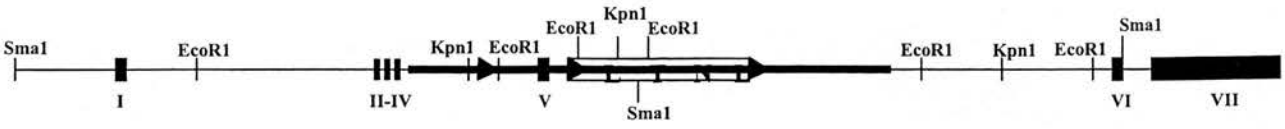

5' probe - 6 kb

3' probe - 9.2 kb

Wildtype

5' probe - 10.5kb

3' probe - 8.5kb

b:

Floxed Periaxin sequence

5' probe - 6kb

3' probe - 20kb

Periaxin knock-out sequence

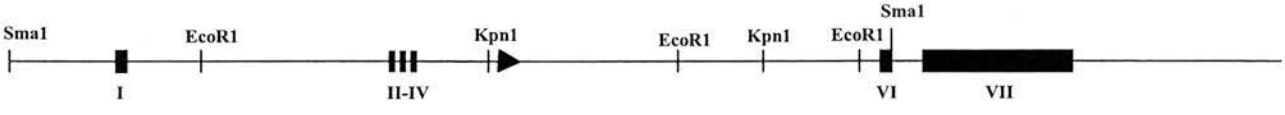

5' probe - 9kb

3' probe - 18.5kb

FIGURE 13 – MORPHOLOGICAL MEASUREMENTS

Photograph with overlay of Iplab colour enabling measurements of axon number, diameter and myelin thickness. The myelin is coloured in green, with preset levels of density recognised by the program. The perimeter of each fibre is encircled in red, and the axon given a number.

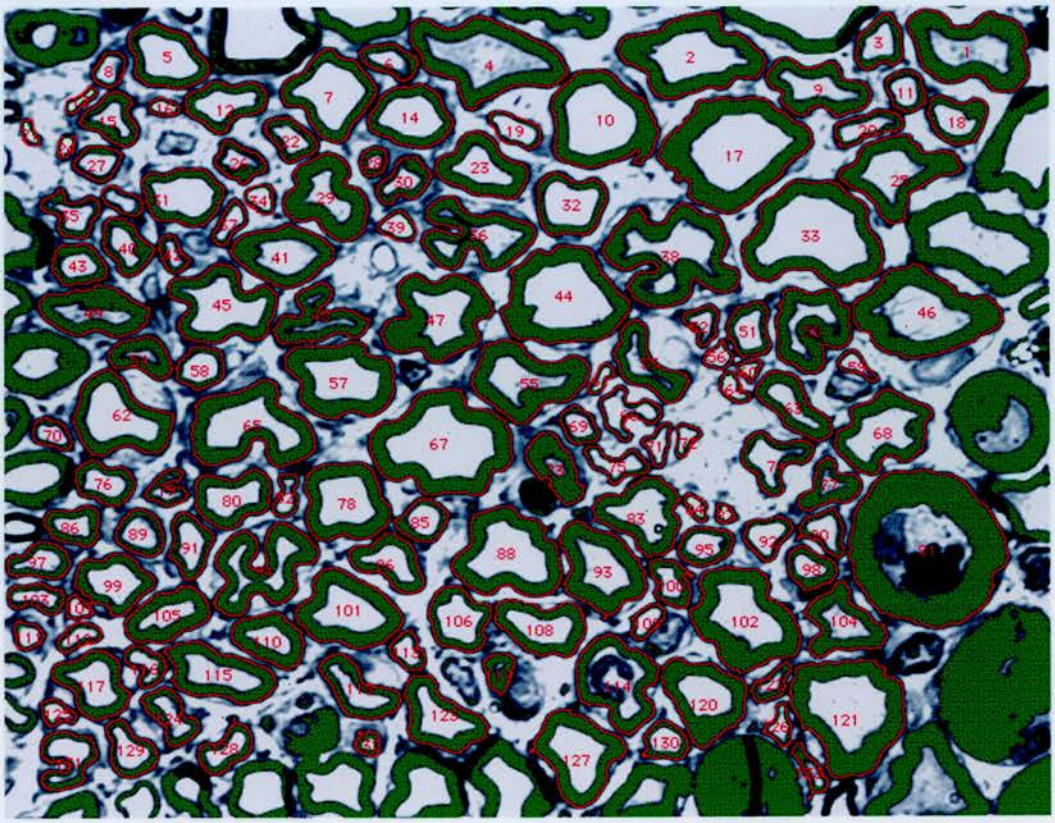

Table 2: Primers used in cloning and sequencing human *PERIAXIN*.

Primer	Sequence 5' to 3'	Orientation and position
Human 1	TCTGGGGGTCCCCGCTGAGC	Reverse exon 7
Human 5	CTGGGGCTCAGGCTCCTGTT	Reverse exon 4
Human11	GCTGACCTGGCCCCTGTTGA	Forward exon 7
Human 12	TCAGTGGGCCTCCAGACGC	Reverse exon 1
AW5	GTACAGGCACTCCTGCCAG	Reverse end of exon 7
AW6	GTCGAACCTCTGGAAGGGCTG	Reverse exon 7
AW7	TGGCTGCAGGAGCTCGTT	Forward exon 7
AW10	TCAACAGAGGGCACTCGG	Reverse exon 7
AW12	AGCTGCATTCCACTGACG	Reverse exon 7
AW13	AGTTCAAGGTGATCGTGC	Forward exon 7
AW15	CGTCAGTGGAATGCAGCT	Forward exon 7
LMD1	AACTCTGGAGGTGTCTGGAGG	Forward exon 2
LMD2	AGGTAGCTGGAACTGACCCTCA	Forward exon 2
LMD19	TCAGCGCTGCGGCTCCTGGCCTCCA T	Reverse exon 4
LMD30	CGGTGAGTCCTCTCGCAGCTC	Reverse exon 5
LMD48	CTTTGGGTGACATCACAGCA	Forward 5' to exon 1
CSG27	CGATAATCTCCACCAACT	Reverse exon 5
CSG36	GAGCTGCGAGAGGACTCACCG	Forward exon 5

Table 3: Peptide sequences used to raise the periaxin antibodies

Antibody	peptide sequence	Human equivalent sequence	Detection of human Periaxin
N-terminal	EARSRSAEELRRAE (rat and mouse identical)	EARSRSAEELRRAE	Yes
Repeat (Anti-170pep1)	VPEMKLPKVPEAQRKS (rat)	**A**PE**V**KLP**RA**PE**V**Q**L**K**A**	Yes
C-terminal (rabbit)	KARSGSKDREEGGFRVRLPS (rat)	KARSGS**G**D**Q**EEGG**L**RVRVRLPS	No
C-terminal (sheep) (PeriC2)	SGSKDREEGGFRVRLPSVGFSETA (rat)	SGS**G**D**Q**EEGG**L**RVRLPSVGFSET**G**	No
S-periaxin	AKLVRVLSPVPVQDSPSDRVAAA (mouse)	AKLVRVLSP**A**P**A**L**D** **C**PSD**P**V**S**A**P**	No

Differences in the human peptide sequence compared to the rodent sequence are shown in bold.

Table 4: Dilutions and source of antibodies

Antibody	Dilution	Company
N-terminal periaxin (rabbit)	1 in 4000	In house
170pep1 (Repeat) periaxin (rabbit)	1 in 4000	In house
Human C-terminal periaxin (rabbit)	1 in 1000 1 in 500 (affinity purified)	In house
Neurofilament (200kD)	1 in 2000	Sigma
Myelin basic protein (clone 12) (mouse)	1in 100	Groome
FITC-conjugated goat anti-rabbit	1 in 200	Cappell
TRITC-conjugated goat anti-mouse IgG1	1 in 100	Southern Biotechnology

Table 5: Primers used in construction of conditional construct

Primer	Sequence 5' to 3'	Orientation and position
LMD2	AAGTAGCTGGAACTGACCCTCA	Forward exon 2
MP1	TCCTTCTGCTGCAGGACCAC	Reverse exon 4
LMD13	GGAGAGTGAAGAGACAACCA	Forward intron 5
MP5	ACAGTGCGCTTCAAGCAGA	Reverse exon 6

Table 6: Fbl6 primers used to build Flag-tagged Fbl6 constructs

Primer	Sequence 5' to 3'	Orientation
F9	TAGAATTCGGATCCGCTCCTGTGGCCC CTGGGCGAGT	Forward, with *BamH*I and *EcoR*I sites in place of start codon
R10	GCTCACAAAGCTGCAGGTGGA	Reverse
F2	GAGAAGAAGCTCCTTGCTT	Forward
F8	GATCATGTCGACTGTGGACTCTCTGGA AGAG	Reverse, with *Sal*I site in place of stop codon

3. RESULTS - THE HUMAN *PERIAXIN* GENE.

3.1. Cloning the human *PERIAXIN* gene

We wished to determine the sequence of the human *PERIAXIN* gene to enable us to screen patients with undefined CMT disease for mutations in this gene. We initially relied on the supposition that the human *PERIAXIN* sequence was similar to that of rat and mouse and used primers and probes designed from rodent sequence to identify human sequence. However, there were known to be some differences, as the human Periaxin protein ran with a lower mobility than the mouse version in SDS gels (Gillespie, unpublished observations).

The methods used to obtain the sequence are described in Section 2.1.

RT-PCR was used to obtain most of the sequence of exons II, III, IV and V. PCR of genomic DNA using rat specific *Periaxin* primers revealed the sequence of exon VI and a small amount of exon VII. The sequence of exons II, III and IV, and intervening introns 2 and 3 was determined by PCR directly from the PAC68 using rat-specific primers (Table 2)

The PAC clone 68 was digested with the frequently cutting enzymes *EcoR*I and *Hind*III (Figure 14a), and the DNA fragments hybridising to a full-length rat periaxin cDNA probe by Southern blot were subcloned into pGEM7. In the digests using *EcoR*I, two bands hybridised to the periaxin probe. The bands were approximately 14 kb and 7 kb in size. Again, on the *Hind*III digest there were two bands of approximately 15 kb and 8 kb (Figure 14b). These bands were cut from a gel, purified, and ligated into pGEM7 plasmid cut with the corresponding enzyme – *EcoR*I or *Hind*III. Hence four plasmids containing four different inserts were generated. To ensure that the correct fragments had been subcloned, these plasmids were digested to release the insert and probed again with the rat full-length periaxin cDNA on a Southern blot (Figure 14c and d). The ends of the inserts in these plasmids were sequenced using vector primers M13F and M13R. This revealed that the sequence generated from the M13R primer in both plasmids generated from the *Hind*III digested fragments were identical to each other and to the PAC vector

sequence in the databank 1kb from the PAC vector insert site. The other end of each insert was different, and had some sequence similarity to human intronic sequence in the data bank. For the plasmids generated by the *EcoR*I digest, the sequences generated from the M13F vector primer were identical to each other but had no significant similarity to databank sequence, and the other ends were different. This suggested that partial digests of the PAC had occurred and that the smaller fragments were identical to part of the larger ones (Figure 15a).

At this point, the human genome project groups who were working on chromosome 19 entered a working draft of sequence on the database (Genbank accession no. AC010271). This corresponded almost exactly to the sequence I had already obtained and showed 80-90% sequence similarity to rat and mouse *Periaxin* sequence across exons. This allowed me to characterise my plasmids more fully.

The unique sequence at the end of the smaller insert (8kb) of the plasmids generated by the *Hind*III digest is identical to that in intron 4, and the orientation of this sequence meant that it contains most of intron 4, all of exon V and 4 kb of intron 5. As the other ends of the subcloned *Hind*III fragments are identical, and the bigger fragment is 15 kb, this subclone contains all the sequence upstream of this point in intron 5, ending upstream of exon I. The 5' sequence of the larger *Hind*III subclone corresponds to sequence more than 1 kb upstream of exon I.

The identical ends of the subcloned inserts generated by an *EcoR*1 digest lie in intron 5. Again, the smaller subclone has its 5' end in intron 4, and the larger subclone has its 5' end upstream of exon I (Figure 15b).

It is surprising that none of the subcloned fragments of *PERIAXIN* contain exon VII, as 90% of the whole length rat periaxin cDNA probe used consists of exon VII sequence. In fact, the smaller subclones were detected with the probe binding to only 157 bases, the size of exon V. However, this does explain the failure of trials of PCR with primers corresponding to rat exon VII sequence using the PAC as template, and with southern blots using exon VII rat probes. These results were previously put down to probable dissimilarity between human and rat exon VII sequence.

Exon I, and the remaining parts of exon V, were sequenced from these subclones directly using human specific primers. New primers were made corresponding to the working draft sequence of exon VII in the databank to allow PCR of this sequence from human genomic DNA. We wished to ensure that the human exonic sequence of *PERIAXIN* was correct before looking for possible mutations. Human expressed sequence tags (ESTs) from the database were found that matched part of the sequence of exon V and also exon VII (AA984421, AW590908, AI637869, AW125547 and AW337783). The subcloned fragments and ESTs are shown aligned to the *PERIAXIN* sequence in diagrammatic form in Figure 16.

The DNA sequence of the human *PERIAXIN* gene differs from that of rat and mouse. Exonic structure is very similar, with the major differences occurring in exon VII. Exon VII in humans is larger than in rodents, encoding for more of the repeat units of the protein: rat L-periaxin has 45 repeats, mouse 47 repeats and human 55 repeats. Comparison of the intronic size shows more differences. These results are summarised in Table 7 and Figure 17. The larger size of exon VII accounts for the larger size of the human L-periaxin protein, which was seen formerly by western blot. The human L-periaxin protein is a 1462 amino acid protein, 71 amino acids longer than the mouse protein. Human and mouse L-periaxin proteins share 77.6% sequence similarity.

A comparison of the amino acid sequence of the L-periaxin isoform of human, rat and mouse is shown in Figure 18.

The human *PERIAXIN* DNA sequence also encodes for the alternative isoform S-periaxin. Similarly to rodent *Periaxin* sequence, there are suboptimal 5' and 3' splice sites in the final intron causing possible retention of intron 6. This introduces a stop codon preceded by sequence encoding a unique 20 amino acid C-terminus. Comparison of the mouse and rat S-periaxin isoforms shows just two amino acid differences at the C-terminus. However, the human isoform is more dissimilar (Figure 19).

3.2. Mutations in *PERIAXIN* causing human CMT disease

We formed a collaboration with Dr. LeGuern and his group at the Hôpital de la Salpetrière in Paris. They localised the *PERIAXIN* gene to the long arm of human chromosome 19 by fluorescent in situ hybridisation (FISH), confirming our prediction based on mouse / human chromosome synteny (Gillespie et al., 1997).

In June, 2000, Delague et al. published a paper describing a large consanguineous Lebanese family with autosomal recessive demyelinating CMT disease (CMT4F) showing linkage to chromosome 19q13.1-13.3 (Delague et al., 2000). Clinically, the patients had delay in motor development, with an early ataxic gait, but obvious weakness and sensory changes in the lower limbs by age 10 years, and in the upper limbs by age 15 years. Progression of the disease was slow, and only one patient out of the thirteen investigated was unable to walk. All patients presented with a demyelinating neuropathy with undetectable sensory or motor nerve velocities on neurophysiology. Of particular importance, sensory loss was severe. Pathology of a sural nerve biopsy done in one patient revealed a severe depletion of myelinated fibres, and Schwann cell proliferation with onion bulbs surrounding the remaining myelinated fibres. This suggested axonal loss secondary to chronic demyelination and remyelination. The group screened the gene for myelin associated glycoprotein (MAG) for mutations in two patients of this family as this gene is at the locus 19q13.1. However, sequencing of the entire gene in these patients revealed no mutations. Further linkage analysis placed the MAG gene outwith the homozygous candidate region for the gene responsible for the disease.

We felt that it was a matter of urgency to screen this family for mutations in the *PERIAXIN* gene.

3.2.1. R196X mutation

Our Paris collaborators designed primers from our human *PERIAXIN* sequence to specifically amplify and sequence the four coding exons of *PERIAXIN* (IV-VII) and their flanking splice sites and the intron 6 in patients from the Lebanese CMT family. Fourteen members (three parents, three non-affected members and eight affected

patients) of this Shiite Muslim family were investigated. They identified a homozygous C-T transition at position 860 which leads to a premature stop codon at the beginning of exon VII (R196X) (Figure 20a). This nonsense mutation truncates the C-terminus of L-periaxin by 1266 amino acids and leads to the absence of the large repeat-rich domain and the C-terminal acidic domain. It also abolishes a recognition site for the restriction enzyme *Rsa*I, which was used to confirm the segregation of the mutation with the disease (Figure 20b). *Rsa*I restriction analysis of one hundred chromosomes from Lebanese controls confirmed that the R196X mutation was specific to the affected patients.

The genetic evidence for a mutation in the *PERIAXIN* gene is supported by comparative immunocytochemical analyses of control and patient sural nerve biopsies. Although the number of myelinated fibres was severely reduced in the patient nerve, it was possible to detect a restricted number of small diameter fibres that were positive for the myelin constituent myelin basic protein (MBP) (Figure 21a). MBP was also detected in the myelin sheaths of fibres in control nerve (Figure 21c). However, Periaxin was undetectable by immunohistochemistry in the affected nerve using an antibody that recognises the N-terminus of L-periaxin (Figure 21b), whereas it was readily demonstrable in the control sample (Figure 21d). In support of the view that the deficit was unique to Periaxin, P0, a characteristic component of PNS myelin co-localised with MBP in the myelin sheaths of both control and affected nerves.

The dearth of myelinated axons in the CMT4F patient's sural nerve was confirmed by light microscopy of plastic sections (Figure 22a). On electron microscopy, a striking feature of the CMT4F nerve was the incidence of both 'onion bulb' structures (Figure 22b) and hypermyelinated outfoldings (Figure 22c). The former represent supernumerary Schwann cells associated with abortive attempts to remyelinate demyelinating nerves. The similarities of the pathology to that of the periaxin-null mouse are striking and support the case that the mouse mutant is a convincing model for the human disease (Figure 22d). This data was reported in a paper in Human Molecular Genetics in 2001 (Guilbot et al., 2001).

In the same month three more families with mutations in *PERIAXIN* and CMT4F disease/ Dejerine-Sottas disease were described by Boerkoel et al. (Boerkoel et al., 2001b).

3.2.2. C715X mutation

Another collaboration was made with the Antwerp group interested in CMT disease led by Vincent Timmerman, and with James Lupski's group in the USA. By DNA sequencing, Lupski's group screened each coding exon of *PERIAXIN* for mutations in 29 peripheral neuropathy patients who had tested negative for mutations involving *PMP22*, *MPZ*, *GJB1*, and *EGR2*. Two siblings were found, born to consanguineous parents, who were homozygous for the mutation 2145T>A that by conceptual translation causes a nonsense stop codon at amino acid 715 that normally encodes a cysteine (C715X). The unaffected parents, sister and brothers either did not carry the mutation or were heterozygous carriers (Figure 23). They did not observe this mutation in 180 control chromosomes. In this family, another sister had died at the age of 48 years due to a cardiomyopathy, but the alive, affected sister and brother were available for study. Both had gait problems from early childhood and developed scoliosis, and the sister attended a school for children with a motor handicap. They were examined at age 50 and 54 respectively, and both showed weak foot and hand muscles, but severely decreased sensitivity for all sensory modalities to the level of the knees and elbows. Thus, the sensory impairment was much worse than the motor deficit. There was no palpable nerve hypertrophy. Electrophysiological studies of the median and ulnar nerves of the sister showed slow motor nerve conduction velocities (motor NCV, 3 m/sec), reduced compound muscle action potentials (CMAP, median: 1.1 mV, ulnar: 0.45 mV, control: > 6mV), and undetectable median sensory nerve action potentials. Despite early onset of disease, these siblings had a relatively slow disease progression and adult motor impairment typical for classical demyelinating CMT neuropathy. We were fortunate to obtain a frozen sural nerve biopsy specimen from the sister.

Immunofluorescence analysis of a normal (frozen) human sural nerve biopsy showed positive double labelling for myelin basic protein (MBP) and for Periaxin labelled with the anti-N-terminal, the anti-170pep1 (repeat region) and the C-terminal L-

periaxin antibodies (Figure 24J). In this patient, there was also labelling with the N-terminal and 170pep1 antibodies, but not with the anti-C-terminal antibody even though there is MBP-positive labelling (Figure 24G-I). This result demonstrates that a truncated L-periaxin is made and indicates that the carboxyl terminal domain of the L-periaxin protein has an important function. Furthermore, these data suggest that interaction with DRP2 (approximately at amino acid positions 118 to 196) is not sufficient for L-periaxin's function.

Light microscopy, carried out in Antwerp, revealed a severe loss of myelinated axons of all diameters and increased connective tissue (Figure 25). Although some remaining myelinated fibres were normal, many showed tomacula formation or small onion bulb formations. On electron microscopy, the tomacula consisted of concentric or eccentric thickenings of the myelin sheath with focally folded myelin surrounding a constricted axon. Multiple paranodal abnormalities were identified including a reduced number of myelin loops and an absence of septate-like junctions between the paranodal myelin and the axon (Figure 26).

An unrelated patient was also discovered homozygous for 247ΔC that results in frameshift mutation R82fsX96 in Periaxin, so affecting both L- and S- periaxin. Unfortunately no nerve biopsy was available for immunohistochemistry. She also had marked sensory involvement but otherwise had a disease course consistent with congenital hypomyelinating disease (CHD). Light microscopy revealed a severe loss of thick myelin sheaths, numerous demyelinated or thinly remyelinated fibres, onion bulbs and occasional tomacula. The details on these two families are published in Annals of Neurology, 2002 (Takashima et al., 2002).

3.2.3. Turkish Mutation R1070X

We entered a further collaboration with Dr. Battaglou's group in Istanbul. This group had discovered a Turkish family with CMT disease caused by the homozygous Periaxin mutation R1070X. We were able to analyse a sural nerve biopsy, which again showed staining with the N-terminal and 170pep1 (repeat region) periaxin antibodies, but no immunoreactivity with the C-terminal antibody (Figure 27). Thus, in these patients, truncated L-periaxin protein is made, missing the C-terminal part.

This is the most 3' site of *PERIAXIN* mutations yet described. The mutation truncates the protein prior to the acidic domain preventing binding to the F-box protein Fbl6 which targets periaxin to the proteasome (Vasiliou in preparation).

3.3. Discussion

We have now identified the fourth gene involved in autosomal recessive CMT disease. There are eight different mutations described so far, in seven different families, as one patient (Boerkoel et al., 2001b) was heterozygous for two different *PERIAXIN* mutations (Figure 28 and Figure 29). The variety of mutations, and the different ethnic groups of the families indicates that this is not a disease with a common founder, such as in HMSN-Lom (Kalaydjieva et al., 2000), but that separate mutations have arisen independently. Obviously, autosomal recessive disease is more evident in families where consanguineous marriages are common, however, sporadic cases of ARCMT disease are becoming more recognised, and *PERIAXIN* mutations are worth considering in such cases.

We have shown that, in three of the cases, the L-periaxin protein is either absent or truncated, concurring with the determined genetic defect. The R196X mutation leads to a truncation at the end of the basic domain of L-periaxin, and this truncated protein is not seen, either due to nonsense mediated RNA decay (Lykke-Andersen, 2001) or instability of the truncated protein. In the other two patients (C715X and R1070X), truncated forms of L-periaxin are generated, but this is not sufficient to prevent demyelination. L-periaxin is an integral constituent of a dystroglycan-dystrophin-related protein 2 (DRP2) complex and possibly other plasma membrane complexes, where it presumably participates in interacting with the basal lamina surrounding the Schwann cell (Sherman et al., 2001). The peripheral demyelinating neuropathy seen in periaxin-null mice (Gillespie et al., 2000) and our patients emphasises the importance of such complexes for stabilising the axon-Schwann cell unit. However, although the interaction between periaxin and DRP2 may be essential for complex formation, the disruption of this interaction is not required to cause demyelinating CMT disease. The patients C715X and R1070X are shown by immunohistochemical studies on nerve biopsy to make stable yet truncated L-periaxin protein containing the DRP2 binding domain. Thus, these truncated proteins

can presumably still interact with DRP2, and this is not sufficient for L-periaxin's function. The C-terminal acidic domain of L-periaxin binds to the F-box protein Fbl6 which targets the protein for ubiquitin-mediated proteolysis (Vasiliou in preparation). The absence of this domain may cause disruption through a loss-of-function but also the truncated protein may have enhanced stability and gain-of-function effects that disrupt interactions of the Schwann cell with the basal lamina.

In each of these three patients (R196X, C715X, and R1070X), it is possible that S-periaxin is still expressed, since the mutations are all downstream of the retained intron that encodes the C-terminus of this shorter isoform. However, the absence of full-length L-periaxin alone appears to be sufficient to lead to demyelination. It is unfortunate that no biopsy material was available from the patient R82fsX96, as this is the first mutation to be described that would disrupt both L- and S-periaxin (Takashima et al., 2002). However, clinically, this patient was indistinguishable from the other patients with *PERIAXIN* mutations. S- and L- periaxin have distinct locations and are likely to have distinct functions. In adult mice, L-periaxin is concentrated at the abaxonal Schwann cell membrane whereas S-periaxin is distributed throughout the cytoplasm (Dytrych et al., 1998). We may gain further understanding of the role of L- and S-periaxin in CMT4F by studying the involvement of these isoforms in the assembly and stabilisation of mouse peripheral nervous system myelin.

There are marked similarities in the histopathology of peripheral nerve from these patients compared to those of the periaxin-null mice (Gillespie et al., 2000). In the patients, there were supernumerary Schwann cells surrounding thinly myelinated or naked axons forming 'onion-bulb' structures, and hypermyelinated regions of the nerve in which the myelin was extensively folded. The accumulation of this excess of myelin is a likely forerunner of massive demyelination. There was also detachment of terminal paranodal myelin loops from the axon with loss of septate-like junctions (Takashima et al., 2002). The formation of axoglial junctions at the paranode has been shown to require at least three proteins: contactin and Caspr on the axonal surface and an isoform of neurofascin, NF155, on the glial surface, which together form an adhesion complex (Charles et al., 2002). These disrupted axoglial junctions

may suggest that L-periaxin is necessary for the formation or maintenance of the adhesion complex.

As with other mutations in CMT genes, there is a spectrum of clinical phenotypes associated with *PERIAXIN* mutations, including CMT4F and Dejerine-Sottas disease. Again, the phenotype is not clearly related to the position of the mutation, though correlations are difficult due to the scarcity of patients with *PERIAXIN* mutations as yet. However, in contrast to mutation of other CMT genes, mutation of *PERIAXIN* causes a prominent sensory neuropathy.

An unusual and early feature of the periaxin-null mouse phenotype is the presence of neuropathic pain behaviour characterised by mechanical allodynia and thermal hyperalgesia. In the mouse mutant, this neuropathic pain behaviour can be abrogated by intrathecal injection of an NMDA antagonist, suggesting that there have been plastic changes in the spinal processing of sensory input from the extremities (Gillespie et al., 2000). Thus, drugs licensed for neuropathic pain may help CMT4F patients, and the periaxin-null mouse may be a useful model in which to study neuropathic pain generated from demyelination. These similarities support the view that the mouse model will lead to a better understanding of human disease.

FIGURE 14 – SOUTHERN BLOTS OF DIGESTED PAC68

a: PAC68 digested with *EcoRI* (1-4) and *HindIII* (5-8)

b: Southern blot of digested PAC68, probed with the full-length rat periaxin cDNA probe. Lane 1- *EcoRI* digest. Lane 2 - *XhoI* digest. Lane 3 - *HindIII* digest.

c: Southern blot of subclones from *HindIII* digest probed with full-length rat periaxin cDNA. Lane 1 - PAC68. Lanes 2-11 - subclones of *HindIII* smaller fragment (positive in lanes 3, 5, 6, 7, 9, 11. Sample 8 is partially digested). Lanes 12 and 13 - subclones of *HindIII* larger fragment (both positive).

d: Southern blot of subclones from *EcoRI* digest probed with full-length rat periaxin cDNA. Lane 1 - PAC68. Lanes 2-11 - subclones of *EcoRI* smaller fragment (positive in lanes 3 and 5. Extra bands represent uncut plasmid). Lanes 12 -15 - subclones of *EcoRI* larger fragment (positive in lane 12).

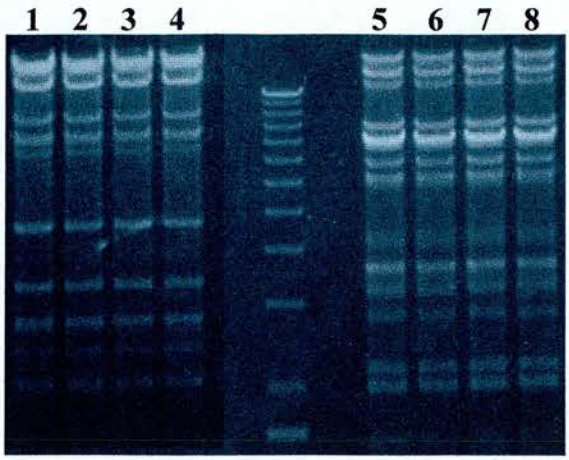

a

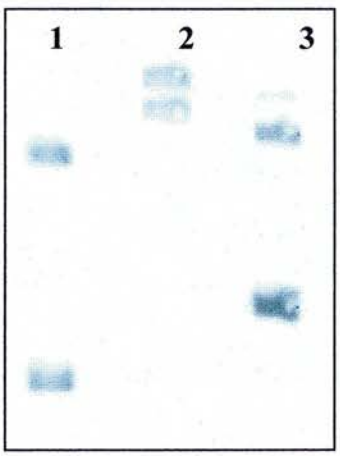

b

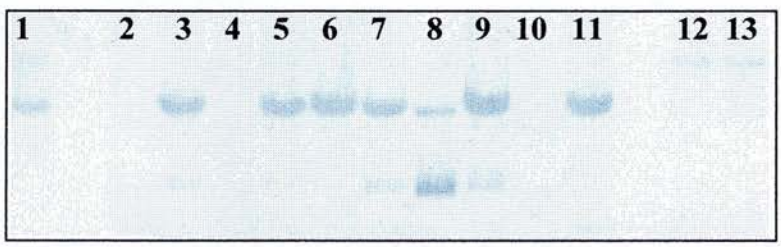

c

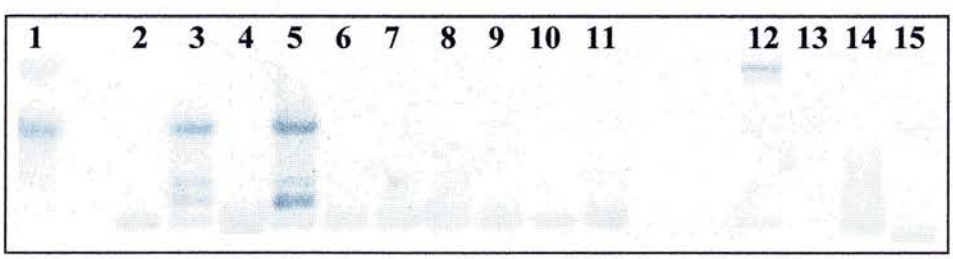

d

FIGURE 15 – PLASMIDS GENERATED BY DIGESTION OF PAC68

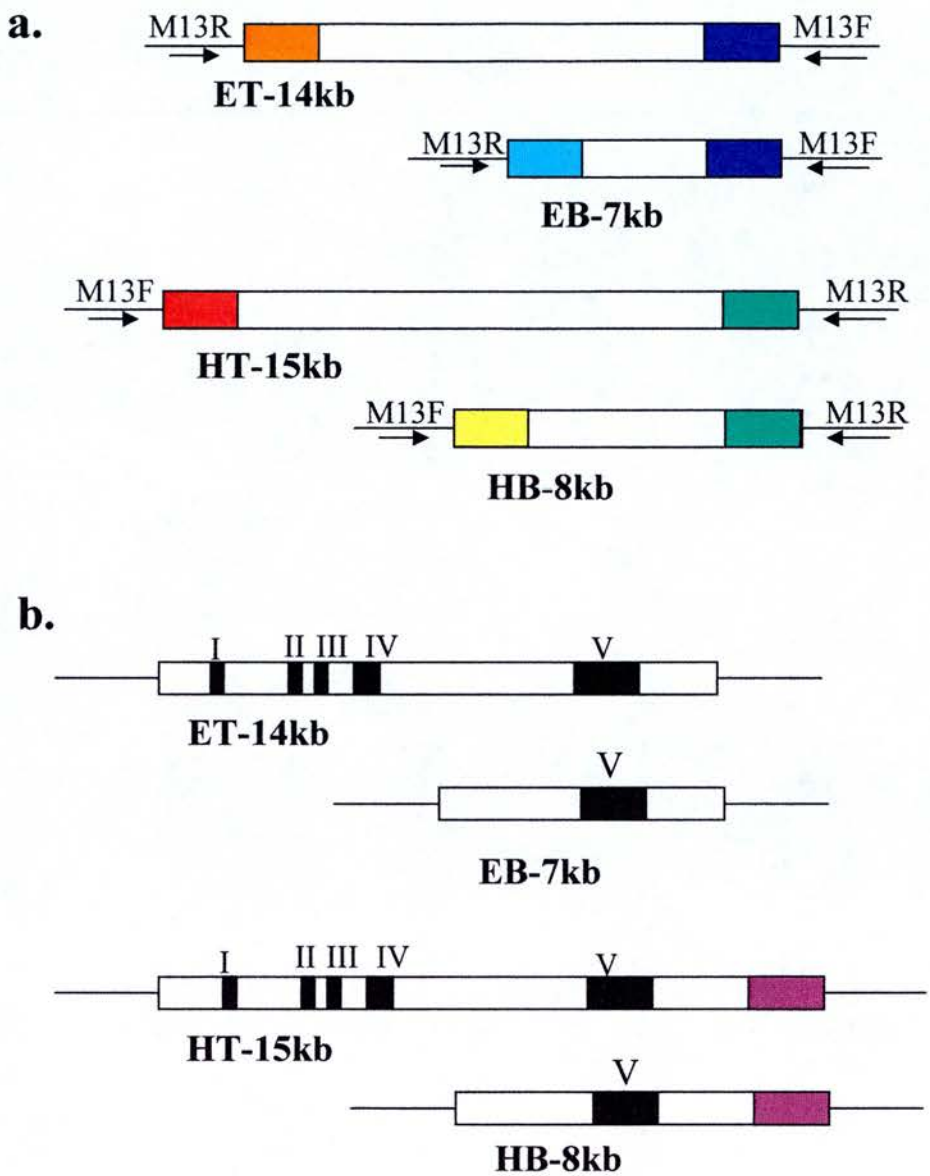

a: Plasmids generated by digestion of PAC68 with *EcoRI* (ET and EB) and *HindIII* (HT and HB) and subcloned into pGEM7. Coloured boxes indicate similarities or differences of insert ends by sequencing.

b: Plasmids as in (a) with exons of human *PERIAXIN* marked in roman numerals as determined by comparison to the Genbank sequence.

FIGURE 16 – DNA FRAGMENTS USED TO OBTAIN HUMAN *PERIAXIN* SEQUENCE

Diagram of the fragments of sequence used to obtain the human *PERIAXIN* gene sequence. EST sequences are labelled. HB and HT sequences and EB and ET sequences indicate sequence obtained from PAC68 through HindIII and EcoRI digests respectively.

Genebank Periaxin
genomic sequence

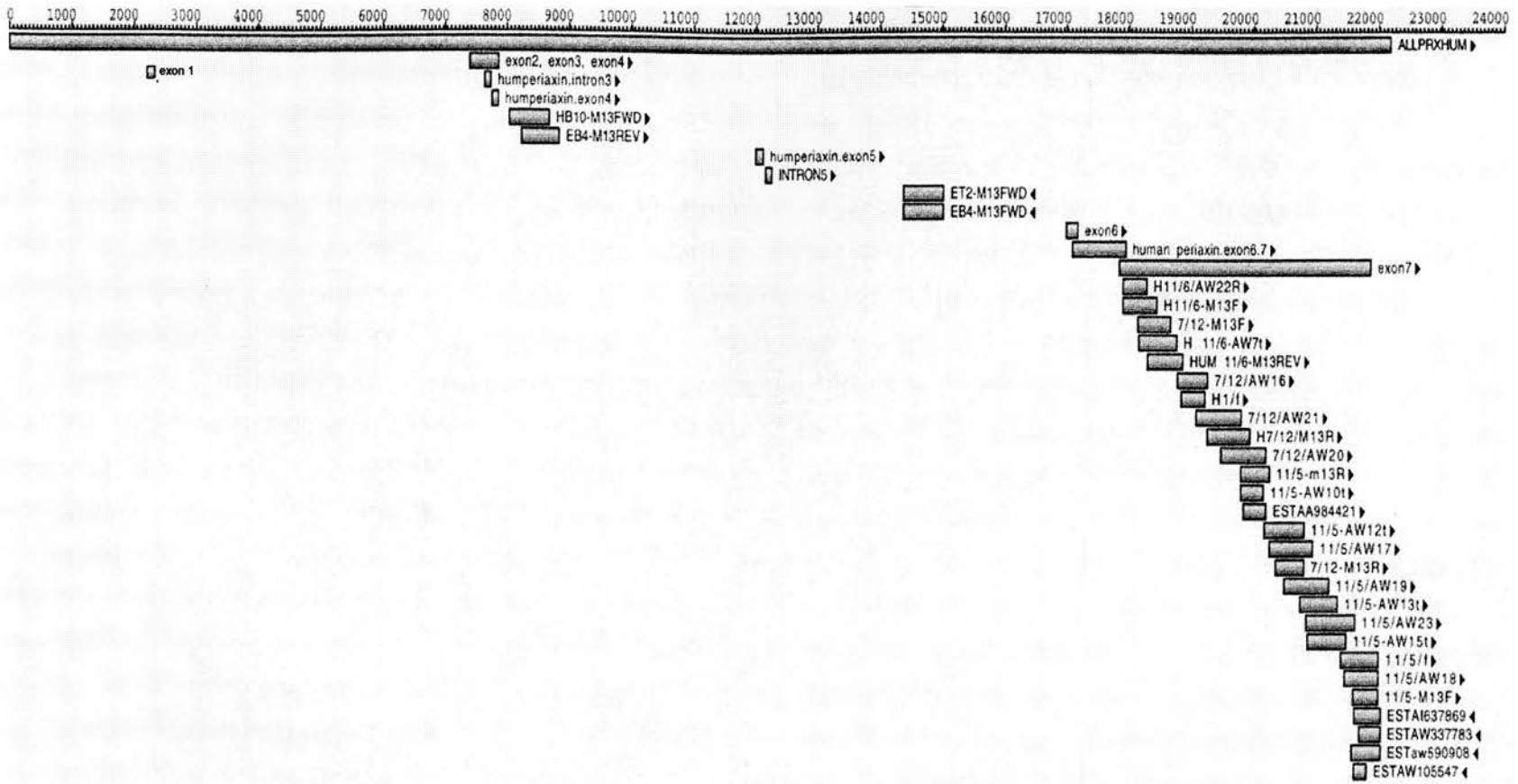

FIGURE 17 - STRUCTURE OF THE HUMAN *PERIAXIN* GENE

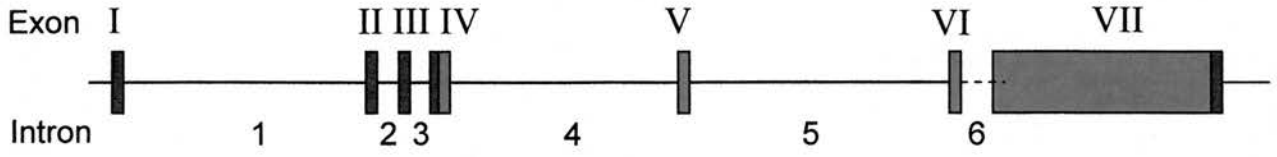

Exon no. (size in bp)	Intron no. (size in bp)
I (32)	1 (4954)
II (44)	2 (83)
III (99)	3 (127)
IV (126)	4 (4090)
V (157)	5 (4816)
VI (197)	6 (649)
VII (4005)	

Structure of the human *PERIAXIN* gene with exon and intron sizes.

FIGURE 18 - COMPARISON OF HUMAN, RAT AND MOUSE L-PERIAXIN AMINO ACID SEQUENCE.

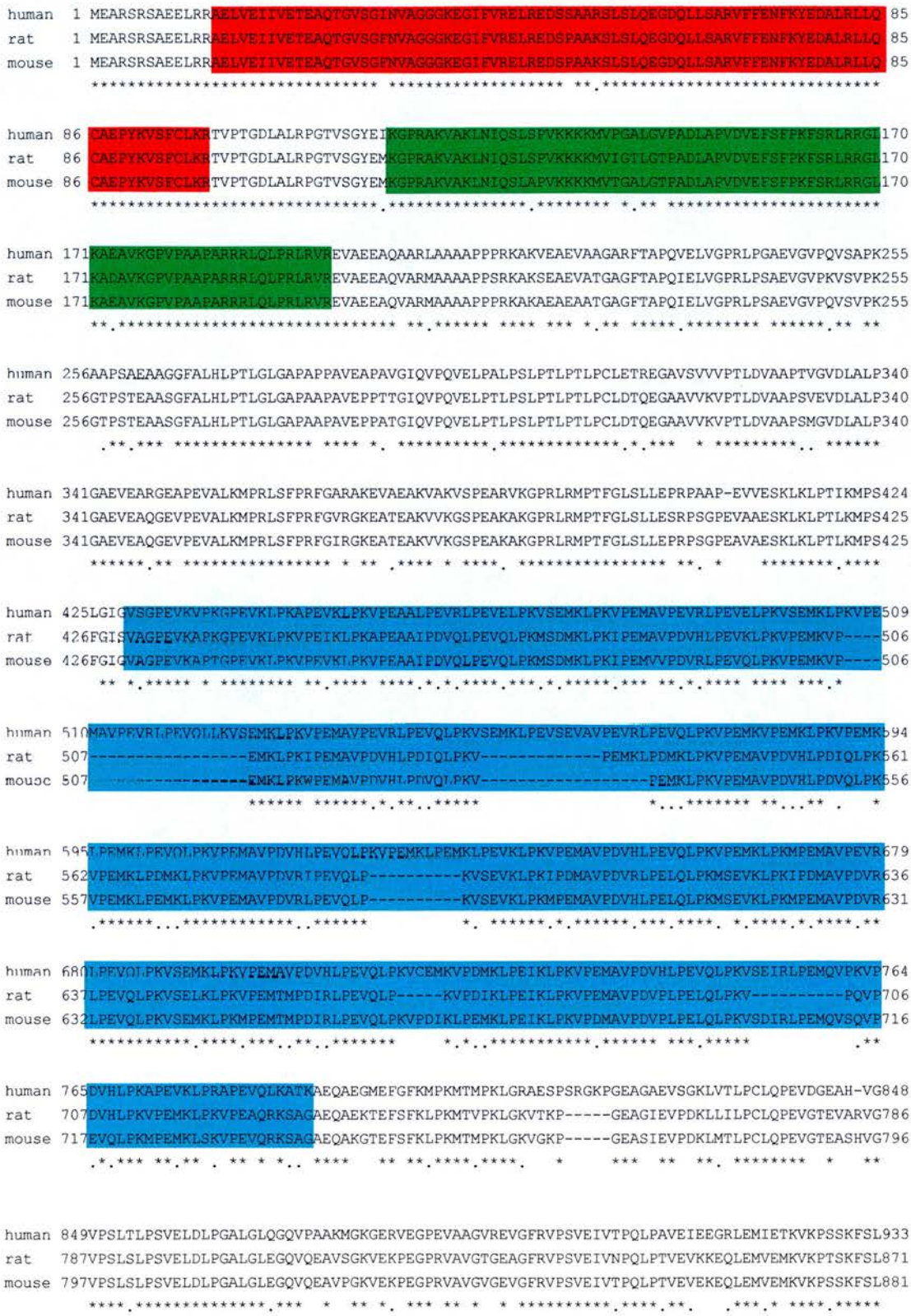

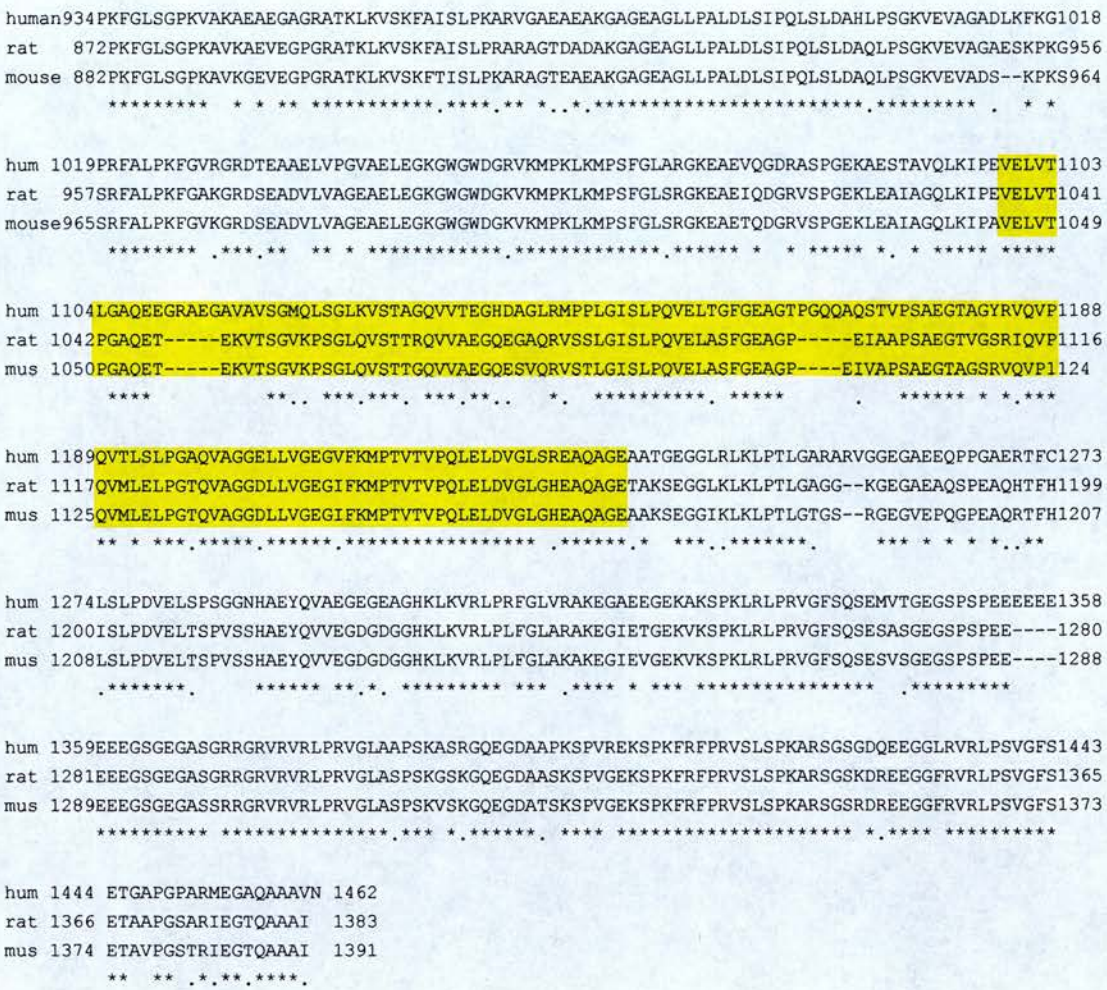

PDZ domain(red), basic domain (green), repeat domain (blue) and acidic domain (yellow)

FIGURE 19 - COMPARISON OF HUMAN, RAT AND MOUSE S-PERIAXIN AMINO ACID SEQUENCE.

This alternative isoform is generated by retention of intron 6 that codes for 21 or 22 amino acids (green) forming a new C-terminus, before reaching an in-frame stop codon. PDZ domain (red).

FIGURE 20 –R196X MUTATION

a: ABI tracing from the sequence of the proband showing a C to T transition resulting in a premature stop codon. This disrupts an *RsaI* restriction site.

b: Family tree of the Lebanese family showing that digestion of a PCR product containing the sequence of interest with *RsaI* produces two bands of 380bp and 320bp in normal *PERIAXIN* sequence and a 700bp band in *PERIAXIN* sequence containing this mutation. Inheritance of the homozygous absence of this *RsaI* site co-segregates exactly with the disease (black circles or squares).

(Published in Guilbot et al., 2001)

a:

Control

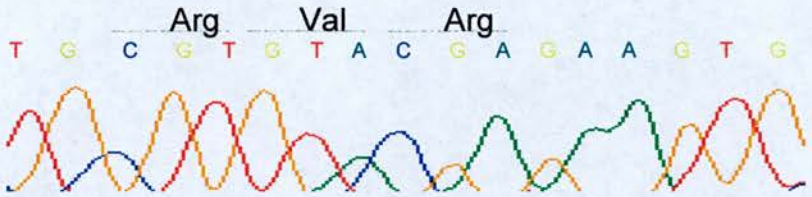

Proband

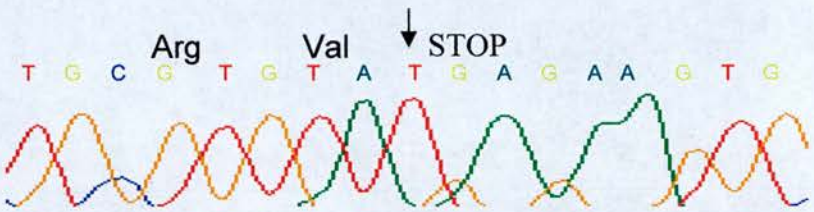

b:

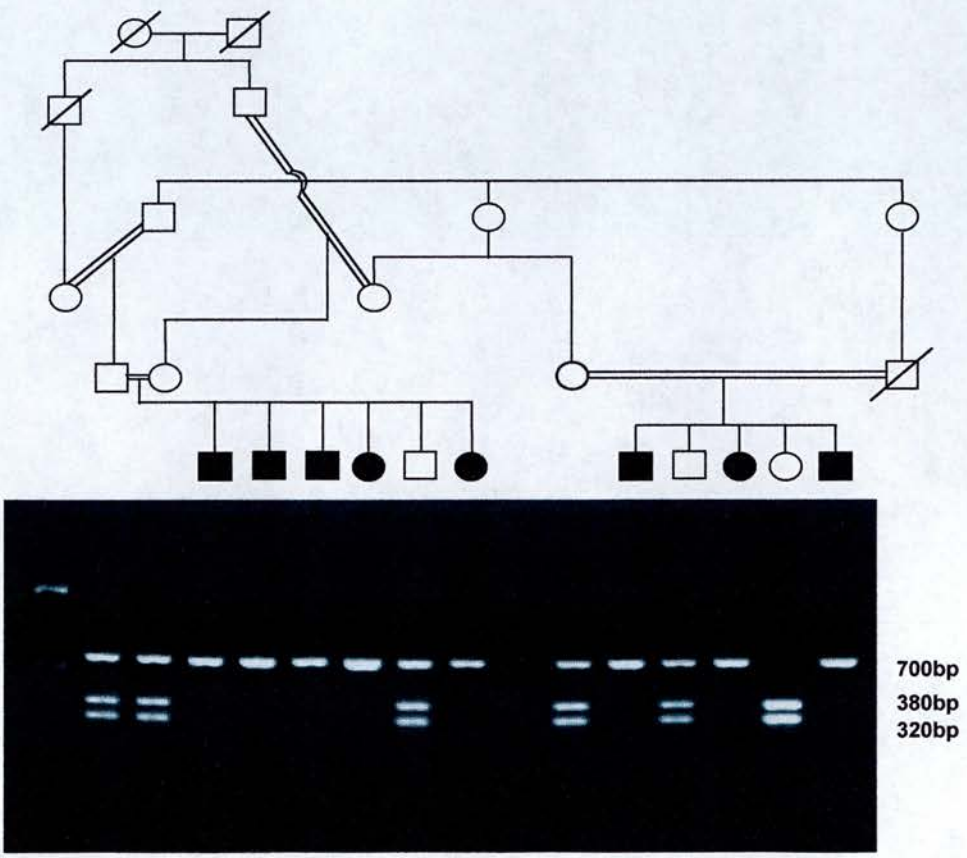

FIGURE 21 - IMMUNOFLUORESCENCE ANALYSIS OF SURAL NERVE BIOPSY FROM PATIENT R196X.

a, b: Nerve fibres from patient R196X show staining with MBP (a) but no staining with the N-terminal PRX antibody (b). The myelinated fibres are much smaller and sparser than in the control.

c, d: Nerve fibres from control show staining with MBP (c) and N-terminal PRX antibody (d).

(Confocal pictures of these slides were taken by Diane Sherman)

(Published in Guilbot et al., 2001)

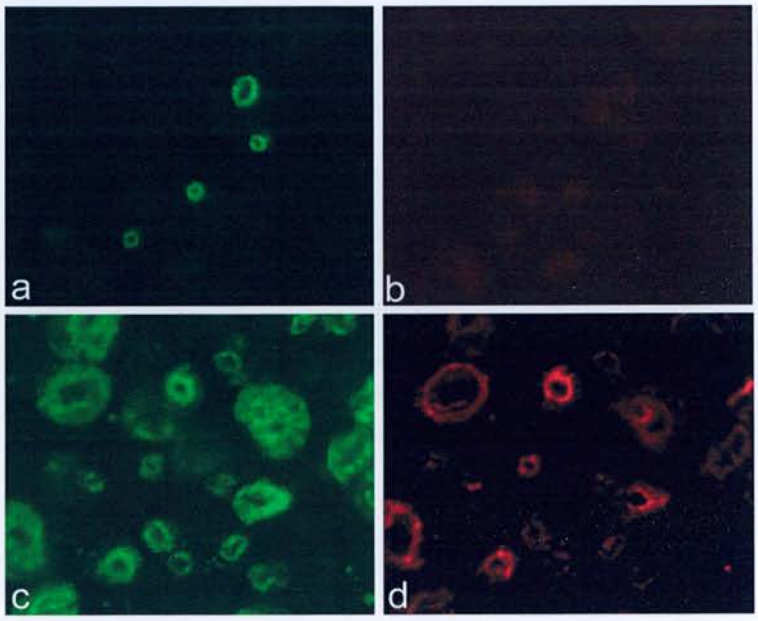
a
b
c
d

FIGURE 22 - PATHOLOGY OF SURAL NERVE BIOPSY FROM PATIENT R196X.

a: Semi-thin section stained with toluidine blue. There is almost complete absence of normal myelinated fibres. Arrows indicate onion bulb structures and arrowheads thinly myelinated fibres. Scale bar 10μm.

b: Electron micrograph of an onion bulb structure showing supernumerary Schwann cells. Arrows indicate Schwann cell nuclei. Scale bar 2μm.

c: Electron micrograph showing abnormal foldings of myelin sheath with the axon marked A. Scale bar 1μm.

Sections cut and photographed by Diane Sherman.

(Published in Guilbot et al., 2001)

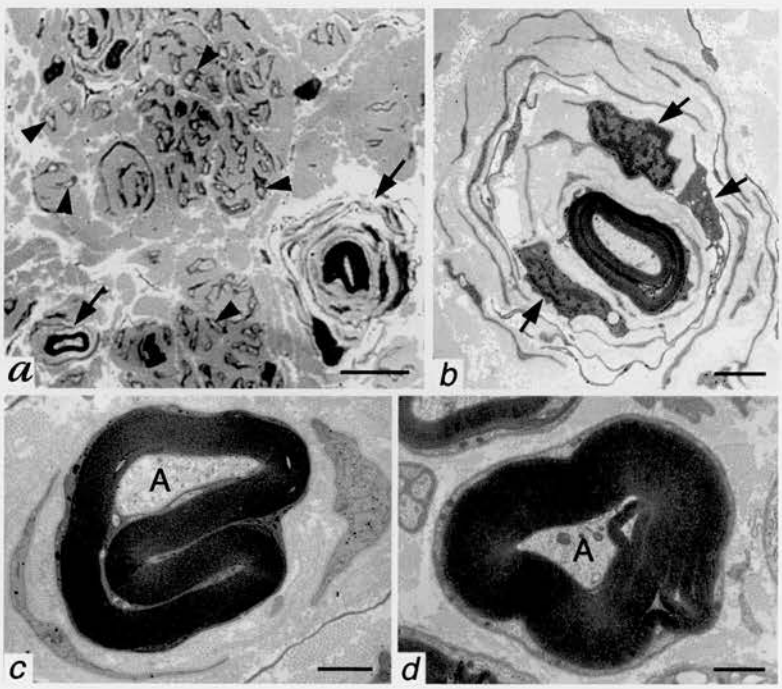
a
b
A
c
A
d

FIGURE 23 – FAMILY TREES OF C715X AND R82fs96X PATIENTS

a.

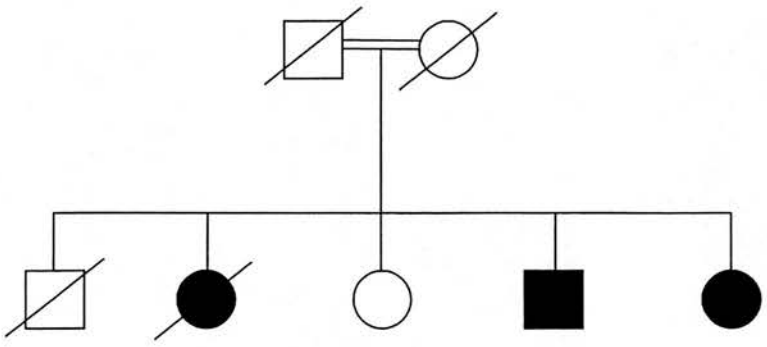

b.

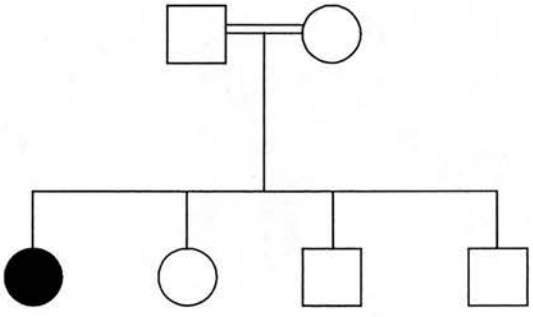

a: Family tree of patients with C715X mutation.

b: Family tree of patient with R82fs96X mutation.

FIGURE 24 - IMMUNOFLUORESCENCE ANALYSIS OF SURAL NERVE BIOPSY FROM PATIENT C715X.

A, B, C : Nerve fibres from patient C715X show staining with N-terminal PRX antibody (A), and MBP (B) , which co-localise (C).

D, E, F : Nerve fibres from patient C715X show staining with 170pep1 (repeat region) PRX antibody (D), and MBP (E) , which co-localise (F).

G, H, I : Nerve fibres from patient C715X show no staining with C-terminal PRX antibody (G), but staining with MBP (H), indicating that a truncated PRX protein is formed.

J, K, L : Nerve fibres from a normal control show staining with the C-terminal PRX antibody (J), and MBP (K) , which co-localise (L).

Scale bar 5μm

(Published in Takashima et al., 2002)

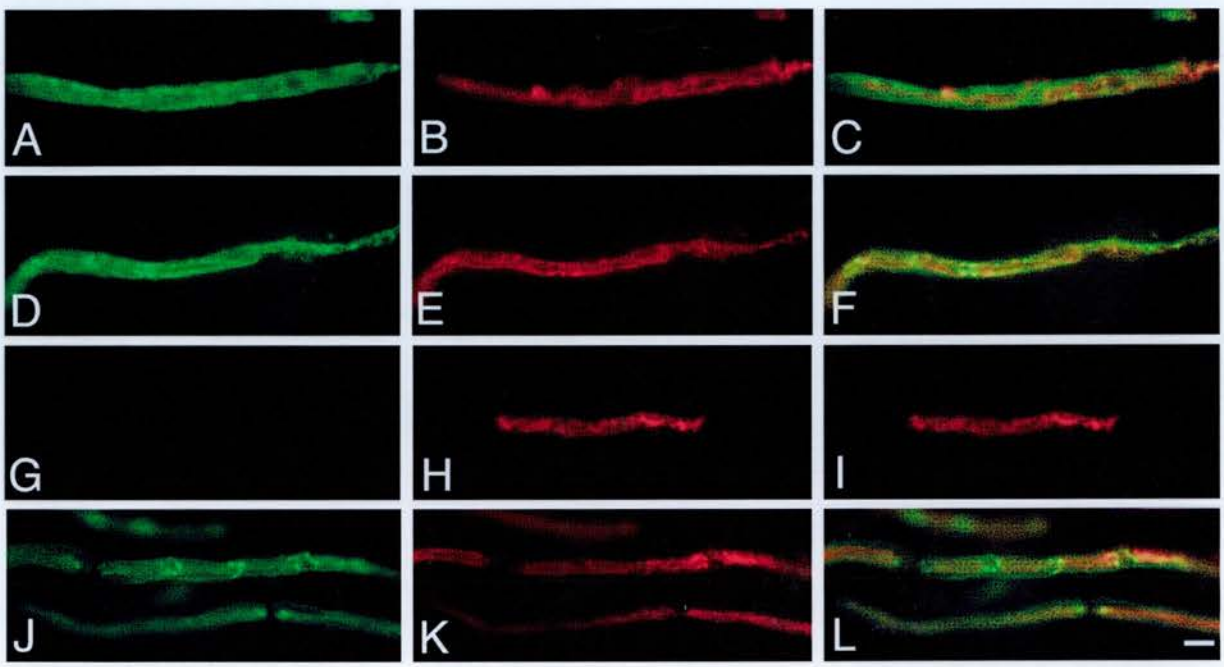
A
B
C
D
E
F
G
H
I
J
K
L

FIGURE 25 - LIGHT MICROSCOPY OF SEMI-THIN RESIN SECTIONS FROM SURAL NERVE BIOPSIES OF PATIENTS C715X AND R82fsX96

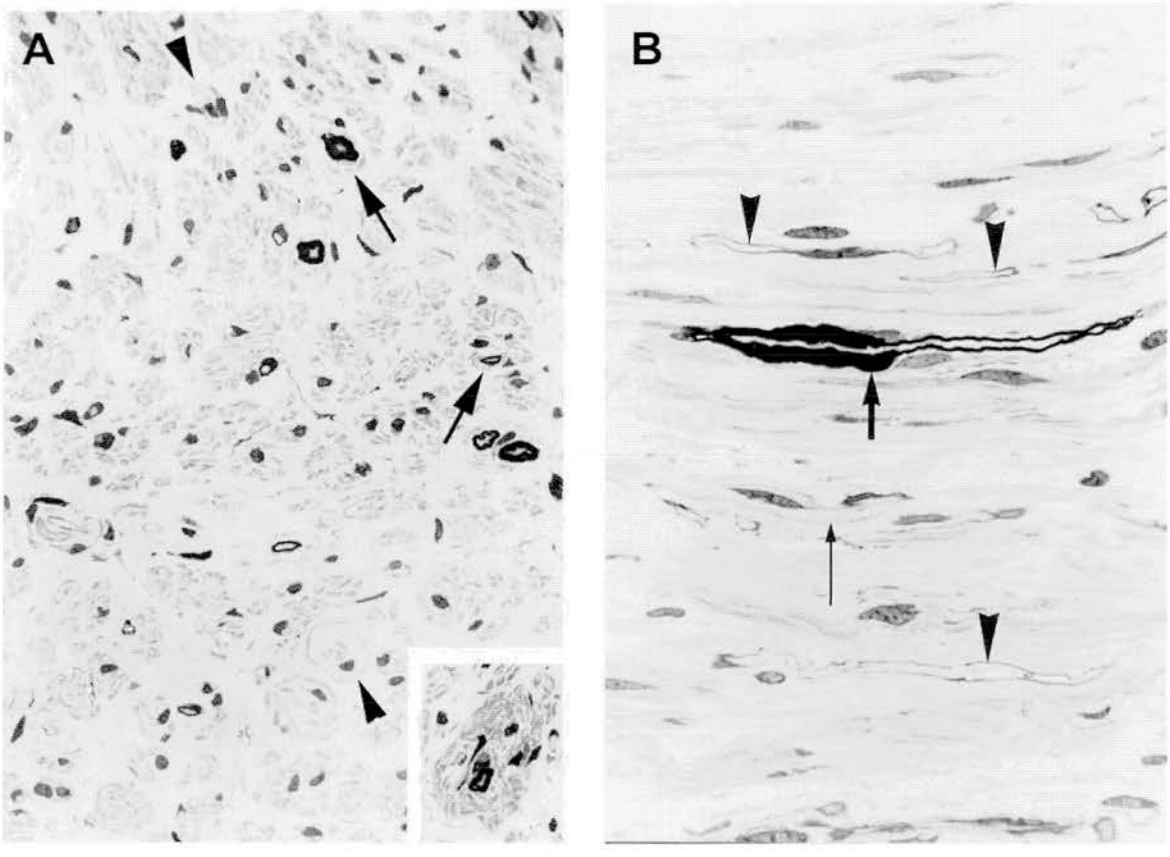

A: Biopsy from Patient R82fsX96

Transverse section showing loss of myelinated fibres of all sizes, onion bulbs (arrows) which were sometimes denervated (arrowheads) and tomacula formations. A complex of grouped, proliferated Schwann cell processes surrounded a myelinated axon (inset). Magnification x 637.

B: Biopsy from Patient C715X

Longitudinal section showing increased connective tissue and demyelinated (thin arrows) or thinly remyelinated (arrowheads) nerve fibres. A tomaculous fibre is indicated by a thick arrow. Magnification x 900.

(Sections cut and photographed by colleagues in Antwerp) (Published in Takashima et al., 2002)

FIGURE 26 - ELECTRON MICROSCOPY OF LONGITUDINAL SECTIONS IN PATIENTS R82fsX96 AND C715X

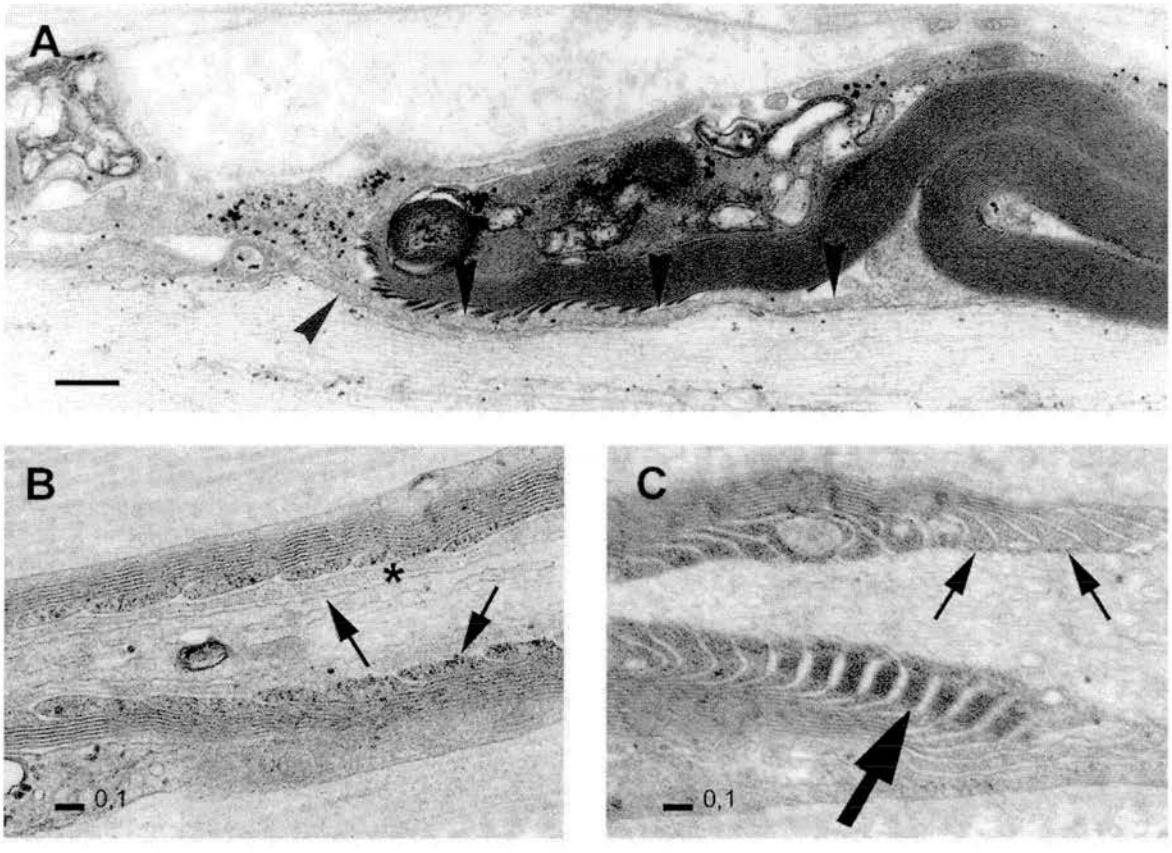

A: Biopsy from Patient R82fsX96.

Heminode showing paranodal myelin folds and a Schwann cell process separating terminal myelin loops from the axon. Scale 1 μm.

B: Biopsy from Patient C715X.

There are abnormalities of paranodal myelin loops and the absence of septate-like junctions or transverse bands (arrows). The myelin loops and axon are separated by a Schwann cell process (*). Scale bar 0.1 μm.

C: Normal sural nerve biopsy.

Normal myelin. There are well-developed septate-like junctions or transverse bands (arrows) of normal paranodal myelin and desmosome-like structures (big arrow). Scale bar 0.1 μm.

(Published in Takashima et al., 2002)

(Sections cut and photographed by colleagues in Antwerp)

FIGURE 27 - IMMUNOFLUORESCENCE ANALYSIS OF SURAL NERVE BIOPSY FROM PATIENT R1070X.

a, b, c : Nerve fibres from patient R1070X show staining with N-terminal PRX antibody (a), and MBP (b), in the same fibres (c).

d, e, f : Nerve fibres from patient R1070X show staining with 170pep1 (repeat region) PRX antibody (d), and MBP (e), in the same fibres (f).

g, h, i : Nerve fibres from patient R1070X show no staining with C-terminal PRX antibody (g), but staining with MBP (h), indicating that a truncated PRX protein is formed.

j, k, l : Nerve fibres from a normal control show staining with the C-terminal PRX antibody (j), and MBP (k), in the same fibres (l). These fibres are much larger than those of the patient.

Scale bar 5μm

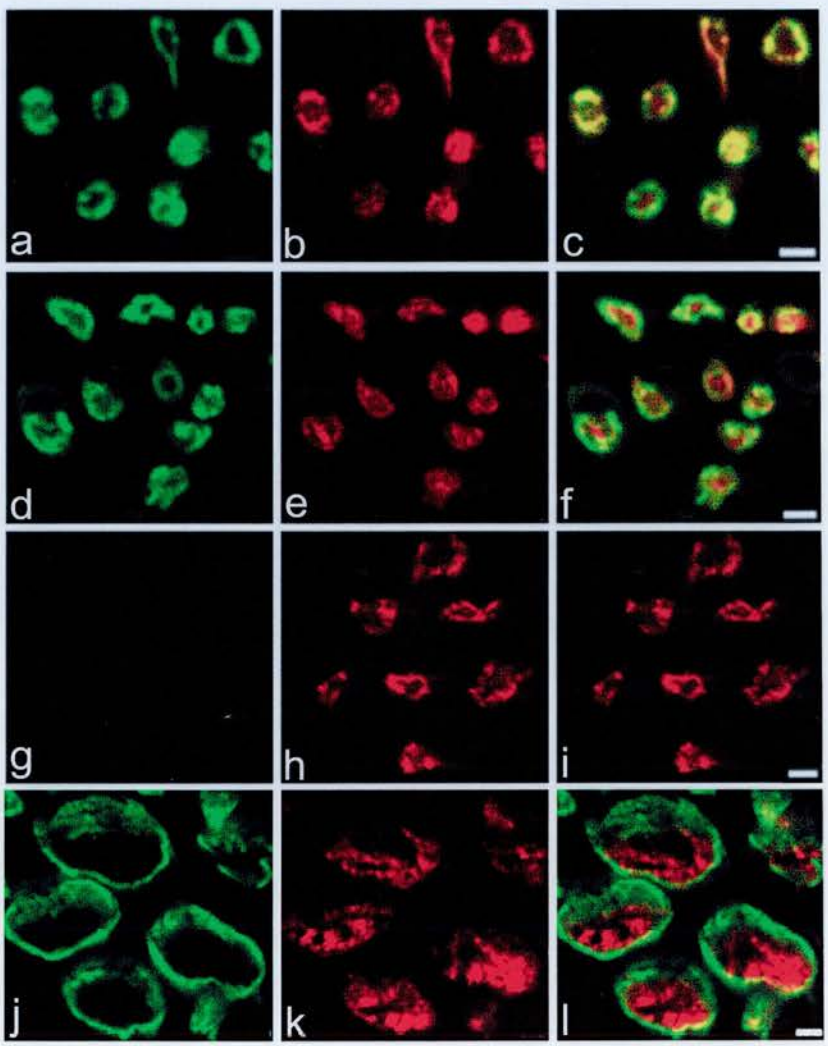
a
b
c
d
e
f
g
h
i
j
k
l

FIGURE 28 –*PERIAXIN* MUTATIONS

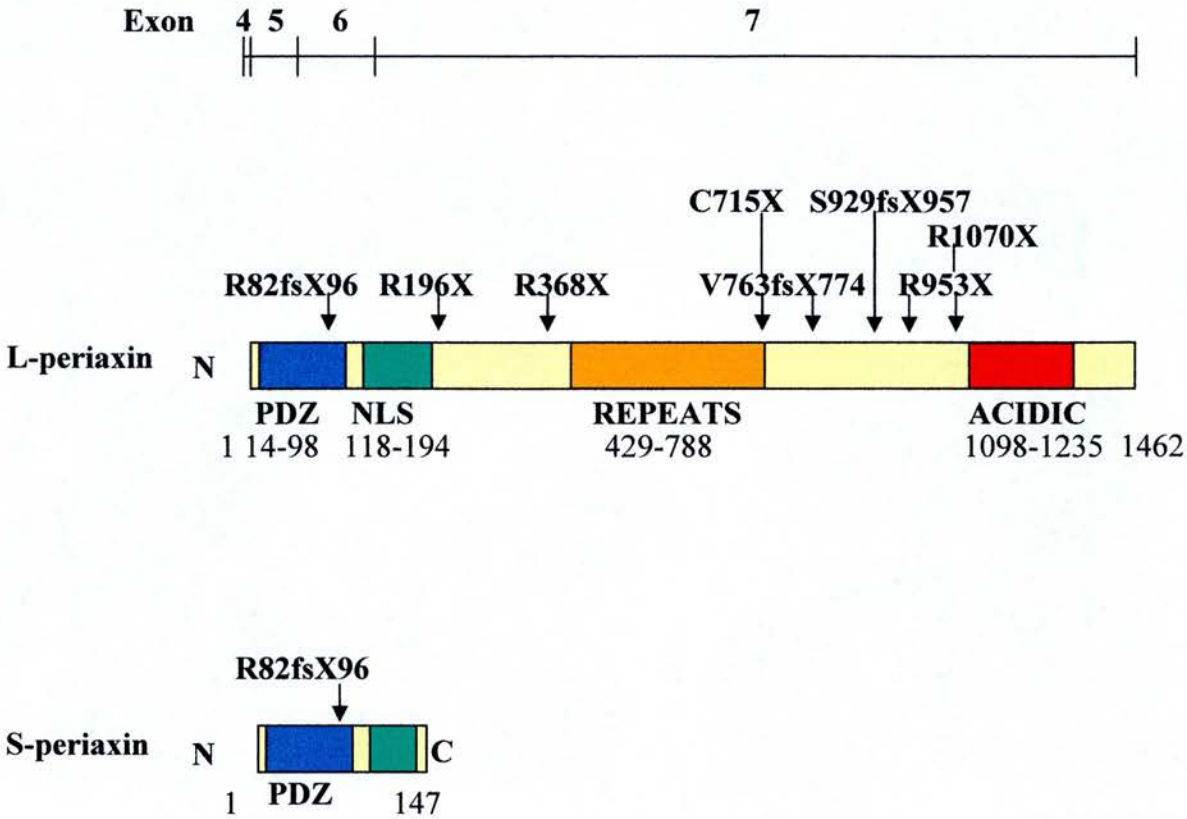

All currently known *PERIAXIN* mutations causing CMT4F/Dejerine-Sottas disease marked on the protein structure of Periaxin, with the corresponding position in the exons above.

FIGURE 29 - LINE-UP OF THE AMINO ACID SEQUENCE PRODUCED BY MUTATIONS R196X, C715X AND R1070X

```
L-periaxin     1 MEARSRSAEELRRAELVEIIVETEAQTGVSGINVAGGGKEGIFVRELREDSSAARSLSLQ  60
R196X          1 MEARSRSAEELRRAELVEIIVETEAQTGVSGINVAGGGKEGIFVRELREDSSAARSLSLQ  60
C715X          1 MEARSRSAEELRRAELVEIIVETEAQTGVSGINVAGGGKEGIFVRELREDSSAARSLSLQ  60
R1070X         1 MEARSRSAEELRRAELVEIIVETEAQTGVSGINVAGGGKEGIFVRELREDSSAARSLSLQ  60

L-periaxin    61 EGDQLLSARVFFENFKYEDALRLLQCAEPYKVSFCLKRTVPTGDLALRPGTVSGYEIKGP 120
R196X         61 EGDQLLSARVFFENFKYEDALRLLQCAEPYKVSFCLKRTVPTGDLALRPGTVSGYEIKGP 120
C715X         61 EGDQLLSARVFFENFKYEDALRLLQCAEPYKVSFCLKRTVPTGDLALRPGTVSGYEIKGP 120
R1070X        61 EGDQLLSARVFFENFKYEDALRLLQCAEPYKVSFCLKRTVPTGDLALRPGTVSGYEIKGP 120

L-periaxin   121 RAKVAKLNIQSLSPVKKKKMVPGALGVPADLAPVDVEFSFPKFSRLRRGLKAEAVKGPVP 180
R196X        121 RAKVAKLNIQSLSPVKKKKMVPGALGVPADLAPVDVEFSFPKFSRLRRGLKAEAVKGPVP 180
C715X        121 RAKVAKLNIQSLSPVKKKKMVPGALGVPADLAPVDVEFSFPKFSRLRRGLKAEAVKGPVP 180
R1070X       121 RAKVAKLNIQSLSPVKKKKMVPGALGVPADLAPVDVEFSFPKFSRLRRGLKAEAVKGPVP 180

L-periaxin   181 AAPARRRLQLPRLRVREVAEEAQAARLAAAAPPPRKAKVEAEVAAGARFTAPQVELVGPR 240
R196X        181 AAPARRRLQLPRLRV                                              195
C715X        181 AAPARRRLQLPRLRVREVAEEAQAARLAAAAPPPRKAKVEAEVAAGARFTAPQVELVGPR 240
R1070X       181 AAPARRRLQLPRLRVREVAEEAQAARLAAAAPPPRKAKVEAEVAAGARFTAPQVELVGPR 240

L-periaxin   241 LPGAEVGVPQVSAPKAAPSAEAAGGFALHLPTLGLGAPAPPAVEAPAVGIQVPQVELPAL 300
R196X        196                                                             195
C715X        241 LPGAEVGVPQVSAPKAAPSAEAAGGFALHLPTLGLGAPAPPAVEAPAVGIQVPQVELPAL 300
R1070X       241 LPGAEVGVPQVSAPKAAPSAEAAGGFALHLPTLGLGAPAPPAVEAPAVGIQVPQVELPAL 300

L-periaxin   301 PSLPTLPTLPCLETREGAVSVVVPTLDVAAPTVGVDLALPGAEVEARGEAPEVALKMPRL 360
R196X        196                                                             195
C715X        301 PSLPTLPTLPCLETREGAVSVVVPTLDVAAPTVGVDLALPGAEVEARGEAPEVALKMPRL 360
R1070X       301 PSLPTLPTLPCLETREGAVSVVVPTLDVAAPTVGVDLALPGAEVEARGEAPEVALKMPRL 360

L-periaxin   361 SFPRFGARAKEVAEAKVAKVSPEARVKGPRLRMPTFGLSLLEPRPAAPEVVESKLKLPTI 420
R196X        196                                                             195
C715X        361 SFPRFGARAKEVAEAKVAKVSPEARVKGPRLRMPTFGLSLLEPRPAAPEVVESKLKLPTI 420
R1070X       361 SFPRFGARAKEVAEAKVAKVSPEARVKGPRLRMPTFGLSLLEPRPAAPEVVESKLKLPTI 420

L-periaxin   421 KMPSLGIGVSGPEVKVPKGPEVKLPKAPEVKLPKVPEAALPEVRLPEVELPKVSEMKLPK 480
R196X        196                                                             195
C715X        421 KMPSLGIGVSGPEVKVPKGPEVKLPKAPEVKLPKVPEAALPEVRLPEVELPKVSEMKLPK 480
R1070X       421 KMPSLGIGVSGPEVKVPKGPEVKLPKAPEVKLPKVPEAALPEVRLPEVELPKVSEMKLPK 480

L-periaxin   481 VPEMAVPEVRLPEVELPKVSEMKLPKVPEMAVPEVRLPEVQLLKVSEMKLPKVPEMAVPE 540
R196X        196                                                             195
C715X        481 VPEMAVPEVRLPEVELPKVSEMKLPKVPEMAVPEVRLPEVQLLKVSEMKLPKVPEMAVPE 540
R1070X       481 VPEMAVPEVRLPEVELPKVSEMKLPKVPEMAVPEVRLPEVQLLKVSEMKLPKVPEMAVPE 540

L-periaxin   541 VRLPEVQLPKVSEMKLPEVSEVAVPEVRLPEVQLPKVPEMKVPEMKLPKVPEMKLPEMKL 600
R196X        196                                                             195
C715X        541 VRLPEVQLPKVSEMKLPEVSEVAVPEVRLPEVQLPKVPEMKVPEMKLPKVPEMKLPEMKL 600
R1070X       541 VRLPEVQLPKVSEMKLPEVSEVAVPEVRLPEVQLPKVPEMKVPEMKLPKVPEMKLPEMKL 600

L-periaxin   601 PEVQLPKVPEMAVPDVHLPEVQLPKVPEMKLPEMKLPEVKLPKVPEMAVPDVHLPEVQLP 660
R196X        196                                                             195
C715X        601 PEVQLPKVPEMAVPDVHLPEVQLPKVPEMKLPEMKLPEVKLPKVPEMAVPDVHLPEVQLP 660
R1070X       601 PEVQLPKVPEMAVPDVHLPEVQLPKVPEMKLPEMKLPEVKLPKVPEMAVPDVHLPEVQLP 660

L-periaxin   661 KVPEMKLPKMPEMAVPEVRLPEVQLPKVSEMKLPKVPEMAVPDVHLPEVQLPKVCEMKVP 720
R196X        196                                                             195
C715X        661 KVPEMKLPKMPEMAVPEVRLPEVQLPKVSEMKLPKVPEMAVPDVHLPEVQLPKV        714
R1070X       661 KVPEMKLPKMPEMAVPEVRLPEVQLPKVSEMKLPKVPEMAVPDVHLPEVQLPKVCEMKVP 720

L-periaxin   721 DMKLPEIKLPKVPEMAVPDVHLPEVQLPKVSEIRLPEMQVPKVPDVHLPKAPEVKLPRAP 780
R196X        196                                                             195
C715X        715                                                             714
R1070X       721 DMKLPEIKLPKVPEMAVPDVHLPEVQLPKVSEIRLPEMQVPKVPDVHLPKAPEVKLPRAP 780

L-periaxin   781 EVQLKATKAEQAEGMEFGFKMPKMTMPKLGRAESPSRGKPGEAGAEVSGKLVTLPCLQPE 840
R196X        196                                                             195
C715X        715                                                             714
```

```
R1070X          781 EVQLKATKAEQAEGMEFGFKMPKMTMPKLGRAESPSRGKPGEAGAEVSGKLVTLPCLQPE  840

L-periaxin      841 VDGEAHVGVPSLTLPSVELDLPGALGLQGQVPAAKMGKGERVEGPEVAAGVREVGFRVPS  900
R196X           196                                                            195
C715X           715                                                            714
R1070X          841 VDGEAHVGVPSLTLPSVELDLPGALGLQGQVPAAKMGKGERVEGPEVAAGVREVGFRVPS  900

L-periaxin      901 VEIVTPQLPAVEIEEGRLEMIETKVKPSSKFSLPKFGLSGPKVAKAEAEGAGRATKLKVS  960
R196X           196                                                            195
C715X           715                                                            714
R1070X          901 VEIVTPQLPAVEIEEGRLEMIETKVKPSSKFSLPKFGLSGPKVAKAEAEGAGRATKLKVS  960

L-periaxin      961 KFAISLPKARVGAEAEAKGAGEAGLLPALDLSIPQLSLDAHLPSGKVEVAGADLKFKGPR 1020
R196X           196                                                            195
C715X           715                                                            714
R1070X          961 KFAISLPKARVGAEAEAKGAGEAGLLPALDLSIPQLSLDAHLPSGKVEVAGADLKFKGPR 1020

L-periaxin     1021 FALPKFGVRGRDTEAAELVPGVAELEGKGWGWDGRVKMPKLKMPSFGLARGKEAEVQGDR 1080
R196X           196                                                            195
C715X           715                                                            714
R1070X         1021 FALPKFGVRGRDTEAAELVPGVAELEGKGWGWDGRVKMPKLKMPSFGLA           1069

L-periaxin     1081 ASPGEKAESTAVQLKIPEVELVTLGAQEEGRAEGAVAVSGMQLSGLKVSTAGQVVTEGHD 1140
L-periaxin     1141 AGLRMPPLGISLPQVELTGFGEAGTPGQQAQSTVPSAEGTAGYRVQVPQVTLSLPGAQVA 1200
L-periaxin     1201 GGELLVGEGVFKMPTVTVPQLELDVGLSREAQAGEAATGEGGLRLKLPTLGARARVGGEG 1260
L-periaxin     1261 AEEQPPGAERTFCLSLPDVELSPSGGNHAEYQVAEGEGEAGHKLKVRLPRFGLVRAKEGA 1320
L-periaxin     1321 EEGEKAKSPKLRLPRVGFSQSEMVTGEGSPSPEEEEEEEEEGSGEGASGRRGRVRVRLPR 1380
L-periaxin     1381 VGLAAPSKASRGQEGDAAPKSPVREKSPKFRFPRVSLSPKARSGSGDQEEGGLRVRLPSV 1440
L-periaxin      1441 GFSETGAPGPARMEGAQAAAVN 1462
```

Table 7: Comparison of human, rat and mouse *Periaxin* genes.

	Human	**Rat**	**Mouse**
Exon I	32	30	32
Intron1	4954	-	4900
Exon II	44	44	44
Intron 2	83	-	88
Exon III	99	99	99
Intron 3	127	-	116
Exon IV	126	126	126
Intron 4	4090	-	2900
Exon V	157	157	157
Intron 5	4816	-	7500
Exon VI	197	197	197
Intron 6	649	-	592
Exon VII	4005	3972	3787
No. of amino acids in protein	1462	1383	1391
Calculated size of protein (L-periaxin)	155kD	147kD	147.5kD
Kozak sequence	TCCATGC	GCTATGG	GCTATGG

The sizes of the rat introns are as yet unknown.

4. RESULTS - MORPHOLOGICAL INVESTIGATION OF THE MOUSE MODEL OF CMT4F - THE PERIAXIN-NULL MOUSE

The function of L-periaxin is unknown. However, it is known that periaxin deficient mice can assemble apparently normal compact myelin in the development of the PNS, and so the presence of periaxin is not prerequisite for development of a PNS myelin sheath. Abnormalities in the myelin sheath appear with time in these mice, suggesting that periaxin is required for maintenance of the stability of the sheath, and perhaps in its ability to repair.

We hypothesised that periaxin is essential for the repair or turnover of myelin sheaths which occurs continually in vivo; hence we carried out sciatic nerve crush on wild-type and periaxin-null mice to determine whether regeneration of the myelin sheath could occur. We assessed myelinated axon number, axon diameter, and myelin sheath thickness.

4.1. Nerve crush experiments

Nerve crushes were performed on the sciatic nerves of wild-type and periaxin-null mice at six weeks of age as described in Section 2.5. This age was chosen as myelination is thought to be complete but there is little sign of peripheral nerve pathology in the periaxin-null mice. This was to ensure that any demyelination and remyelination was due to nerve crush and recovery rather than disease. Analysis of regeneration was carried out at two and six weeks after crush (eight and twelve weeks of age). On each occasion the uncrushed, contra-lateral sciatic nerve was taken as an internal control. We examined the nerves four days after crush to ensure that the crush technique was efficient at causing demyelination (secondary to axonotmesis) and found that the efficiency of our crush technique is adequate to affect most myelinated axons (Figure 30). Hence we can confidently attribute the presence of myelin two weeks after crush to remyelination.

4.1.1. Myelinated axon number

We counted the number of myelinated axons to determine if periaxin-null mice and wild-type mice have equivalent baseline numbers of myelinated axons, and if, after crush, the nerves could regenerate the normal number of myelinated axons. It is known that in human demyelinating CMT disease axonal loss contributes much to the symptoms of the disease (Krajewski et al., 2000), so we wanted to determine whether axonal loss was increased after experimental nerve crush in periaxin-null mice.

At baseline, in uncrushed nerves, periaxin-null and wild-type mice have an equivalent number of myelinated axons. At two weeks after crush, the number of myelinated axons in both wild-type and periaxin-null mice is back to normal, suggesting that recovery of the number of myelinated axons is complete by two weeks after crush (Figure 31).

4.1.2. Cross-sectional area of nerve

It has been reported previously that the cross-sectional area of nerves increases in animal models of demyelinating CMT disease (Sahenk, 1999). The average cross-sectional area of a periaxin-null mouse sciatic nerve is significantly larger than that of the wild-type (unpaired t-test $p<0.001$) (Figure 32d). As Figure 31 shows, the number of myelinated fibres is equivalent, so the density of axons in periaxin-null mice is markedly reduced (unpaired t-test $p<0.001$) (Figure 32c). There is no change in density with age over this period.

The reduced density of fibres (Figure 32) and the increase in total area of the nerve in periaxin-null mice is due to an increase in ECM. There is a clinical correlate of this observation in that human patients with inherited demyelinating peripheral neuropathies often have thickened nerves which are palpable on clinical examination. This suggests that this difference is real and not an artefact of the tissue processing. At higher power, this is confirmed, as empty space is not apparent.

4.1.3. Frequency distribution of axon diameters in the nerve

Myelination of an axon causes phosphorylation of neurofilaments, which is believed to increase the axon diameter. Therefore, in causing demyelination, nerve crush reduces neurofilament phosphorylation, which leads to more densely packed neurofilaments and a smaller axon diameter (de Waegh et al., 1992). We determined if there were baseline differences in the frequency distribution of axon diameters between periaxin-null and wild-type mice, and whether this changed after crush.

The frequency distribution of axon diameters in wild-type or periaxin-null mouse sciatic nerve does not fit a normal distribution, but is skewed to the left indicating a higher representation of smaller myelinated axons (Figure 33).

In uncrushed nerves, the axon diameter size distribution does not change with time between eight and twelve weeks of age. Periaxin-null nerves have a higher proportion of smaller axon diameters compared to wild-type nerves, both in the crushed and uncrushed situations (Kolmogorov-Smirnov test $p<0.001$).

Nerve crush, in both wild-type and periaxin-null mice, shifts the curve further to the left, indicating an increase in the proportion of smaller diameter myelinated axons. The difference is not fully resolved by six weeks after crush, indicating that the axon diameters have still not returned to their previous size, even in wild-type mice (Kolmogorov-Smirnov test $p<0.001$).

4.1.4. Myelin thickness

We determined whether the thickness of myelin is different between periaxin-null and wild-type nerves at baseline and after crush. The g-ratio is a measure of the thickness of the myelin sheath around an axon, compared to its diameter, and is derived by dividing the axon diameter by the fibre diameter. Therefore, as the myelin thickness increases, the g-ratio decreases and vice versa. If there is no myelin sheath, then the g-ratio is 1.

The g-ratio is plotted against the axon diameter to directly compare the amount of myelin around a fixed sized axon. Figure 34 shows regression lines for the average g-

ratio values for each axon diameter range from all nerves tested in each experimental group. The regression lines for the crushed and uncrushed wild-type nerves are superimposed at both two weeks and six weeks after crush, indicating repair of the myelin sheath to normal by two weeks. However, in periaxin-null mice, the crushed nerve regression line is significantly higher than the uncrushed line at two weeks after crush ($p=0.007$). The difference is less marked, but still present, at six weeks after crush ($p=0.002$). Thus, crushed nerves have less thick myelin sheaths compared to uncrushed nerves in the periaxin-null mouse. However, on comparing these regression lines to wild-type mice, uncrushed periaxin-null nerves show a lower g-ratio than the corresponding wild-type nerves ($p=0.02$ at 2 weeks, $p=0.01$ at 6 weeks), indicating hypermyelination, especially of smaller diameter fibres. The two regression lines for crushed periaxin-null and wild-type nerves are very similar two weeks after crush, indicating that there had been repair of the myelin sheath at the same rate after demyelination. At six weeks after crush these diverge as the periaxin-null nerve g-ratios decrease, thus indicating hypermyelination. Therefore, crushed periaxin-null nerves become more hypermyelinated and more abnormal with time.

This is shown in a different way in Figure 35 which shows the results of g-ratios for a single experimental mouse at each time point. In the wild-type mice, the g-ratio values from crushed and uncrushed nerves are indistinguishable at two and six weeks after crush, suggesting that myelin thickness returns to normal within two weeks. In the periaxin-null mice, the g-ratio values are lower in the uncrushed nerve compared to the crushed nerve at two weeks, though the difference is less at six weeks after crush when the g-ratio values are lower, indicating hypermyelination.

4.2. Discussion

Nerve crush is a commonly used experimental model in rodents to allow investigations of peripheral nerve injury and regeneration. This has been evaluated and standardised by several groups (Bridge et al., 1994; Nawwar et al., 1995). The failure of patients with demyelinating CMT disease to remyelinate normally or fully is still not understood. Hence there is value in studying this issue in good mouse models of the disease.

There are now several mouse models of human CMT disease, (reviewed in (Young and Suter, 2001)), and the periaxin-null mouse is a model of an autosomal recessive type. Hence, these mice provide an excellent opportunity to study the pathophysiology of disease.

4.2.1. Baseline differences between periaxin-null and wild-type mice

We have shown that there is no difference in the number of myelinated axons in wild-type and periaxin-null sciatic nerves up to twelve weeks of age. Thus, periaxin-null mice have the capacity to form normal numbers of myelinated axons. It is known that peripheral nerve development involves bidirectional axon-glial interactions (de Waegh et al., 1992) suggesting that periaxin is not critical in this signalling at least at early stages. In human demyelinating CMT disease it is thought that most symptoms occur when axons are lost, secondary to demyelination, although myelin abnormalities can be seen earlier on electrophysiological testing (Krajewski et al., 2000). Indeed, at nine months of age, periaxin-null mice also show a reduction in myelinated axons (Sherman et al., unpublished).

However, at the age of this experiment (two to three months), prior to axonal loss, there is a higher proportion of smaller diameter axons in periaxin-null nerves. Shiverer and Trembler mice, which have disordered myelination due to myelin basic protein and peripheral myelin protein-22 mutations respectively, also show this (de Waegh et al., 1992; Kirkpatrick et al., 2001). This may be secondary to the presence of thin myelin around some axons, as it is postulated that the myelin sheath signals to the axon, causing an increase in the number of neurofilaments and state of neurofilament phosphorylation both of which increase axon calibre (Kriz et al., 2000). However, many of the axons in the periaxin-null mouse are hypermyelinated, as shown in Figure 34 and Figure 35. It is known that the rate of slow axonal transport is reduced in Trembler and Shiverer mouse peripheral nerve, where axon diameters are small (de Waegh et al., 1992; Kirkpatrick et al., 2001), and so it may be that these axo-glial units are less stable over time. Therefore, there appears to be disordered axo-glial interactions in periaxin-null mice even at the age of three months.

4.2.2. Extracellular matrix

Periaxin-null sciatic nerves are larger in total cross-sectional area than wild-type nerves, due to an increase in ECM. In some patients with demyelinating CMT disease, peripheral nerves are visible or palpable (Harding and Thomas, 1980a). This is thought to be due to a combination of an increase in ECM and the presence of onion-bulb structures around remyelinated axons. By electron microscopy, patients with an axonal form of CMT also had increased ECM (Barhoumi et al., 2001). The dystroglycan-dystrophin-related protein-2 complex links the Schwann cell cytoskeleton to the extracellular matrix, and it may provide a signalling link as well as a physical one. The absence of periaxin may alter this signalling affecting both the Schwann cell and the ECM.

4.2.3. Differences between periaxin-null and wild-type mice after nerve crush.

After crush, the number of myelinated axons in wild-type and periaxin-null sciatic nerve returns to normal within two weeks. However, the axon diameters decrease in both wild-type and periaxin-null mice, and do not fully recover to normal even after six weeks. Similarly, Bridge et al. (Bridge et al., 1994) found that eight weeks after nerve crush in wild-type rats, axon size had also not returned to normal yet electrophysiological and behavioural testing results were normal.

Crushed wild-type axons repair their myelin sheath to normal by two weeks after crush. Crushed periaxin-null axons initially remyelinate at the same rate as wild-type crushed axons by two weeks after crush, but then become hypermyelinated.

Thus, periaxin-null mice can remyelinate regenerated fibres after nerve crush. Periaxin-null nerves have very similar measurements of myelin thickness to wild-type nerves shortly after crush, but later, hypermyelination occurs. This suggests that although these axons can remyelinate, the mechanisms that regulate myelin thickness are deranged, so abnormally thick myelin sheaths occur. Thus, periaxin may be involved in the regulation of myelin sheath thickness, and it may be that this hypermyelination later leads to the progressive demyelination and dysfunction seen both in the mouse model and in human CMT patients.

At three months of age, in this strain background, the periaxin-null mouse has little pathology and a mild phenotype, but by six months of age the mice are severely affected (Gillespie et al., 2000). The human form of the disease seems more variable with both severe phenotypes (Boerkoel et al., 2001b; Takashima et al., 2002) (Dejerine-Sottas disease) and milder forms described (Guilbot et al., 2001; Takashima et al., 2002). This may partly reflect the different genetic backgrounds on which the *PERIAXIN* mutations are superimposed.

This work was published in the Journal of Anatomy (Williams and Brophy, 2002).

FIGURE 30 - EFFICIENCY OF CRUSH TECHNIQUE.

a: Uncrushed sciatic nerve from wild-type mouse.

Scale bar 9.7μm.

b: Crushed sciatic nerve from wild-type mouse, taken four days after crush, showing disruption of the majority of myelin sheaths.

Scale bar 9.7μm.

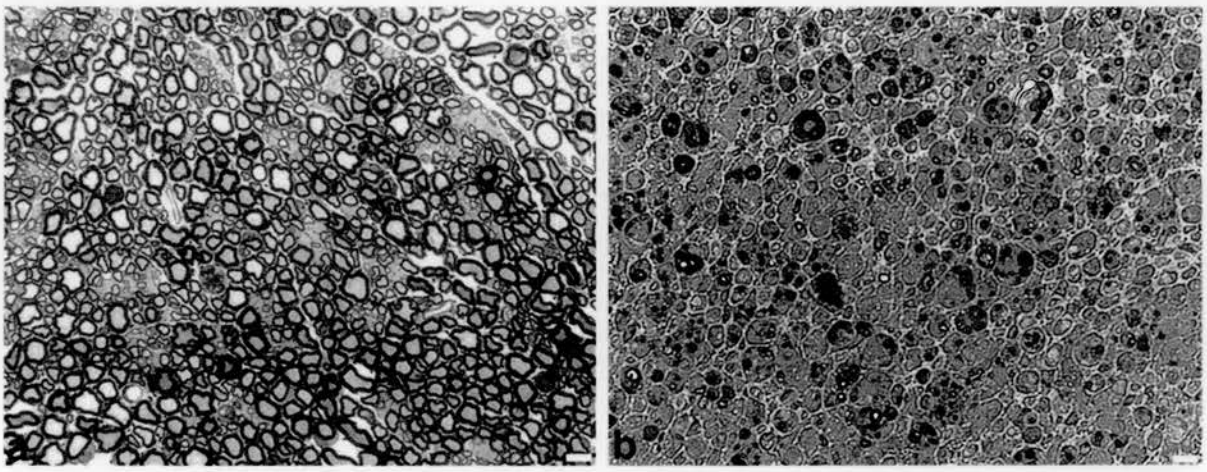
b

FIGURE 31 - MYELINATED AXON NUMBER

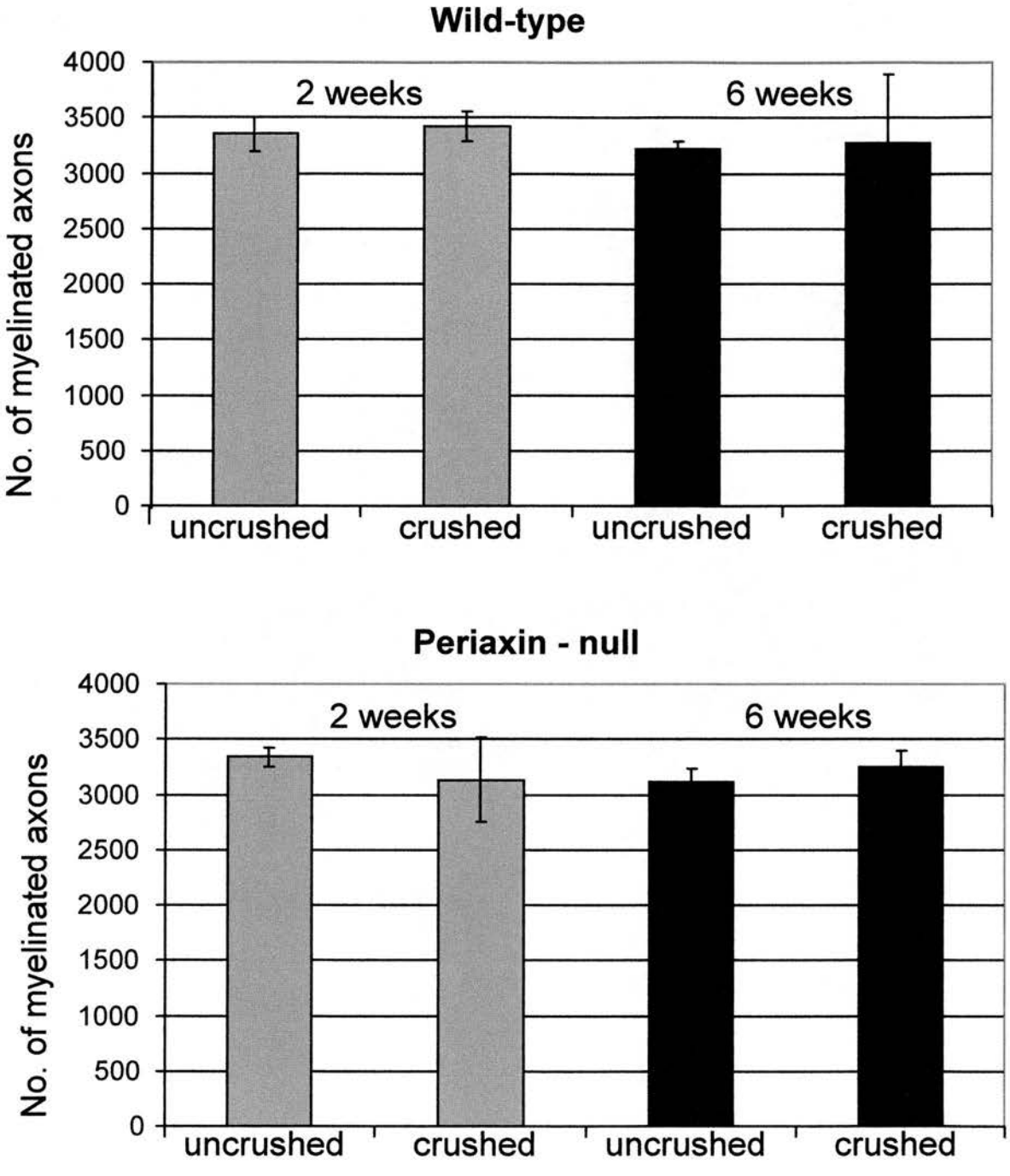

Myelinated axon number in periaxin-null mice is normal at baseline (uncrushed) or 2 and 6 weeks after sciatic nerve crush (crushed). Values shown are mean ± SEM for 3-5 experimental mice.

FIGURE 32 – DENSITY OF MYELINATED AXONS

a + **b**: Light micrographs of wild-type (a) and periaxin-null (b) sciatic nerve show the reduced density of myelinated axons and increased extracellular matrix in the periaxin-null mice. Scale 10μm.

c: The density of myelinated axons is significantly reduced in periaxin-null sciatic nerve. Values shown are means ± SEM for 19 wild-type and 23 periaxin-null mice.

d: The cross-sectional area of periaxin-null sciatic nerve is significantly larger than that of the wild-type.

Asterisks indicate statistically significant differences ($p<0.001$, unpaired t-test).

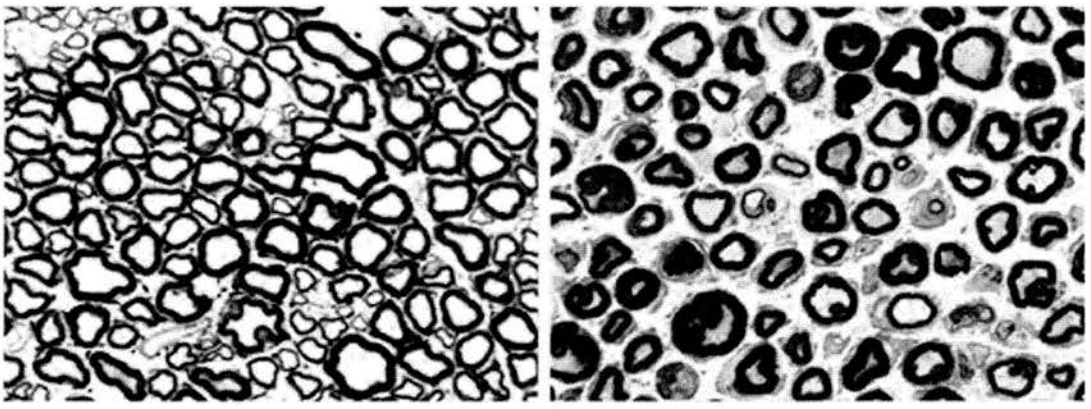

a b

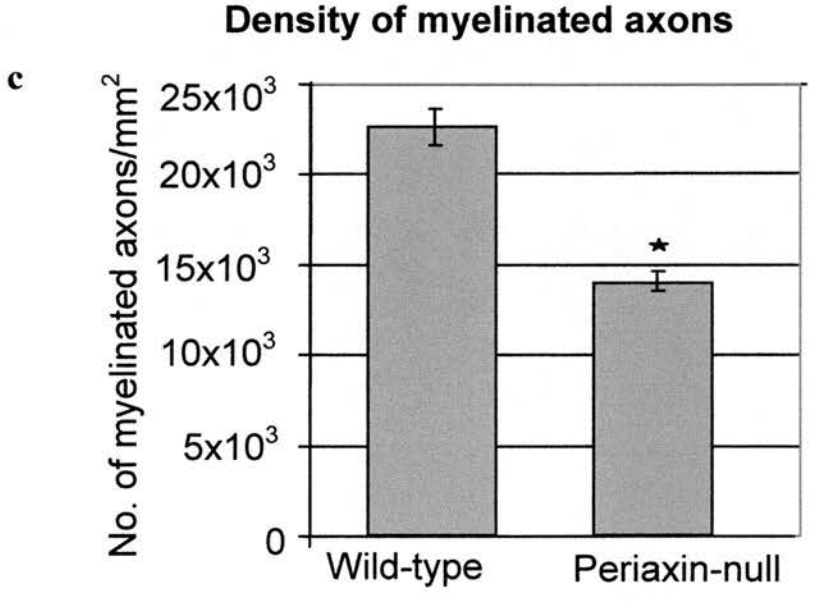
Density of myelinated axons
No. of myelinated axons/mm2
25x10^3
20x10^3
15x10^3
10x10^3
5x10^3
0
Wild-type
Periaxin-null

c

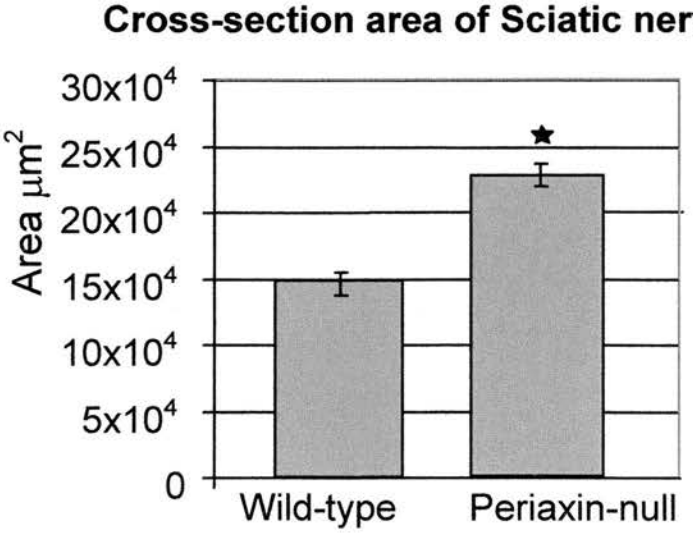
Cross-section area of Sciatic nerve
Area µm2
30x10^4
25x10^4
20x10^4
15x10^4
10x10^4
5x10^4
0
Wild-type
Periaxin-null

d

FIGURE 33 - AXON DIAMETER

Axon diameter frequency distribution in sciatic nerve from wild-type and periaxin-null mice in uncrushed nerves, and 2 and 6 weeks after crush respectively. The percentage frequency is plotted against axon diameter (μm). Uncrushed periaxin-null nerves have a higher percentage of small diameter fibres. After crush, the proportion of small diameter axons increases in both wild-type and periaxin-null nerves and although this reverts slowly towards normal, at 6 weeks there are still more smaller axons. Values shown are means ± SEM of an average of 957 axons per each of 3-5 sciatic nerves for each group.

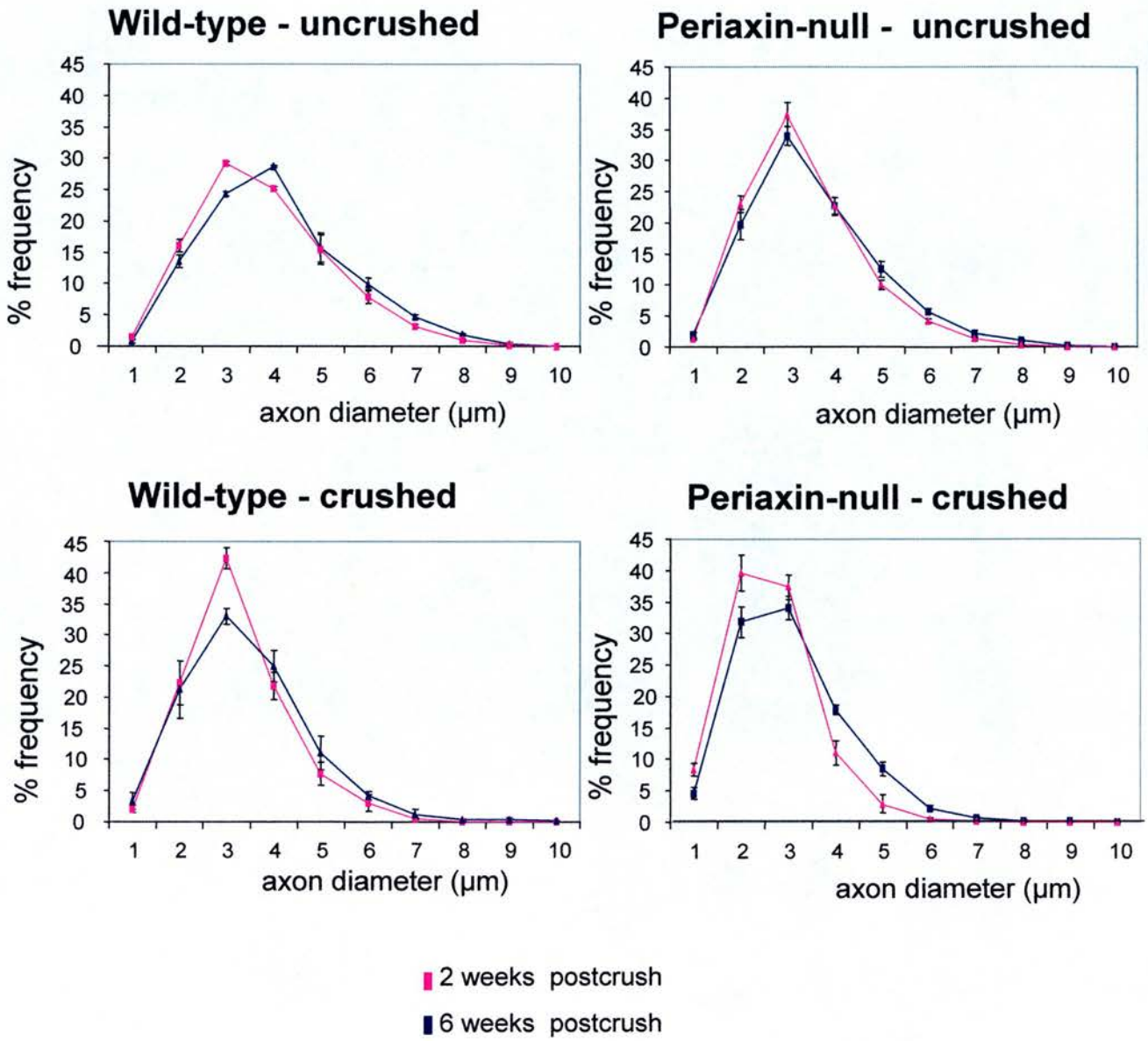
Wild-type - uncrushed
Periaxin-null - uncrushed
Wild-type - crushed
Periaxin-null - crushed
% frequency
axon diameter (µm)
2 weeks postcrush
6 weeks postcrush

FIGURE 34 – MEAN g-RATIO

Graphs of the mean g-ratio plotted against axon diameter for wild-type and periaxin-null mice at 2 and 6 weeks after crush. The axon diameter values are grouped according to size, and the mean g-ratio is plotted for each size range. For ease of comparison, the mean g-ratio is plotted against the natural log of the axon diameter, giving a straight regression line. The equations for the regression lines are displayed. Mean g-ratios are from an average of 957 axons for each of 3-5 sciatic nerves in each experimental group. The mean g-ratio values for the crushed and uncrushed wild-type mice are superimposed at both 2 and 6 weeks after nerve crush and show that remyelination is carried out to completeness by 2 weeks after crush. The mean g-ratio values for the uncrushed periaxin-null nerves are lower than their wild-type equivalents, indicating hypermyelination. After nerve crush, the periaxin-null axon g-ratios are very similar to their wild-type counterparts at two weeks, indicating a similar initial rate of remyelination. However, at 6 weeks after crush, the g-ratio values have decreased, indicating progressive hypermyelination, moving closer to the hypermyelinated state of the uncrushed nerves.

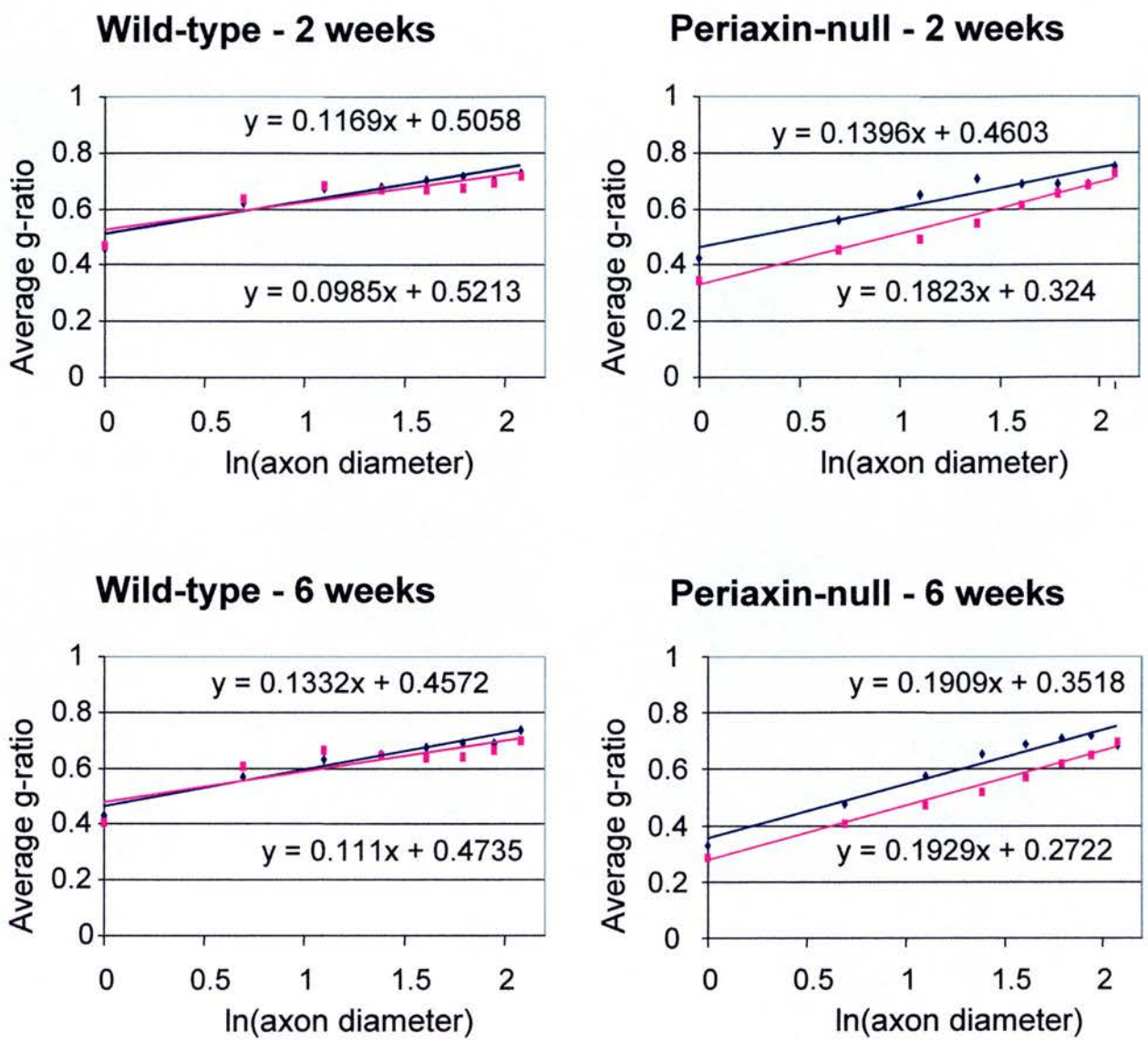
Wild-type - 2 weeks
y = 0.1169x + 0.5058
y = 0.0985x + 0.5213
Average g-ratio
ln(axon diameter)
Periaxin-null - 2 weeks
y = 0.1396x + 0.4603
y = 0.1823x + 0.324
Average g-ratio
ln(axon diameter)
Wild-type - 6 weeks
y = 0.1332x + 0.4572
y = 0.111x + 0.4735
Average g-ratio
ln(axon diameter)
Periaxin-null - 6 weeks
y = 0.1909x + 0.3518
y = 0.1929x + 0.2722
Average g-ratio
ln(axon diameter)
uncrushed
crushed

FIGURE 35 – g-RATIO DISTRIBUTION PER AXON

Graphs of the g-ratio for each axon measured in crushed and uncrushed nerve, plotted against its axon diameter, for one experimental animal for each group. This emphasizes that there is no difference in g-ratio values for crushed and uncrushed wild-type axons at 2 or 6 weeks after crush, indicating complete remyelination. However, there are distinct populations of g-ratio values from crushed and uncrushed periaxin-null axons, at two weeks after crush. The uncrushed values are lower, indicating hypermyelination, and the crushed values are similar to that of crushed wild-type axons at this time point. At 6 weeks after crush, the crushed and uncrushed periaxin-null axon g-ratio values are more similar, and lower, indicating progressive hypermyelination.

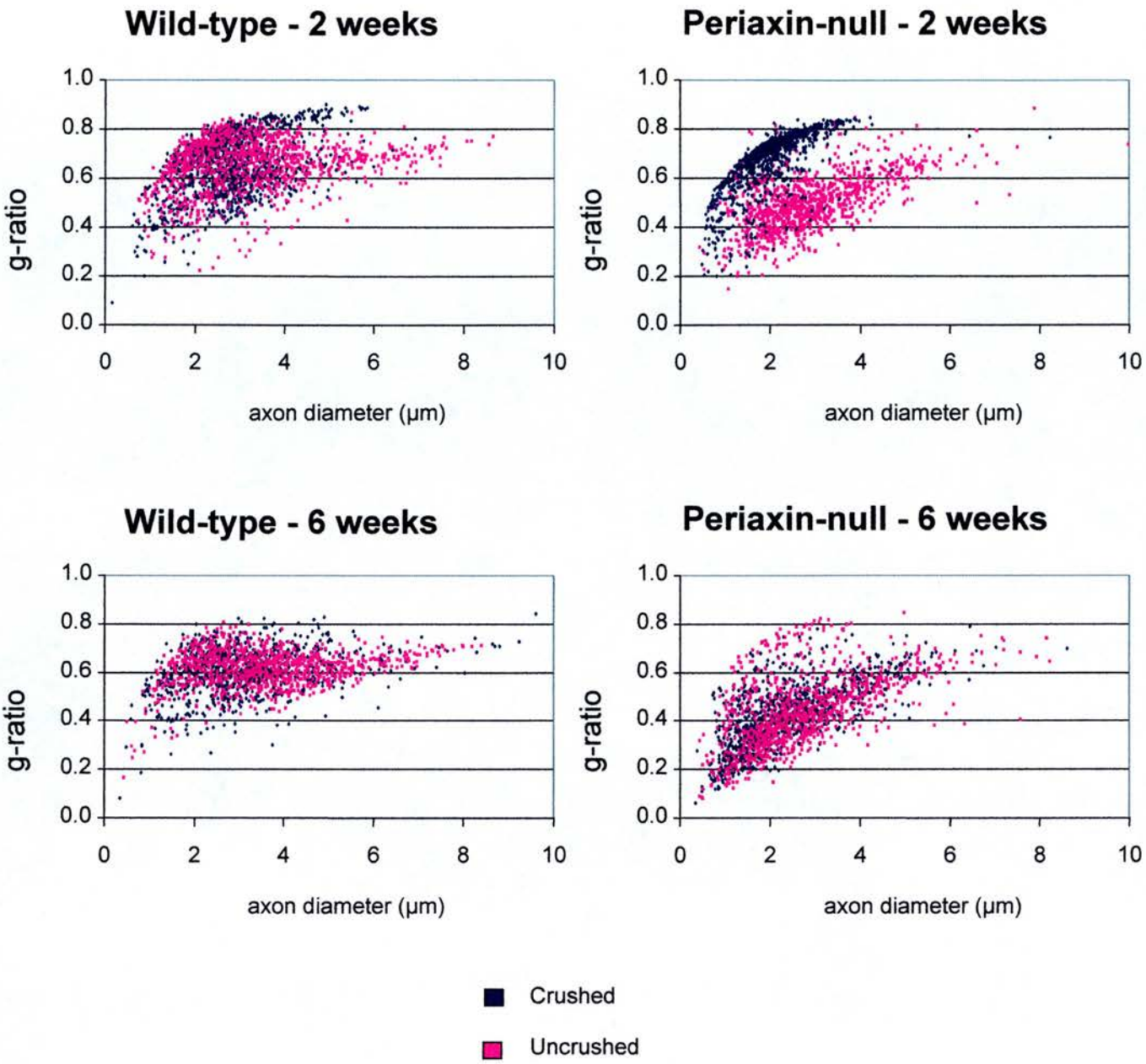
Wild-type - 2 weeks
Periaxin-null - 2 weeks
Wild-type - 6 weeks
Periaxin-null - 6 weeks
g-ratio
axon diameter (μm)
0.0
0.2
0.4
0.6
0.8
1.0
0
2
4
6
8
10
Crushed
Uncrushed

5. RESULTS - EXPERIMENTS WITH Fbl6

Sylvia Vasiliou identified the F-box protein Fbl6 as a binding protein of L-periaxin in a yeast-2 hybrid screen using the C-terminal part of L-periaxin (Vasiliou in preparation). She narrowed down the region of interaction to an 84 amino acid stretch involving part of the acidic domain and sequence upstream of this (Figure 36). L-periaxin was shown to interact with the leucine-rich repeat region of Fbl6 by in vitro pull down assays (Vasiliou in preparation). However, in vivo interaction was not confirmed.

5.1. Fbl6 antibody

We generated an antibody to GST fused to the amino acids 49-115 of the rat Fbl6 protein. This stretch of the sequence was chosen as it was previously thought that the methionine at amino acid 48 was the first amino acid of the protein, by comparison with the mouse sequence in the database. However, on closer examination there is another in-frame methionine residue 48 amino acids upstream of this (Figure 37). The ATG here has a more classical Kozak sequence, and is probably the preferred start codon. This is corroborated by the human equivalent sequence, which is also thought to start at this first methionine (Figure 38).

The antibody was tested on western blot and immunohistochemistry. On western blot, non-specific bands were produced. On immunohistochemistry on mouse sciatic nerve, there was specific staining of the cytoplasm of myelinating Schwann cells. Teased fibre preparations showed that Fbl6 co-localised with S100, a marker of Schwann cell cytoplasm (Figure 39). Double labelling with the sheep C-terminal periaxin antibody on the teased fibres showed periaxin localisation at the membrane of the Schwann cell and in the Schmidt-Lanterman incisures, and Fbl6 in the Schwann cell cytoplasm (Figure 39). From the flattened, confocal image the localisation of the Fbl6 looks to be peripheral to periaxin localisation. However, when confocal images of mouse sciatic nerves are taken in cross-section, it is clear that this is due to the non-cylindrical distribution of Schwann cell cytoplasm (Figure 40 and Figure 41). Periaxin is localised in areas where there is little underlying cytoplasm, and bulges of Fbl6-filled cytoplasm lie in between these areas. Thus,

taking planes through this non-cylindrical structure, and superimposing the pictures, give the erroneous impression that Fbl6 is located peripheral to the position of periaxin (Figure 41).

5.2. Developmental expression of Fbl6

As the Fbl6 antibody is not specific on westerns, I took sections of mouse sciatic nerve from ages postnatal day 2 (P2), P10, P21 and sections through embryonic hindquarter at embryonic day 14.5 (E14.5). At each of these ages, Fbl6 expression was seen in the cell bodies of Schwann cells. Thus, Fbl6 is expressed at a time when it could be involved in the regulation of periaxin, as periaxin is expressed in Schwann cells from day E13.5-14.5.

5.3. Transfection Experiments

Cos-7 cells permanently expressing periaxin were generated and grown up from a single clone under the selection of geneticin. Periaxin expression was not uniform in these cells, but many cells were expressing periaxin at a detectable level by immunofluorescence. Three constructs were made to investigate the interaction of periaxin and Fbl6 in vivo. The first construct contained the full-length Fbl6 sequence with an N-terminus Flag tag, the second was the same with a C-terminal Flag tag and the third consisted of clone 26a with an N-terminal Flag-tag. Each was under the control of a CMV promoter. Sylvia Vasiliou generated clone 26a which contains amino acids 122-487 of Fbl6, incorporating the leucine rich repeat region, but not the F-box (Figure 42). Thus, the protein generated by this construct would theoretically be able to bind L-periaxin but not target it to the SCF complex for ubiquitination.

These constructs were transiently transfected into the permanently L-periaxin expressing Cos 7 cells with the aim of assessing the levels of L-periaxin in the transfected cells, and its localisation. The success of transfection was assessed by growing transfected cells on coverslips and carrying out immunofluorescence with an anti-Flag antibody. There were very few Flag-positive cells found after transfection, in spite of a high transfection efficiency with a control plasmid. Thus, this was thought to be due to a low stability of Fbl6 as F-box proteins themselves can

also be ubiquitinated and degraded in the proteasome pathway (Galan and Peter, 1999; Xirodimas et al., 2001). Lactacystin, a proteasome inhibitor, was added to the culture medium after transfection, and this improved the number of Flag-positive cells seen by a factor of three and allowed the visualisation of Fbl6 and periaxin in the same cell.

Cells transfected with full-length Flag-tagged Fbl6 (N-terminus) showed targeting of Flag labelling to the nucleoli. In cells also expressing L-periaxin, L-periaxin was not seen in these nucleoli (Figure 43). Transfection with the Flag-tagged 26a construct showed no increase in stability of the protein with the addition of lactacystin, and Flag labelling was not directed to the nucleoli (Figure 44).

5.4. Discussion

It is traditionally taught that a myelinated nerve forms a symmetrical, cylindrical uniform structure in the internodes, like the common analogy of insulation on wires. However, Ramon y Cajal identified an apparent cobblestone effect on the surface of myelinated nerves, and recently it was described that periaxin and its binding partner DRP2 are clustered in patches at the myelinated nerve surface, over cytoplasmic-poor areas, with cytoplasmic-rich areas in between (Sherman et al., 2001). It is now clear that Fbl6 is predominantly localised in these cytoplasmic bulges in Schwann cells. The reason for this complex architecture is open to speculation. Periaxin underpins the DRP2-dystroglycan complex which may stabilise the Schwann cell by its interaction with the basal lamina externally and with the actin cytoskeleton internally. It is unclear why large quantities of cytoplasm are excluded from these areas, but it is clear that the cytoplasm of a cell is not a homogeneous structure, but has well regulated areas with structural and functional differences. The Schwann cell is already known to be an excellent example of this due to its formation of the compact myelin sheath. Perhaps the exclusion of large quantities of cytoplasm from these areas where the periaxin/DRP2 complex lies is to allow closer contact of the compact myelin sheath to its anchor in the basal lamina, and so promote stability further. This might make the compact myelin sheath more resistant to shear forces. We also know that these complexes do not cluster in periaxin-null mice, and demyelination occurs, possibly through this lack of stability (Sherman et al., 2001).

An alternative hypothesis is that Fbl6 is predominantly removed from these areas as Fbl6 targets L-periaxin for degradation via the ubiquitination pathway. Thus, spatial separation of these molecules may play a role in the regulation of periaxin breakdown.

In transfected Cos7 cells, Fbl6 appears to be predominantly targeted to the nucleoli, whereas the sequence without the F-box domain (26a) is absent from these structures. When L-periaxin is transfected into the same cells, it is mislocalised, in that it is found both in the cytoplasm and the nucleus, but the not the nucleoli, rather than associated with the membrane, as in Schwann cells. This mislocalisation of periaxin is thought to be due to the absence of the DRP2-dystroglycan complex in the cell membrane of these cells, so L-periaxin is not targeted to these areas. It is possible that Fbl6 is localised in a different area of the transfected cell compared with its in vivo localisation for similar reasons.

Fbl6 contains two sequences which may be nucleolar targeting sequences: QLQRL (amino acids 187-191) and ALQRG (amino acids 314-318). The optimal nucleolar targeting sequence is thought to be the highly basic sequence RRQRR with the most important amino acids being the QR (Scott et al., 2001). However, these sequences are also present in the clone 26a, which is not targeted to the nucleolus. Other work has shown that proteins may be targeted to the nucleolus not only by endogenous target sequence, but also via other interacting proteins (Henderson et al., 1995). In Schwann cells, the interaction of Fbl6 with other members of the SCF complex and with its target proteins may localise the protein to the cytoplasm, yet in cell lines these mechanisms may not all be in place, hence the disparity of localisation.

Ribosomal proteins and proteins involved in ribosomal RNA proteins are located in the nucleolus. However, an increasing number of other proteins are also found to be localised in the nucleolus, including proteins involved in cell cycle and growth regulation, DNA protective factors and recognition factors regulating translation on cytoplasmic ribosomes (Carmo-Fonseca, 2002).

E3 ubiquitin ligase proteins have also been found to be localised to the nucleolus in cell culture systems. The E3 ubiquitin ligase Mdm2 ubiquitinates the tumour

suppressor gene p53, targeting it for degradation by the proteasome in response to hyperproliferative signals such as activation of the myc oncogene. This process is antagonised by another tumour suppressor protein ARF, thereby stabilising p53. ARF is predominantly localised in the nucleolus, while Mdm2 and p53 are mostly nucleoplasmic. Export of Mdm2/p53 complexes is required for p53 degradation in the cytoplasm. However, when Mdm2 was transfected into H1299 cells, in the presence of a proteasome inhibitor, it was shown to accumulate in the nucleoli. This was also shown to happen when Mdm2 and p14ARF were co-transfected into cells, suggesting that the appearance in the nucleoli was related to the increase in levels of Mdm2. Similarly, the nucleolar localisation of Mdm2 was decreased by overexpression of its substrate p53 (Xirodimas et al., 2001). ARF may sequester Mdm2 in the nucleoli, preventing the interaction of p53 and Mdm2, and allowing accumulation of p53 in the nucleoplasm, consistent with its role as a tumour suppressor protein (Weber et al., 1999) and inhibiting export of p53/Mdm2 complexes from the nucleus to the cytoplasm (Tao and Levine, 1999; Zhang and Xiong, 1999). Tumour-associated mutations in ARF disrupt both its nucleolar localisation and its ability to stabilise p53 (Weber et al., 1999; Zhang and Xiong, 1999). However, more recently, mutant forms of ARF have been described that do not accumulate in the nucleolus and yet retain the ability to stabilize p53. Hence it may be that the small quantity of nucleoplasmic ARF is the functionally active protein (Llanos et al., 2001). It is thought that sequestration of Mdm2 in the nucleolus may still play a part in inactivating Mdm2 in response to some p53-activating signals. Mdm2 has been found to contain a cryptic nucleolar localisation signal that does not function in unstressed cells, but in response to abnormal proliferative signals ARF is expressed and Mdm2 is necessary to cooperate with nucleolar localisation signals in ARF to allow relocalisation of both proteins (Lohrum et al., 2000).

Another putative E3 ubiquitin ligase was also found to localise to the nucleoli in embryonic stem cells, colocalising with small nucleolar RNP proteins (snRNP) (Tate et al., 1998).

It may be that the Fbl6, which forms part of the SCF complex E3 ligase, is localised in a similar manner. Thus, overexpression of Fbl6 in transfected Cos-7 cells allows targeting to the nucleolus, whereas endogenous Fbl6 in vivo in Schwann cells is mainly cytoplasmic. Fbl6 may be sequestered in the nucleoli in this system, to prevent the interaction with L-periaxin, which is present in the nucleoplasm and it may be that the lower amount of nucleoplasmic Fbl6 is the functionally active protein, directing ubiquitination of periaxin. As the 26a construct, lacking the N-terminal of Fbl6 including the F-box domain, does not localise to the nucleolus, it suggests that this region is required for this targeting, either directly, through an as yet unrecognised nucleolar targeting sequence or by interaction with another protein which performs this function.

There is a precedent for F-box proteins to be intrinsically unstable. Epitope-tagged Cdc4p and Grr1p, F-box proteins involved in regulating the cell cycle in yeast, have half lives of only 5 minutes and 15 minutes respectively when expressed in yeast cells. If a proteasomal inhibitor was added to the culture system, Grr1p levels were shown to stabilise on a Western blot. Ubiquitinated forms of Grr1p and Cdc4p were detected, and ubiquitination required all the core components of the SCF complex indicating that ubiquitination of the F-box occurs via an autocatalytic mechanism. A mutant form of Grr1p lacking the F-box was intrinsically stable in yeast, unaffected by use of the proteasome inhibitor, and not degraded in an ubiquitin-dependent manner. Thus the autocatalytic mechanism relies on an intact F-box (Galan and Peter, 1999). My experiments indicate that Fbl6 is also intrinsically unstable, and as stability of Flag labelling in Flag-Fbl6 transfected cells is enhanced by use of the proteasomal inhibitor lactacystin, they also suggest that Fbl6 is degraded via the ubiquitin/proteasomal pathway. The mutant protein 26a is unaffected by the use of lactacystin similarly to the mutant Grr1p mutant missing the F-box region, suggesting that Fbl6 is also degraded in an autocatalytic manner within the SCF complex requiring an intact F-box domain.

FIGURE 36 – Fbl6 INTERACTS WITH PeriC1 AND PeriA7

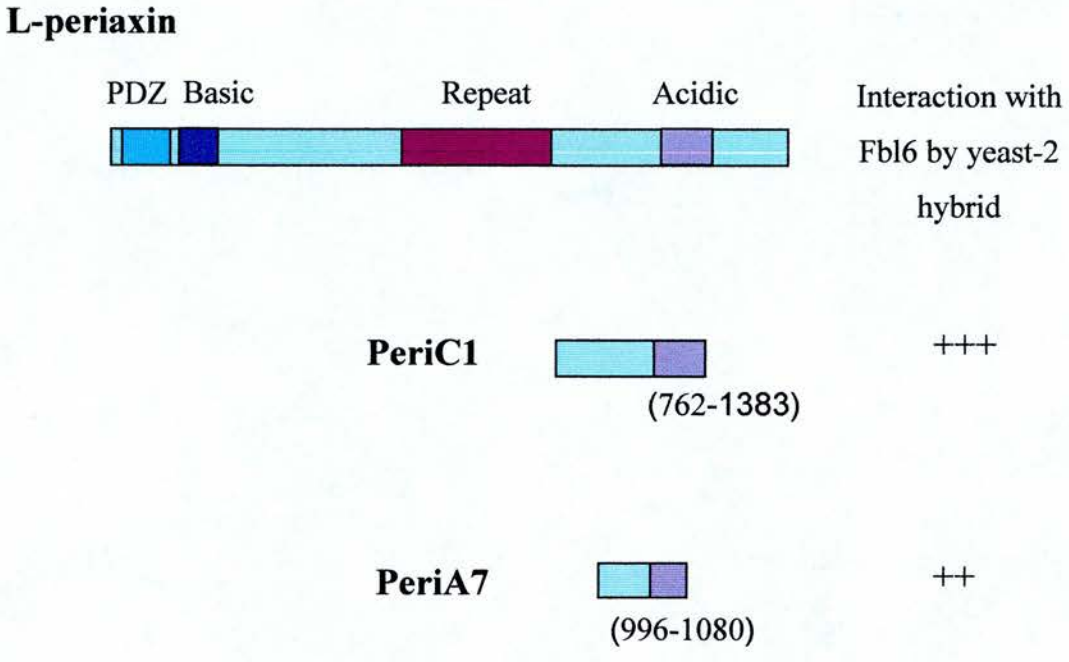

Fbl6 was found to interact with the construct PeriC1 in a yeast - 2 hybrid screen. PeriA7 is the smallest construct tested that still interacts with Fbl6 in this system.

(Vasiliou in preparation)

FIGURE 37 - AMINO ACID SEQUENCE OF RAT Fbl6

MAPVAPGRVRRRVRGSKRPDARGRSAEDWWWDRLAPRGSGYHLLQADSMLLVLPDL
EPTRARAHRRAPRRAPRSLARGPTAVAKPRAKPRPEPSLDQGLDSGWGDRIPLEVL
VHTFGLLVAAHGPMPFLGRAARVCRHWHEATSHPSLWHTVTLSPALVGRAAKGNLK
GEKKLLACLEWLIPNRFSQLQRLTLIHWKSQVHSVLELVSKFCPRLTFLKLSDCHG
VTAETLVMLAKACCQLHSLDLHHSMVESTAVVSFLEEAGSRMRRLWLTYSSQTTAI
LGALLGNCCPQLQVLEVSAGMSCNNTPLQLPVEALQRGCPQLQVLRLLNLIWLPKP
CGRGAPQGPGFPSLEELCLAGSTCSFVSNEVLGRLLHCSPKLRLLDLRGCARITPT
GLCHLPCQELEQLYLGLYGMSDGLALAKDGSPLLTQKWYHTLRELDFSGQGFSEKD
LEQALAVFSGTTEGLPPALCSLNLRGTRVTPSTVSSVISSCPGLLYLNLESCRCLP
RGLKRAYRGLEEVQWCLEQLLTSPPSSREST*

Amino acid sequence of rat Fbl6 with F-box domain (green) and Leucine-rich repeat domain (blue). The red letters indicate the amino acids fused to GST to make the Fbl6 antibody.

FIGURE 38 - ALIGNED AMINO ACID SEQUENCE OF RAT, MOUSE AND HUMAN Fbl6

```
rat     1 MAPVAPGRVRRRVRGSKRPDARGRSAEDWWWDRLAPRGSGYHLLQADSMLLVLPDLEPTR 60
mouse   1                                                MLLVLPDLEPPR 12
human   1 MAAPASRQVRRRARAAPRP----RSAEDWWWDRLAPRGSGYHLLQSDSMLLVLSEPGPAR 56
                                                         ***** .  * *

rat    61 ARAHRRAPRRAPRSLARGPTAVAKPRAKPR-----------PEPSLDQGLDSGWGDRIP108
mouse  13 ARAHRRARRRAPRSLARGPTAVAKPRTKPR-----------PEPSLDQGLDSGWGDRIP 60
human  57 PRAQRRASRRTPRQPPRGPSAAAKPKAGLRSEAAAAPAPAPAPTPTPEEGPDAGWGDRIP116
          **.*** **.**   ***.* ***..  *           * *. ..* *.*******

rat   109LEVLVHIFGLLVAAHGPMPFLGRAARVCRHWHEATSHPSLWHTVTLSPALVGRAAKGNLK168
mouse  61 LEVLVHIFGLLVAAHGPMPFLGRAARVCRHWHEATSHPSLWHTVTLSPSLVGRAGKGNLK120
human 117LEILVQIFGLLVAADGPMPFLGRAARVCRRWQEAASQPALWHTVTLSSPLVGRPAKGGVK176
          **.**.******** **************.*.**.*.*.********  ****  **..*

rat   169 GEKKLLACLEWLIPNRFSQLQRLTLIHWKSQVHSVLELVSKFCPRLTFLKLSDCHGVTAE228
mouse 121GEKKLLACLEWLVPNRFSQLQSLTLIHWKSQVHSVLELVSKFCPRLTFLKLSDCHTVTAE180
human 177AEKKLLASLEWLMPNRFSQLQRLTLIHWKSQVHPVLKLVGECCPRLTFLKLSGCHGVTAD236
           ******.****.******** ********** ** **   ********** ** ***.

rat   229 TLVMLAKACCQLHSLDLHHSMVESTAVVSFLEEAGSRMRRLWLTYSSQTTAILGALLGNC288
mouse 181TLVMLARACCQLHSLDLHHSMVESTAVVSFLEEAGSRMRKLWLTYSSQTTAILGALLDNC240
human 237ALVMLAKACCQLHSLDLQHSMVESTAVVSFLEEAGSRMRKLWLTYSSQTTAILGALLGSC296
          .*****.**********.*********************.****************  *

rat   289 CPQLQVLEVSAGMSCNNTPLQLPVEALQRGCPQLQVLRLLNLIWLPKPCGRGAPQGPGFP348
mouse 241CPQLQVLQVSTGMNCNNTPLQLPVEALQKGCPQLQVLRLLNLIWLPKPCGRGVPQGPGFP300
human 297CPQLQVLEVSTGINRNSIPLQLPVEALQKGCPQLQVLRLLNLMWLPKPPGRGVAPGPGFP356
          *******.**.*.  *  **********.*************.***** ***   *****

rat   349 SLEELCLAGSTCSFVSNEVLGRLLHCSPKLRLLDLRGCARITPTGLCHLPCQELEQLYLG408
mouse 301SLEELCLAGSTCNFVSNEVLGRLLHRSPKLRMLDLRGCARVTPSGLCHLPCQELEQLYLG360
human 357SLEELCLASSTCNFVSNEVLGRLLHGSPNLRLLDLRGCARITPAGLQDLPCRELEQLHLG416
          ******** *** ************ ** **.********.**.**  ***.***** **

rat   409 LYGMSDGLALAKDGSPLLTQKWYHTLRELDFSGQGFSEKDLEQALAVFSGTTEGLPPALC468
mouse 361LYGISDGLTLAKDGSPLLTRKWYHTLRELDFSGQGFSEKDLEQALAVFSGTPGGLHPALC420
human 417LYGTSDRLTLAKEGSPFLTQKWCHTLRELDLSGQGFSEKDLEQALAAFLSTPGGSHPALC476
          *** ** *.***.*** **.** ******* *************** *  *  *  ****

rat   469 SLNLRGTRVTPSTVSSVISSCPGLLYLNLESCRCLPRGLKRAYRGLEEVQWCLEQLLTSP528
mouse 421SLNLRGTRVTPSTVSSVISGCPGLLYLNLESCRCLPRGLKRVYRGLEEVQWCLEQLLTSP480
human 477SLNLRGTRVTPSTVSSVISSCPGLLYLNLESCRCLPRGLKRAYRGLEEVQWCLEQLLTSP536
          ****************** ********************* *****************

rat   529 -PSSRESTNLKTAPRFALP 546
mouse 481-PSAKEPT            487
human 537SPS                 539
           **
```

Aligned amino acid sequence of rat, mouse and human Fbl6 indicating the first methionine in rat and human, compared to that in mouse.

FIGURE 39 - IMMUNOFLUORESCENCE ON TEASED FIBRES OF MOUSE SCIATIC NERVE SHOWING Fbl6.

a, b, c: Fbl6 labels the Schwann cell cytoplasm (a) and periaxin labels the abaxonal membrane (b), with little co-localisation (c).

Scale bar 5.5μm.

d, e, f: Fbl6 labelling (d) co-localises with S100 labelling (e) in the Schwann cell cytoplasm (f).

Scale bar 8μm.

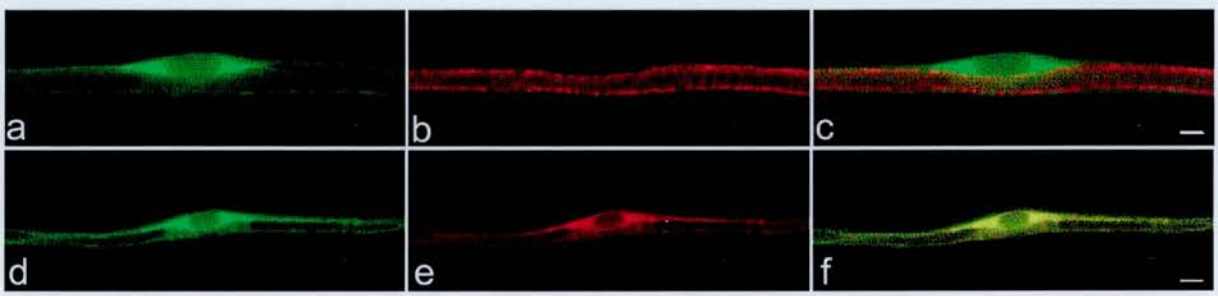
a
b
c
d
e
f

FIGURE 40 – IMMUNOFLUORESCENCE ON CROSS-SECTION OF MOUSE SCIATIC NERVE SHOWING Fbl6

Immunofluorescence study of a cross-section of mouse sciatic nerve showing Fbl6 labelling (green) in the Schwann cell cytoplasm and periaxin labelling (red) in clusters in-between this labelling. The continuous brighter periaxin staining represents sections through Schmidt-Lanterman incisures.

Scale bar 7.5μm.

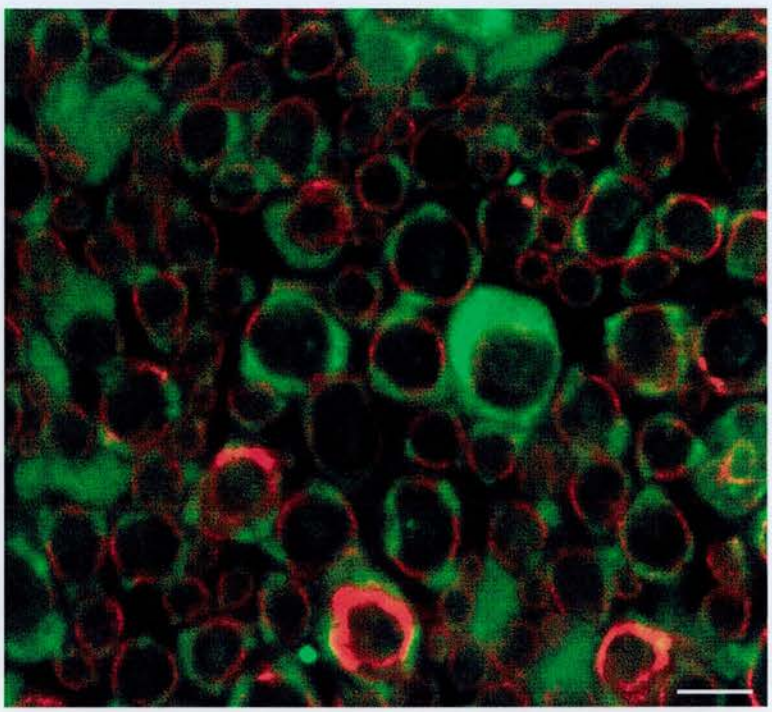

FIGURE 41 – LOCALISATION OF Fbl6 IN SCHWANN CELLS

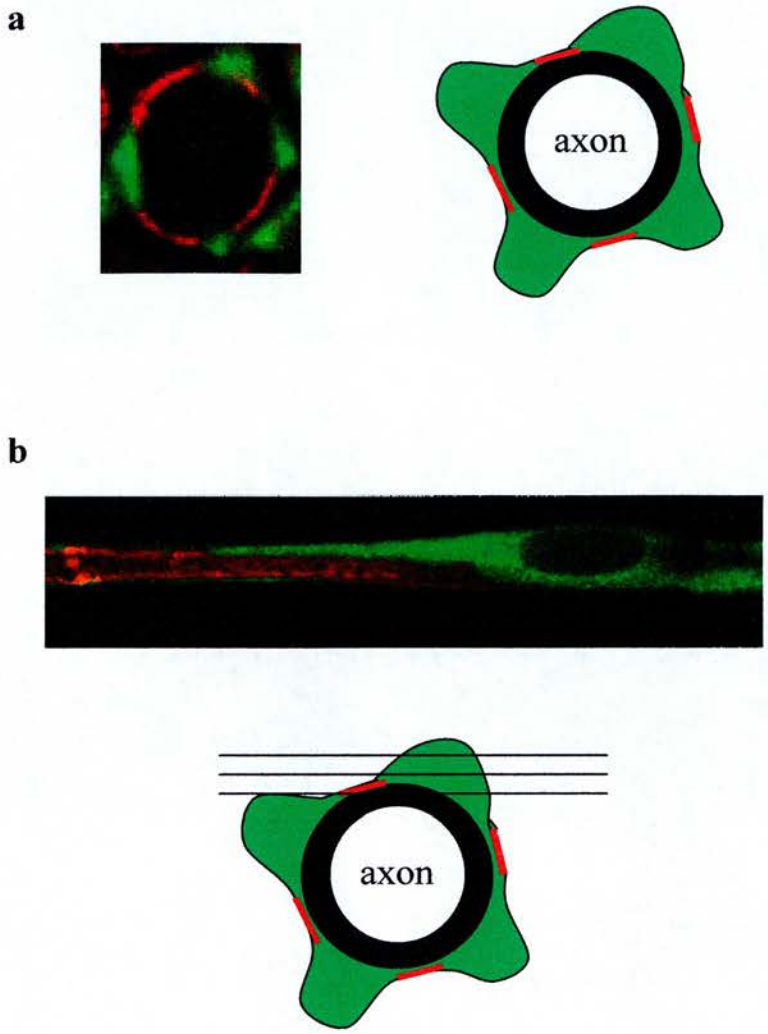

a: Cross-section of a myelinated axon showing periaxin labelling (red) and Fbl6 labelling (green). This is illustrated in the diagram, indicating clustering of periaxin and DRP2 with cytoplasmic rich areas in-between.

b: Labelling of periaxin (red) and Fbl6 (green) in a teased fibre of sciatic nerve appears to show Fbl6 labelling outside of periaxin labelling. However, the diagram shows that the photograph is constructed from multiple photographs taken at planes through the axon and merged. Thus, this impression is produced by flattening an image of a non-uniform structure.

FIGURE 42 - RAT Fbl6 AND 26a PROTEINS

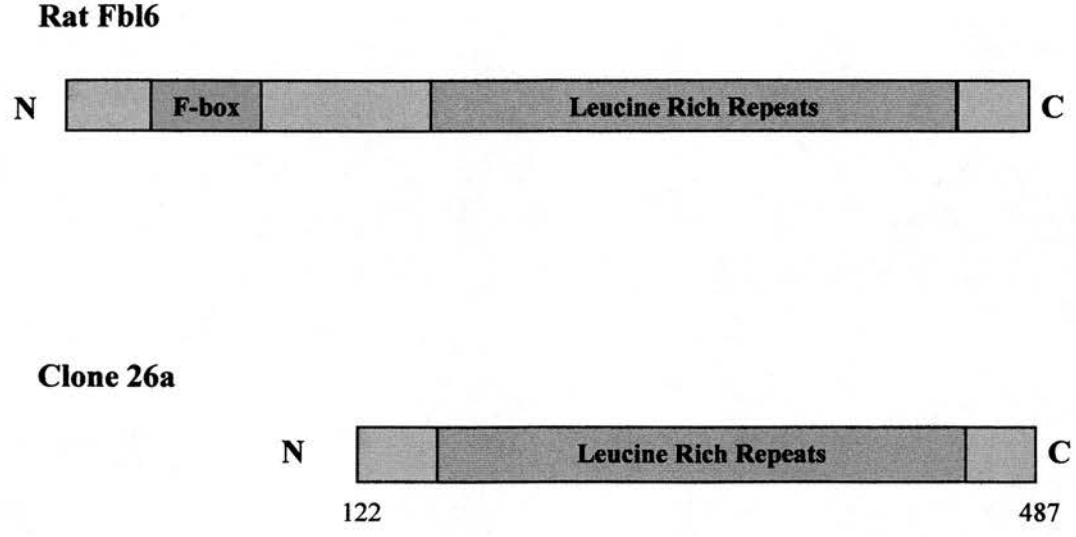

Diagrammatic representation of the rat Fbl6 protein showing the F-box and Leucine rich repeat domains. Clone 26a contains amino acids 122-487 of Fbl6, lacking the F-box domain.

FIGURE 43 - FLAG-TAGGED Fbl6 IS LOCALISED TO NUCLEOLI IN TRANSFECTED COS-7 CELLS.

a, b, c: In this permanently expressing Cos-7 cell, periaxin is localised to the cytoplasm and nucleus (a), but Fbl6 is localised to the nucleus and nucleolus (b). Merged picture in (c).

d, e, f : Periaxin is localised to the nucleus, and not the nucleoli (d), where Fbl6 is seen (e). Merged picture in (f).

g, h, i : Again, periaxin is present in the nucleus (g) with Fbl6 located in the nucleoli and the cytoplasm (h). Merged picture in (i).

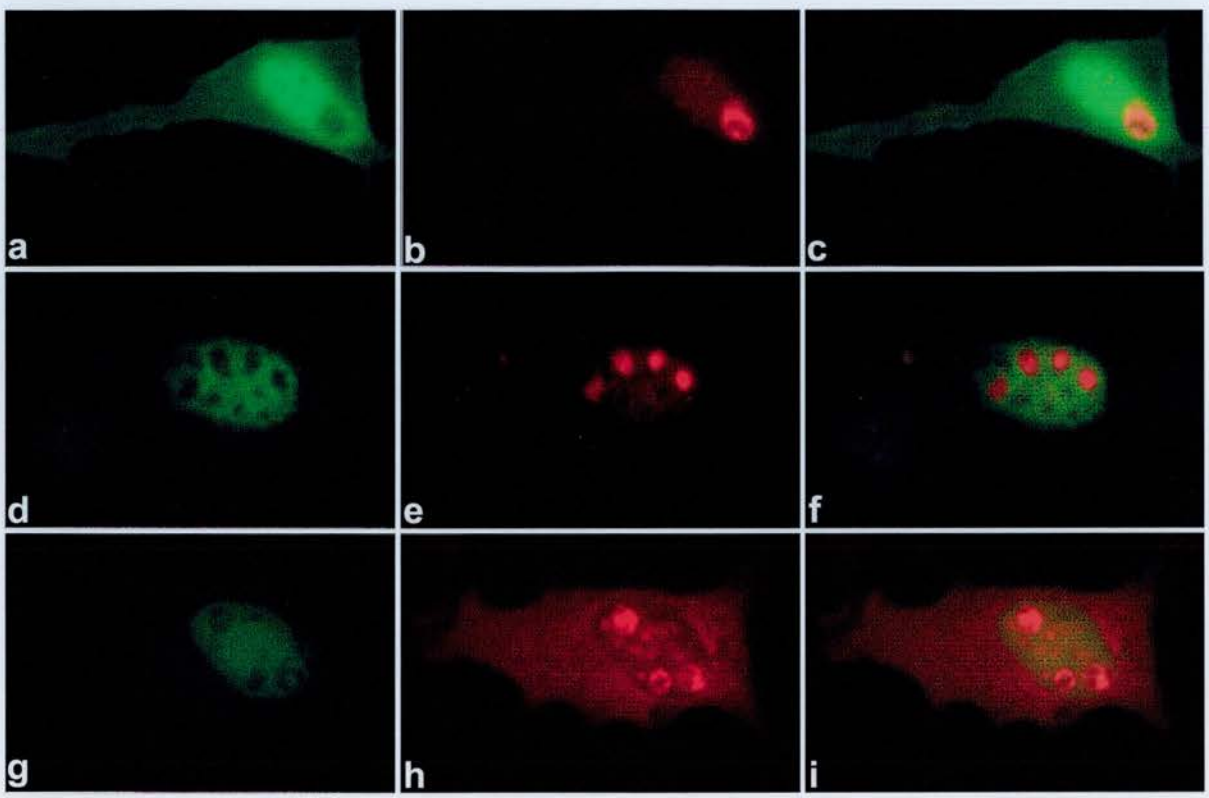
a
b
c
d
e
f
g
h
i

FIGURE 44 - FLAG-TAGGED 26a DOES NOT LOCALISE TO NUCLEOLI IN TRANSFECTED COS-7 CELLS.

a, b, c : Three transfected cells showing the distribution of Flag-tagged 26a in the cytoplasm, and nucleus but not the nucleoli. These cells were grown in the absence of lactacystin.

d, e, f : A cos-7 cell permanently transfected with periaxin present in the nucleus and cytoplasm (d), and transiently transfected with 26a, which is present mainly in the cytoplasm and not localised to the nucleoli (e). Merged picture in (f). This cell was grown in the presence of lactacystin.

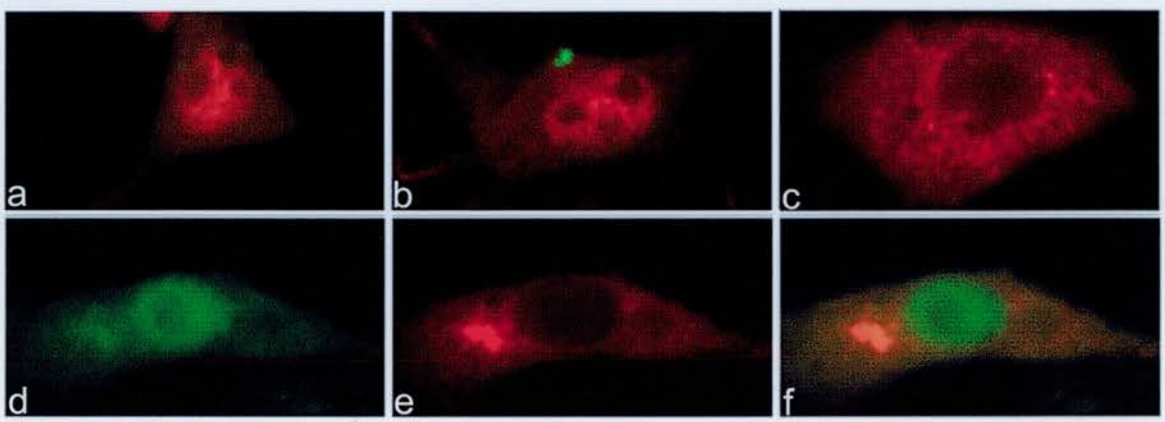
a
b
c
d
e
f

6. DISCUSSION

The discovery of mutations in the human *PERIAXIN* gene that cause CMT disease expands the classification of CMT disease subtypes. The position of the mutations in the L-periaxin protein that produce truncated proteins has helped in the understanding of the function of periaxin, since we now know that binding to DRP2 is not sufficient to rescue the Schwann cell from demyelination. As yet, none of the truncated proteins formed by the mutations are likely to be able to bind the F-box protein Fbl6 so it will be interesting to see whether mutations are described further towards the C-terminal of the periaxin protein. This will help us determine whether there are other interactions of the periaxin protein that are important in maintaining myelination.

The antibodies generated by the group have been invaluable in characterising these mutations. We can use these antibodies in a quick and simple test to screen potential patients by immunofluorescence by looking for truncated Periaxin protein in peripheral nerve biopsy material.

Much effort has been put into making genotype and phenotype correlations within CMT disease but with limited success. There are phenotype differences between patients who have the same mutation in the same causal gene between unrelated families (Thomas et al., 1997). There are also intrafamily differences in phenotype, in that different siblings with the same mutation are variably affected (Auer-Grumbach et al., 2000a; Senderek et al., 2001). This suggests that the CMT phenotype is not only reliant on a mutation in the causal gene, but on genetic background and environmental influences.

The genetic background in mice is known to affect the phenotype of transgenic mice (Dubois et al., 2002; Shusterman et al., 2002). Thus, transgenic mice can be bred onto different backgrounds to investigate phenotype modulating genes. Microarray analysis of gene expression in mice transgenic for CMT genes with different genetic backgrounds may help identify modifying factors determining the vulnerability of Schwann cells and axons to the CMT mutation leading to the CMT phenotype.

Similarly this could be performed in human monozygotic twins or patients with identical mutations but disparity of phenotype.

There are reports of CMT disease occurring in human monozygotic twins, where genetic background is identical. Two pairs of identical twins were studied with *PMP22* duplication (Garcia et al., 1995), and another pair with a novel *P0* mutation (Marques et al., 1999), and each pair showed variation in clinical expression between siblings. This variation included age of onset of the disease, degree of disability, presence or absence of sensory symptoms and neurophysiological test results. The phenotype differences in these patients with identical genetic backgrounds suggest that the expression of these mutations is susceptible to external, non-genetic influences that modulate the CMT phenotype.

If environmental modulators influence phenotype, what could these be? Nutrition may have an influence, as nutritional deficiency, for example of vitamin E, is known to cause acquired peripheral neuropathy (Martinello et al., 1998). Thus, minor nutritional changes in susceptible individuals may change the time of onset of the disease, and its severity. Functional use of neurones has also been associated with vulnerability to damage and death. Motor activity enhances the peripheral nerve toxicity of lead (Ray, 1997). In models of Amyotrophic Lateral Sclerosis (ALS), glutamate excitation of neurones contributes to neurodegeneration (Cluskey and Ramsden, 2001). Hence, difference in phenotype in CMT disease may be associated with differences in nerve activity.

There are too few mutations in the *PERIAXIN* gene to allow any meaningful phenotype-genotype correlations at present. The human disease appears variable with both severe phenotypes (Boerkoel et al., 2001b; Takashima et al., 2002) (Dejerine-Sottas disease) and milder forms described (Guilbot et al., 2001; Takashima et al., 2002). The mouse phenotype within the mouse strain C57BL/6 is much less variable, though these mice appear to be affected at a later age than may be expected from correlation with the human condition, substantiating the argument for the role of genetic background in the production of the phenotype.

However, the human condition has a prominent sensory disturbance compared to patients with most other forms of CMT disease. There is pathological evidence to substantiate this from work with the periaxin-null mouse. Experiments have suggested selective vulnerability of sensory nerves compared to motor nerves in the periaxin-null mouse. In this mouse, at six months of age, there is more loss of myelinated axons in the pure sensory nerves (saphenous and dorsal roots) than in the pure motor nerves (quadriceps and ventral roots) (Sherman et al., in preparation). There is no evidence that unmyelinated fibres, that carry most pain and temperature sensation, are affected in the periaxin-null mouse. The mechanism for the increased sensory nerve vulnerability is unknown, but there are precedents for differential vulnerability of motor and sensory neurones in disease.

Motor neurones are specifically damaged in motor neurone disease. In ALS, putative mechanisms for this specificity in nerve degeneration include persistent viral infection, glutamate-mediated excitotoxicity, oxidative stress, altered neurofilament and peripherin expression, disrupted axonal transport, neurotrophin deficiency and mitochondrial dysfunction (reviewed in (Cluskey and Ramsden, 2001)). Familial ALS accounts for approximately 10% of patients, and 20% of these have mutations in the gene encoding cytosolic Cu/Zn superoxide dismutase (SOD1). The mutant SOD1 causes neuronal degeneration by a gain of toxic property (Cleveland and Rothstein, 2001). Although these mechanisms are not unique to motor axons, selective disruption of the motor axons can be explained by the increased energy requirements of long, large diameter motor axons and so their heightened vulnerability to insults. There may also be a glial role in the neurodegeneration of ALS, as astrocytes also express mutant SOD1. Selective expression of a mutant form of SOD1 (G85R) in astrocytes provoked glial pathology but not motor neurone death, indicating that only part of the toxicity is derived from glia (Gong et al., 2000).

Other diseases are selective for the sensory peripheral nerves. A variety of chemotherapy drugs cause acquired peripheral neuropathy, as a side-effect. Vincristine is a Vinca alkaloid which binds intracellular tubulin. This leads to oedema of the fast and slow conducting axons, and dorsal root ganglion (DRG) cell

damage, manifesting as a painful and primarily sensory neuropathy (Postma et al., 1993). Cisplatin, a platinum compound, has a predilection for sensory nerves. This drug forms intra- and interstrand crosslinks in DNA, inducing apoptotic cell death in dividing cells, but it may also act in peripheral nerve by a disturbance of axonal transport. It is not clear why platinum compounds affect sensory nerves and spare the motor nerves, however, it may be related to the preferential accumulation of the drug in DRG cells. Damage to these cells prevents repair once the drug is removed. Pathologically, the small and thinly myelinated axons are most affected (Quasthoff and Hartung, 2002). Suramin is another chemotherapeutic agent, which acts by inhibiting growth factors and by blocking P2 purinergic receptors, which are divided into two subtypes: the metabotropic P2Y and the ionotropic P2X receptors. In the PNS, P2X receptors are found on DRG neurones and P2Y receptors on Schwann cells (Wachtler et al., 1996). Activation of these P2 receptors induces intracellular calcium ion transients which play an important role in intracellular signal transduction pathways (Mayer et al., 1998). Pathology shows demyelination with axonopathy, and sensory symptoms are much more frequent than motor.

In the periaxin-null mouse, the increased sensory fibre loss is equally not explained. It may be that sensory fibres, with smaller diameter fibres and with corresponding thinner myelinated sheaths are either more prone to demyelination or to sustaining permanent damage after demyelination. Periaxin-null sensory nerves may be more vulnerable due to their cell bodies lying in the dorsal root ganglia, outside of the central nervous system, thus they are proportionately more reliant on Schwann cells as their glial support. In comparison, motor neurones, whose cell bodies lie in the anterior horn of the spinal cord, use proportionately more oligodendrocytes for glial support, which do not express periaxin. Sensory nerves may have different axon-Schwann cell interactions than motor nerves, which may confer the properties of a small axon diameter and a thin myelin sheath, but also may confer vulnerability to damage in the absence of periaxin.

Behavioural tests in periaxin-null mice substantiate the pathological findings as there is evidence of an early sensory disturbance. At six weeks of age these mice show behaviour suggestive of neuropathic pain with allodynia in response to mechanical

stimulation with Von Frey hairs, and thermal hyperalgesia, in spite of a normal mechanical grip test. These sensory disturbances were abrogated by intrathecal injection of NMDA antagonist, suggesting that a central sensitisation occurs in response to disruption of the myelin sheath (Gillespie et al., 2000).

Initially, periaxin-null mice develop an apparently normal myelin sheath, thus periaxin is not prerequisite for myelination in development. However, it is not fully understood why both in these mice, and in the comparable human CMT diseases, demyelination should occur later. Our morphology experiments addressed this issue, as it was speculated that periaxin was required for remyelination after demyelinating damage, as this may not exactly recapitulate developmental myelination. These experiments clearly showed the ability of periaxin-null Schwann cells to remyelinate crushed, regenerated sciatic nerve at six weeks of age, but the periaxin-null Schwann cells failed to limit the thickness of the regenerated myelin sheath. Hypermyelination is thought to be the forerunner of massive demyelination, but it may also lead to axonal loss, in addition to that generated by several rounds of demyelination and remyelination. There is clinical evidence that much of the disability from CMT disease occurs when axons are lost, rather than purely through demyelination, which probably explains the lag of symptomatology behind pathology in humans (Krajewski et al., 2000; Sahenk, 1999). We also know that there is considerable interaction between the Schwann cell and the axon to maintain the health of both. Myelination controls the phosphorylation of neurofilament within axons, and we know that in trembler mice, a point mutation in *Pmp22* causes a change in neurofilament phosphorylation, increased neurofilament density and decreased axonal transport (de Waegh et al., 1992). Conversely, myelin sheaths are not sustainable in the absence of axons. It is not clear how myelin thickness is controlled, but a clue may be present in the binding of L-periaxin to DRP2 in the DRP2/dystroglycan complex at the Schwann cell membrane, linking in to the basal lamina. These complexes are clustered in areas of the abaxonal membrane of the Schwann cell overlying cytoplasmic poor regions, thus presumably anchoring the compact myelin sheath more strongly by bringing it closer to the basal lamina and therefore making it more resistant to shear forces. It may also function as a signalling complex, perhaps controlling the number of myelin lamellae. In periaxin-null mice,

these complexes are not able to cluster, making the Schwann cell more structurally vulnerable. There is no expression of periaxin in the CNS, and one can speculate that this is because of the absence of a basement membrane here, thus making its anchoring/signalling function redundant. Thus, the later onset of demyelination in periaxin-null mice and their human counterparts may be related to an accumulation of damage to the myelin sheath via reduced mechanical stability and an alteration in the correct communication between Schwann cell and axon necessary to produce an appropriately sized myelin sheath, and a healthy axon and Schwann cell. Although periaxin-null Schwann cells can remyelinate axons, the repeated cycle of demyelination and remyelination may fail with age, either due to a reduced ability of Schwann cells to remyelinate with age, or because of increased axonal loss, which prevents remyelination. There is evidence of reduced nerve repair potential with age in mice. When nerve grafts were used from young rats to repair femoral nerve transection in old rats, preferential reinnervation of motor pathways by motor axons was vigorous, compared to using grafts from older rats in old rats (Le et al., 2001). Nerve grafts rely on intact endoneural pathways for regenerating axons to grow down, and the presence of glial cells, and so this disparity of repair potential with age may reflect glial cell competence. It may be that periaxin-null Schwann cells 'age' early accounting for the lack of successful repair later. This could be tested by doing the same sciatic nerve crush experiments in periaxin-null mice at a later age, to examine the remyelination potential.

In development, the transcription factor EGR2 activates periaxin expression (Nagarajan et al., 2001). However, the control of levels and localisation of periaxin later in development may be regulated by Fbl6 and the ubiquitin/proteasome pathway. Free L-periaxin, not bound to the membrane DRP2/dystroglycan complex, may bind Fbl6 in the cytoplasm and be targeted for degradation. L-periaxin that is not able to bind Fbl6 may be transported to the nucleus where it has unspecified downstream effects. It may act as a transcription factor regulating other genes encoding proteins involved in myelination, as it is present in the nucleus of Schwann cells prior to the expression of the myelin proteins P0, MBP and MAG (Scherer et al., 1995; Sherman and Brophy, 2000). The disparity in localisation of Fbl6 in Schwann cells in vivo and Fbl6 transfected into Cos-7 cells is yet to be fully

explained, but may be related to the mislocalisation of periaxin in Cos-7 cells due to the lack of the DRP2-dystroglycan complex, so failing to target L-periaxin to the membrane. Alternatively, the Fbl6 antibody labelling in sciatic nerve may be misleading. The antibody appears specific on immunohistochemistry, as the labelling in Schwann cell cytoplasm disappears when the antibody is blocked with the GST fusion protein used to raise the antibody. However, this cannot be checked fully as the antibody does not work on western blots. Formation of another Fbl6 antibody, currently in progress, may resolve this issue.

F-box proteins usually bind phosphorylated target proteins but although we know that L-periaxin has potential phosphorylation sites, we do not know whether this is the regulatory mechanism. Abnormalities in the molecules involved in this pathway may disrupt Schwann cell function, and so these molecules, including Fbl6, are candidate genes for as yet undefined CMT disease. The *DRP2* gene, located at Xq22.1, has been screened for mutations occurring in autosomal recessive CMT disease but as yet has not been linked to any families with CMT disease, at least in the 168 potential patients examined thus far (Takashima et al., 2002).

There is an underlying similarity between the phenotype and pathology in all types of demyelinating CMT disease and even considerable overlap with axonal CMT disease. This suggests that abnormalities in many parts of the network of molecules maintaining health and function in the Schwann cell and axon can produce the same end result of demyelination and axonal damage.

This work has shown the benefit of studying rare human disease and the cell biology and molecular genetics of Schwann cells, in increasing the knowledge of both.

7. FURTHER WORK

7.1. Human mutations

The characterisation of further *PERIAXIN* mutations in patients with CMT disease should help to define the functional areas of periaxin further as well as assisting in diagnosis.

Screening for truncated forms of Periaxin using our spectrum of antibodies would be a quick and simple way of screening for mutations in patients with autosomal recessive or sporadic forms of CMT disease. This becomes increasingly important as the number of autosomal recessive genes to screen increases. However, peripheral nerve biopsies, usually of the sural nerve, are associated with risk and morbidity. A sural nerve biopsy produces a permanently numb area on the side of the foot, which can generate neuropathic pain. An alternative would be to examine the myelinated nerves present in skin biopsies. This procedure is associated with much less risk and morbidity, leaving a small (4mm diameter), round scar which can be positioned under the arm, so it is less noticeable. Myelinated nerves are visible in both the dermis and epidermis of skin in both mouse and human by immunofluorescence using antibodies against neurofilament (labelling axons - Figure 45b and e), and periaxin (Figure 45a and d). Skin biopsies have been used occasionally in the diagnosis of CMT disease to provide nerve for electron microscopy (Ceuterick-de Groote et al., 2001). They have also been used to look for small fibre neuropathy in some cases of diabetic neuropathy and impaired glucose tolerance neuropathy where the density of intraepidermal nerve fibres is calculated (Griffin et al., 2001; Smith et al., 2001). Assays of nerve growth factors have been performed on skin biopsies in order to investigate the peripheral neuropathy associated with diabetes mellitus (Diemel et al., 1999; Kennedy et al., 1998). Immunohistochemistry has been carried out on skin biopsies from Leprosy patients showing a reduction in staining with antibodies to the pan-neuronal marker PGP (protein gene product) 9.5 in lesions (Facer et al., 1998). Thus, nerve tissue is available from skin biopsies. If a battery of antibodies was generated against the proteins involved in autosomal recessive CMT disease, then this technique may be extremely useful in providing a quick and

inexpensive screen directing the clinician to the correct gene involved with minimal discomfort to the patient.

7.2. Periaxin-null mouse nerve morphology

The morphological experiments showed that periaxin-null Schwann cells are able to remyelinate axons at the age of six weeks albeit producing hypermyelinated axons, due to an abnormal limit on myelin thickness. Although there are signs of attempts at remyelination later in life in both the mice and in biopsies from human CMT patients, permanent damage ensues, with axonal loss and demyelination. It is possible that the periaxin-null Schwann cells lose the ability to remyelinate with age, and so it would be interesting to perform the same experiment on older mice to test this hypothesis.

Further work is currently underway to quantify the loss of sensory and motor axons in periaxin-null mice with age. The sensory myelinated fibres appear more vulnerable than motor fibres, and counts of the DRG neurone number, and expression of ATF3, which is expressed in damaged axons, are helping to substantiate this. Unmyelinated fibres appear unaffected, and previous work in other forms of CMT disease concurs with this. In one case of autosomal recessive axonal CMT disease, there was a normal number of unmyelinated axons yet a decrease in myelinated axons (Barhoumi et al., 2001). Another patient, with CHD from a *PMP22* point mutation, showed an increase in the total area of the cross-section of the sural nerve, a decrease in number of myelinated fibres and a normal number of unmyelinated fibres (Simonati et al., 1999). Yet, these patients did not show a predominant sensory neuropathy and so we wish to investigate unmyelinated fibres in these mice at the electron microscopy level, as these C-fibres carry the sensations of pain and temperature.

7.3. Vectors constructed for future transgenic and targeted mice

7.3.1. Overexpression of Schwann cell molecules

The molecular architecture of the myelin sheath depends on a precisely regulated stoichiometry of myelin proteins. Naturally occurring and induced mutations reveal

the importance of correct gene dosage for normal myelination. Gain of an allele for proteolipid protein (PLP) causes the central nervous system myelinopathy Pelizaeus-Merzbacher disease, and gain of an allele for PMP22 causes CMT disease type 1A. Mouse models replicating the overexpression of PMP22 show a correlation between the level of PMP22 expression and the degree of demyelination and reduction in conduction velocity (Huxley et al., 1998). Contrived overexpression of the structural myelin protein P0 similarly disrupts myelination, in a dose-dependent manner. Transgenic mice, overexpressing P0 with a low and high copy number, showed a dose-dependent arrest of nerve development, ranging from transient hypomyelination, with mild overexpression, to inability of Schwann cells to segregate axons, with the highest overexpression. This dose dependent problem was reflected in their behavioural and neurophysiological phenotype (Wrabetz et al., 2000). P0 overexpression has not yet been found in human disease but the pathology in transgenic mice resembles congenital hypomyelinating disease. These studies suggest that caution is necessary in possible replacement gene therapy for CMT patients where a mutation predicts underexpression of P0 or PMP22, as precise regulation of expression would be essential to avoid additional myelin disruption.

No models of overexpression of non-structural Schwann cell proteins have yet been published. The importance of L-periaxin in its DRP2-dystroglycan complex in stabilising the myelinating Schwann cell membrane is clear. Overexpression of L-periaxin may disrupt this, but also may cause an alteration in signalling as excess L-periaxin may be transported to the nucleus by virtue of the nuclear translocation signal. In the future, it will be interesting to generate transgenic mice overexpressing L-periaxin to reveal down-stream genes and proteins involved in myelinating Schwann cell biology.

7.3.2. Transgenic mice overexpressing L-periaxin

In order to overexpress L-periaxin, mouse L-periaxin cDNA has already been linked to 9kb of MBP promoter including Schwann cell enhancer 1 (SCE1) obtained from Dr. A. Peterson's group in Montreal, Canada. This group had found that use of this sequence without the SCE1 conferred a high level of reporter gene expression in oligodendrocytes only, but addition of the SCE1 sequence also targeted expression to

Schwann cells (Forghani et al., 2001). Periaxin expression in the central nervous system has no obvious phenotype (Sherman and Brophy, 2000), probably as it is confined to the nucleus in oligodendrocytes. The expression of L-periaxin in oligodendrocytes can thus be used to check for expression of the transgene as well as detecting PCR products corresponding to L-periaxin cDNA rather than genomic DNA. We will determine the degree of overexpression of periaxin by doing quantitative western blots. The construct is ready for injection but these mice are yet to be made.

We might expect the overexpression of L-periaxin to disrupt the control of myelination in these mice. Overexpression of L-periaxin may alter the localisation of DRP2 and change the interaction between Schwann cell and basal lamina. Other Schwann cell constituents involved in myelination may also be disrupted by this transgene. MBP levels may be decreased, as regulatory proteins normally involved in controlling MBP expression may be redirected to control *Periaxin* transgene expression. Alternatively, MBP expression may be increased as the SCE1 element may enhance expression even at a distance. Krox-20 (EGR2) acts as a transcription factor regulating *MBP*, *L-PERIAXIN*, *MPZ*, *CX32*, *MAG* and *PMP22*. Therefore, by changing the balance of genes to regulate by introducing the transgene, the expression of the other proteins may alter which independently may lead to disruption of normal myelination. Thus, we should gain information on whether the correct stoichiometry of periaxin is necessary for the health and function of Schwann cells and information on the interactions of periaxin and other Schwann cell proteins involved in the pathogenesis of CMT disease.

7.3.3. Conditional Knock-outs

It is now possible to control the expression of genes in transgenic mice using a conditional and inducible system. There are two arms to this system.

Firstly, gene expression can be confined to a specific tissue by employing a tissue-specific promoter driving a Cre recombinase. The bacteriophage P1 Cre recombinase is a 38kD protein that recognises specific 34 base pair sequences called loxP sites and catalyses site-specific recombination between two loxP sites (Sternberg and

Hamilton, 1981). These two loxP sites are engineered within the gene of interest so that when Cre recombinase is activated, the gene is inactivated. This was employed to good effect in a paper disrupting the β1 integrin gene in transgenic mice (Feltri et al., 2002). Here, the Cre recombinase was driven by the MPZ promoter, so that it was activated at E13.5-14.5 when P0 expression is turned on, inactivating the β1 integrin gene in Schwann cells and causing a severe neuropathy with impaired radial sorting of axons.

Secondly, gene expression can be switched on and off using a tetracycline switch. The system uses a modified version of the tetracycline repressor protein from *Escherichia coli* fused to the transactivator region from VP16 protein of herpes simplex virus (called tTA) to control gene expression. The tTA binds to tet operator sequences (tetO) and activates transcription of the gene of interest placed under the control of tetO linked to a minimal CMV promoter (Gossen and Bujard, 1992). However, when tTA is bound to tetracycline it loses this ability. The system can be made tissue-specific by expressing the tTA protein under the control of a tissue-specific promoter. This system was used by Perea et al., (Perea et al., 2001) who put the tTA under the control of the PMP22 promoter, limiting its expression to Schwann cells. PMP22 was overexpressed under the control of the tTA, causing demyelination, but when the tetracycline was reintroduced, turning off overexpression of the transgene, myelination normalised, showing that the Schwann cells were poised to myelinate normally.

These systems can be combined to give an inducible system where a tetracycline-dependent switch activates Cre recombinase expression and controls specific gene expression in a tissue specific manner. This system has been used to produce inducible knockouts in small intestine and colonic epithelium in mice (Saam and Gordon, 1999). This used the reverse tetracycline regulated transactivator (rtTA) under the control of an intestinal epithelium specific promoter. When rtTA binds tetracycline, it acquires the ability to bind to tet operator sequences (tetO) and activate transcription of Cre recombinase linked to a minimal CMV promoter. This then allows recombination between loxP sites in a reporter gene (Figure 46). In this

case the system was leaky, as background recombination in the absence of the inducer was not zero (Saam and Gordon, 1999).

However, in spite of more complicated cloning and complex animal husbandry, these systems will facilitate definition of gene function at different times throughout development, in specific tissues, or under certain physiological or pathological conditions.

We wished to produce an inducible and conditional periaxin knockout transgenic mouse to further investigate the role of periaxin in Schwann cells, and to see whether periaxin-null mice were able to recover normal myelination at different stages of their development by reactivating periaxin expression. In preparation for these experiments, embryonic stem cells carrying a 'floxed' *Periaxin* allele have been generated.

7.3.4. The conditional periaxin construct

A construct was built to produce targeted mice with a floxed *Periaxin* gene. In the presence of Cre recombinase, there is recombination between the loxP sites, removing exon V of *Periaxin*, and changing the translation frame, leading to a premature stop codon thirteen amino acids into the protein. It is highly likely that this peptide will be unstable and not functional. Thus, a normal mouse can be converted into a periaxin-null mouse in vivo.

The Centre for Genome Research in Edinburgh transfected this construct into embryonic stem cells and have generated several clones of these cells with the targeted floxed *Periaxin* gene construct. However, as yet, there has been no germ line transmission.

When germ line transmission is achieved, we would like to cross these mice with mice that are transgenic for a Schwann cell switch mechanism that will allow us to turn on and off L-periaxin expression. An ideal switch mechanism would consist of the tTA gene under the control of the PMP22 promoter, making tTA expression specific to Schwann cells, with the TetO with a minimal CMV promoter driving expression of Cre recombinase. Thus, we would be able to obtain Schwann cell

specific expression of Cre recombinase that is controllable by the administration of tetracycline (Figure 47).

Thus, there are several steps left to achieve before these mice will be generated. However, once made, they will be invaluable at assessing the role of periaxin at different stages of development by switching on and off periaxin expression at different times. It would also be interesting to assess whether Schwann cells, surrounding demyelinating nerves in mice with periaxin expression switched off, are competent to regenerate normal nerves when it is switched back on. This has implications for understanding the cell biology of myelin development and repair, but also for the possible use of gene therapy in patients with demyelinating CMT disease in the future.

7.4. Fbl6

There is scope for further work examining the role of Fbl6 in the control of L-periaxin levels and localisation, and myelination. We are generating a transgenic mouse that contains a Flag-tagged form of Fbl6 lacking the F-box domain (26a clone). Thus, the protein formed will theoretically be able to bind L-periaxin, but not direct it to the SCF complex for ubiquitination and degradation. This may stabilise the protein, leading to accumulation in the cell, and potentially causing a toxic gain of function effect.

We are raising a further antibody to the new putative N-terminus of the Fbl6 protein to help us further characterise the in vivo interaction of L-periaxin and Fbl6.

Transfection experiments show that full length Fbl6 is directed to nucleoli of cos-7 cells, but L-periaxin appears absent from these structures. The Fbl6 construct missing the F-box domain (26a) is not targeted to these areas (Figure 43 and Figure 44). By analogy to the E3 ubiquitin ligase Mdm2, whose target protein is the tumour suppressor protein p53, it may be that overexpression of Fbl6 in the cell culture system directs the protein to a nucleolar localisation. Thus, it would be interesting to look at the localisation of endogenous Fbl6 in a variety of cell lines with the new antibody against Fbl6.

Proteins interacting with Fbl6 may help to explain its biology. There may be interacting proteins which direct the protein to the nucleolus, which presumably interact with the N-terminal part of the protein as 26a is not directed to nucleoli. As Fbl6 appears to be sequestered in the nucleolus, away from the localisation of L-periaxin, then there may well be other interacting proteins, such as p14ARF with Mdm2, which regulate formation of an Fbl6/L-periaxin complex. A yeast 2-hybrid screen using the N-terminal part of Fbl6 would thus be potentially very interesting. A similar screen using the leucine rich repeat domain would indicate other target proteins of Fbl6 directed to the ubiquitin/proteasomal pathway.

My experiments have indicated the likelihood that Fbl6 degradation is also controlled by the ubiquitin/proteasomal pathway, as Flag labelled Fbl6 is more stable in the presence of a proteasomal inhibitor. This could be determined by immunoprecipitation experiments using an anti-Flag antibody or the newly generated Fbl6 antibody, and blotting with an ubiquitin antibody to detect ubiquitinated forms of Fbl6. The addition of a proteasomal inhibitor to the culture system should increase the amount of ubiquitinated Fbl6 and may increase Fbl6 polyubiquitination.

FIGURE 45 - IMMUNOFLUORESCENCE OF HUMAN SKIN BIOPSY

a, b, c: Human nerve from skin biopsy labelled with anti-170 pep-1 periaxin antibody (a), and neurofilament (b) with a merged picture (c). The periaxin antibody labels myelinated nerve.

d, e, f: Human nerve from skin biopsy labelled with anti-170 pep-1 periaxin antibody (d), and neurofilament (e) with a merged picture (f). This shows unmyelinated and myelinated fibres.

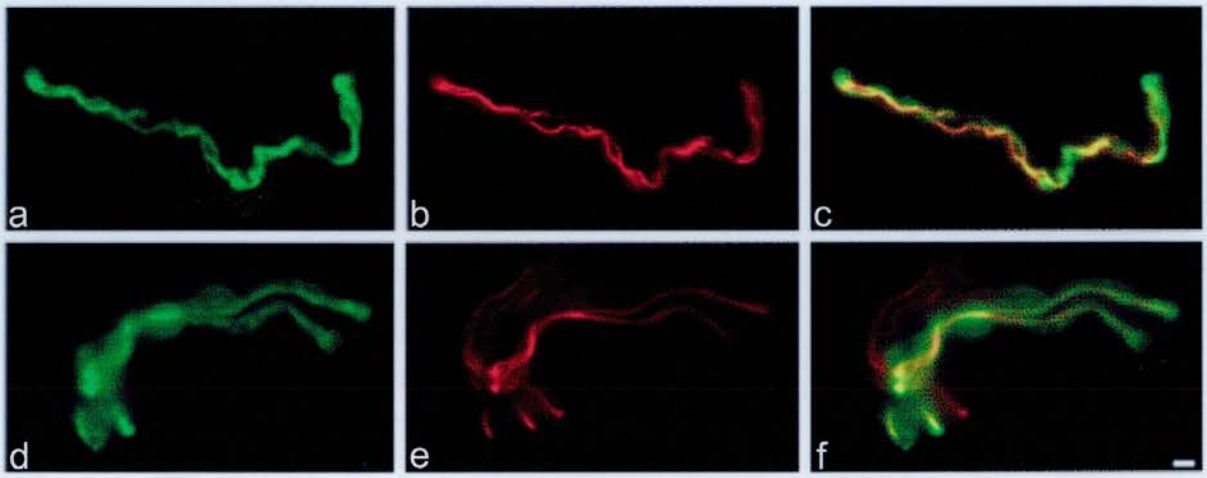
a
b
c
d
e
f

FIGURE 46 - THE TET ON AND OFF SYSTEMS

a: The TET - off system.

A tissue-specific promoter drives the expression of tTA which binds TETO sequence and allows transcription of Cre recombinase. This catalyses the removal of DNA sequence between loxP sites. In the presence of Tetracycline, tTA cannot bind to TETO sequence and does not activate Cre recombinase expression.

b: The TET - on system.

A tissue-specific promoter drives the expression of rtTA which only binds TETO sequence in the presence of tetracycline. This activates Cre recombinase expression which catalyses the removal of sequence between loxP sites.

a.

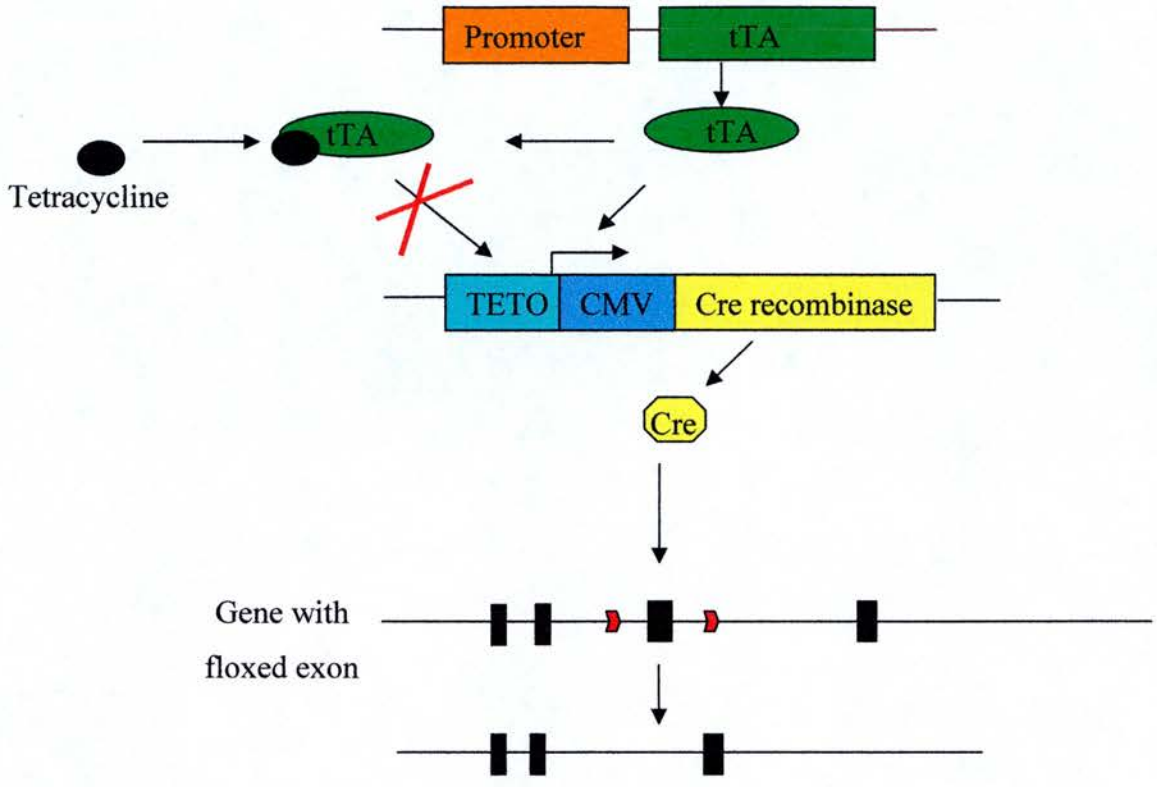
Promoter
tTA
tTA
tTA
Tetracycline
TETO
CMV
Cre recombinase
Cre
Gene with
floxed exon

b.

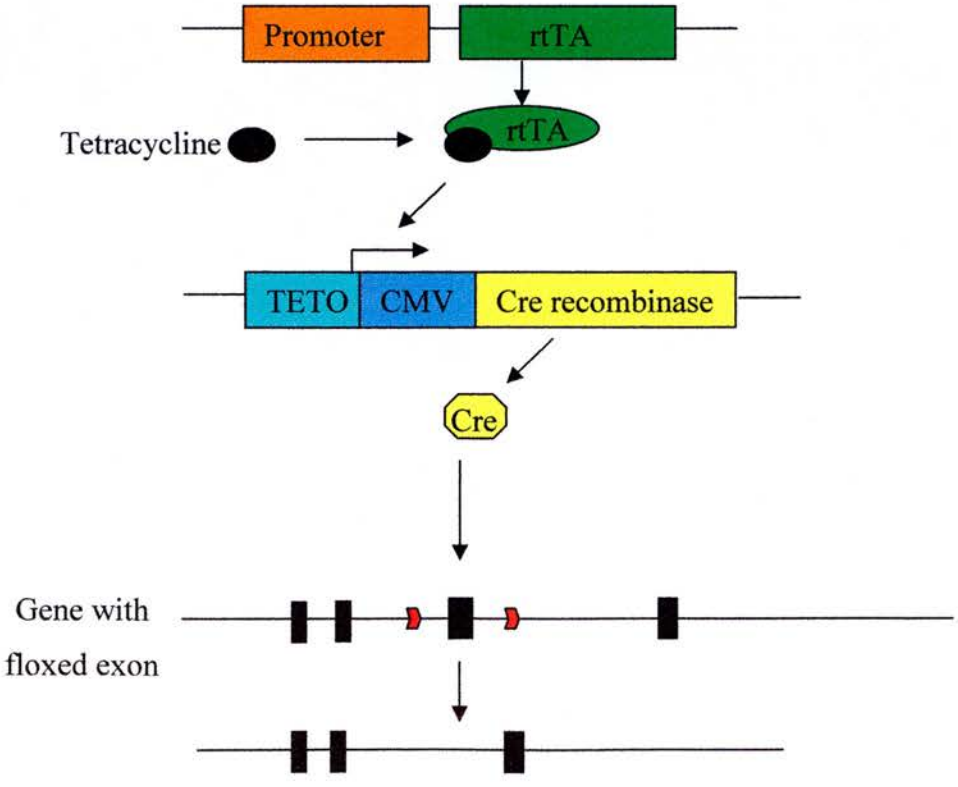
Promoter
rtTA
rtTA
Tetracycline
TETO
CMV
Cre recombinase
Cre
Gene with
floxed exon

FIGURE 47 - PROPOSED SCHEME FOR CONDITIONAL KNOCKOUT OF L-PERIAXIN.

A Schwann cell specific promoter drives expression of rtTA in Schwann cells. In the presence of tetracycline, this binds to the TETO sequence, and activates the expression of Cre recombinase. This catalyses recombination between the loxP sites ( ) that flank exon V of the *Periaxin* gene inactivating the gene due to a frameshift that generates a stop codon.

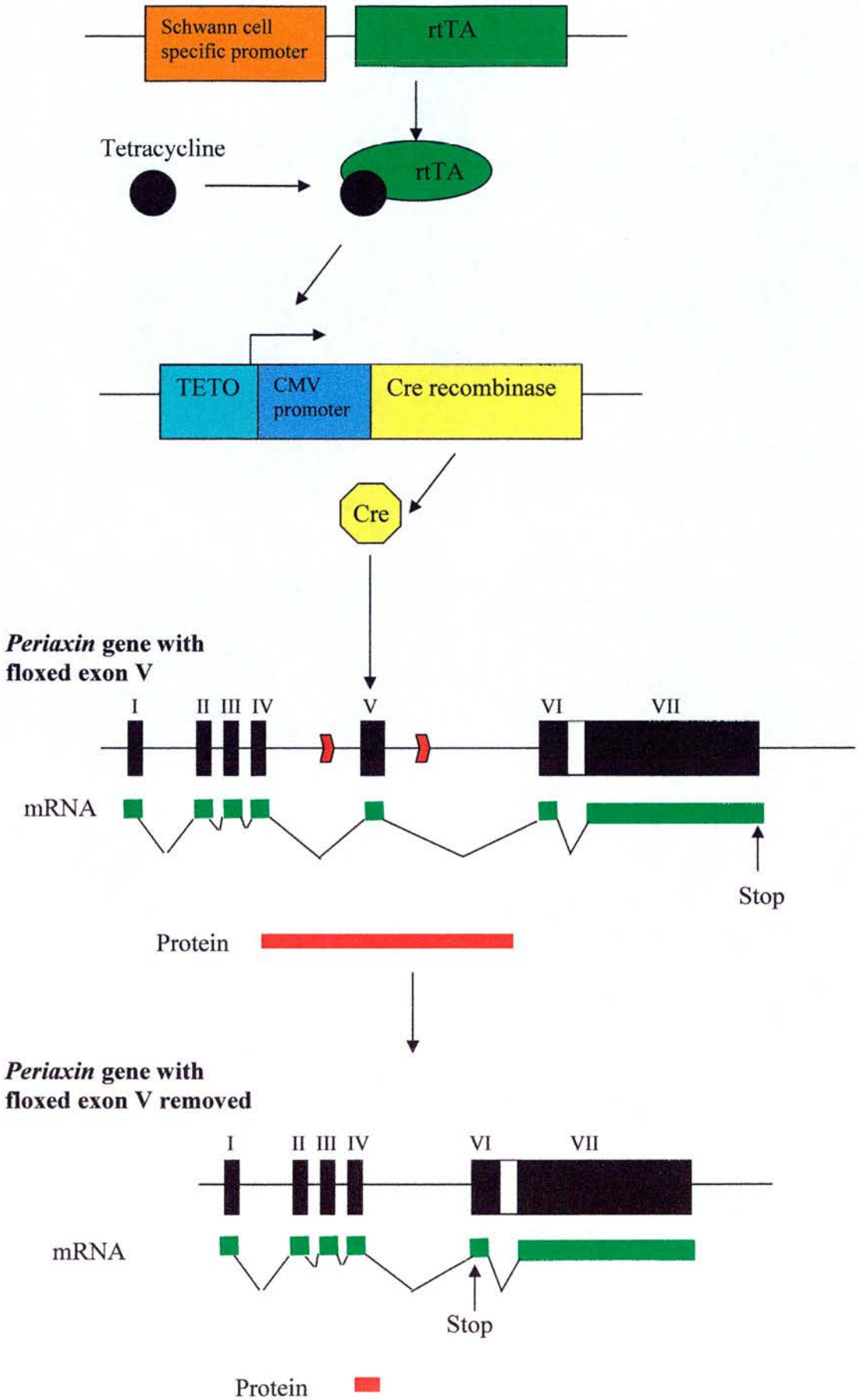
Schwann cell specific promoter
rtTA
Tetracycline
rtTA
TETO
CMV promoter
Cre recombinase
Cre
Periaxin gene with floxed exon V
I
II III IV
V
VI
VII
mRNA
Stop
Protein
Periaxin gene with floxed exon V removed
I
II III IV
VI
VII
mRNA
Stop
Protein

8. REFERENCES

Abrams, C. K., Oh, S., Ri, Y., and Bargiello, T. A. (2000). Mutations in connexin 32: the molecular and biophysical bases for the X- linked form of Charcot-Marie-Tooth disease. Brain Res Brain Res Rev *32*, 203-214.

Anderson, S. L., Coli, R., Daly, I. W., Kichula, E. A., Rork, M. J., Volpi, S. A., Ekstein, J., and Rubin, B. Y. (2001). Familial dysautonomia is caused by mutations of the IKAP gene. Am J Hum Genet *68*, 753-758.

Armstrong, R. N. (1997). Structure, catalytic mechanism, and evolution of the glutathione transferases. Chem Res Toxicol *10*, 2-18.

Auer-Grumbach, M., Loscher, W. N., Wagner, K., Petek, E., Korner, E., Offenbacher, H., and Hartung, H. P. (2000a). Phenotypic and genotypic heterogeneity in hereditary motor neuronopathy type V: a clinical, clectrophysiological and genetic study. Brain *123*, 1612-1623.

Auer-Grumbach, M., Wagner, K., Timmerman, V., De Jonghe, P., and Hartung, H. P. (2000b). Ulcero-mutilating neuropathy in an Austrian kinship without linkage to hereditary motor and sensory neuropathy IIB and hereditary sensory neuropathy I loci. Neurology *54*, 45-52.

Bai, C., Sen, P., Hofmann, K., Ma, L., Goebl, M., Harper, J. W., and Elledge, S. J. (1996). SKP1 connects cell cycle regulators to the ubiquitin proteolysis machinery through a novel motif, the F-box. Cell *86*, 263-274.

Barhoumi, C., Amouri, R., Ben Hamida, C., Ben Hamida, M., Machghoul, S., Gueddiche, M., and Hentati, F. (2001). Linkage of a new locus for autosomal recessive axonal form of Charcot- Marie-Tooth disease to chromosome 8q21.3. Neuromuscul Disord *11*, 27-34.

Baxter, R. V., Ben Othmane, K., Rochelle, J. M., Stajich, J. E., Hulette, C., Dew-Knight, S., Hentati, F., Ben Hamida, M., Bel, S., Stenger, J. E., *et al.* (2002). Ganglioside-induced differentiation-associated protein-1 is mutant in Charcot-Marie-Tooth disease type 4A/8q21. Nat Genet *30*, 21-22.

Bebington, C., Doherty, F. J., and Fleming, S. D. (2001). The possible biological and reproductive functions of ubiquitin. Hum Reprod Update *7*, 102-111.

Bejaoui, K., Wu, C., Scheffler, M. D., Haan, G., Ashby, P., Wu, L., de Jong, P., and Brown, R. H., Jr. (2001). SPTLC1 is mutated in hereditary sensory neuropathy, type 1. Nat Genet *27*, 261-262.

Bell, C., and Haites, N. (1998). Genetic aspects of Charcot-Marie-Tooth disease. Arch Dis Child *78*, 296-300.

Bellone, E., Rodolico, C., Toscano, A., Di Maria, E., Cassandrini, D., Pizzuti, A., Pigullo, S., Mazzeo, A., Macaione, V., Girlanda, P., *et al.* (2002). A family with

autosomal dominant mutilating neuropathy not linked to either Charcot-Marie-Tooth disease type 2B (CMT2B) or hereditary sensory neuropathy type I (HSN I) loci. Neuromuscul Disord *12*, 286-291.

Ben Hamida, M., Hentati, F., and Ben Hamida, C. (1990). Giant axonal neuropathy with inherited multisystem degeneration in a Tunisian kindred. Neurology *40*, 245-250.

Ben Othmane, K., Hentati, F., Lennon, F., Ben Hamida, C., Blel, S., Roses, A. D., Pericak-Vance, M. A., Ben Hamida, M., and Vance, J. M. (1993a). Linkage of a locus (CMT4A) for autosomal recessive Charcot-Marie-Tooth disease to chromosome 8q. Hum Mol Genet *2*, 1625-1628.

Ben Othmane, K., Middleton, L. T., Loprest, L. J., Wilkinson, K. M., Lennon, F., Rozear, M. P., Stajich, J. M., Gaskell, P. C., Roses, A. D., Pericak-Vance, M. A., and et al. (1993b). Localization of a gene (CMT2A) for autosomal dominant Charcot-Marie- Tooth disease type 2 to chromosome 1p and evidence of genetic heterogeneity. Genomics *17*, 370-375.

Bergoffen, J., Scherer, S. S., Wang, S., Scott, M. O., Bone, L. J., Paul, D. L., Chen, K., Lensch, M. W., Chance, P. F., and Fischbeck, K. H. (1993). Connexin mutations in X-linked Charcot-Marie-Tooth disease. Science *262*, 2039-2042.

Bermingham, J. R., Jr., Scherer, S. S., O'Connell, S., Arroyo, E., Kalla, K. A., Powell, F. L., and Rosenfeld, M. G. (1996). Tst-1/Oct-6/SCIP regulates a unique step in peripheral myelination and is required for normal respiration. Genes Dev *10*, 1751-1762.

Bhat, M. A., Rios, J. C., Lu, Y., Garcia-Fresco, G. P., Ching, W., St Martin, M., Li, J., Einheber, S., Chesler, M., Rosenbluth, J., *et al.* (2001). Axon-glia interactions and the domain organization of myelinated axons requires neurexin IV/Caspr/Paranodin. Neuron *30*, 369-383.

Blondeau, F., Laporte, J., Bodin, S., Superti-Furga, G., Payrastre, B., and Mandel, J. L. (2000). Myotubularin, a phosphatase deficient in myotubular myopathy, acts on phosphatidylinositol 3-kinase and phosphatidylinositol 3-phosphate pathway. Hum Mol Genet *9*, 2223-2229.

Bodzioch, M., Lapicka, K., Aslanidis, C., Kacinski, M., and Schmitz, G. (2001). Two novel mutant alleles of the gene encoding neurotrophic tyrosine kinase receptor type 1 (NTRK1) in a patient with congenital insensitivity to pain with anhidrosis: a splice junction mutation in intron 5 and cluster of four mutations in exon 15. Hum Mutat *17*, 72.

Boerkoel, C. F., Takashima, H., Bacino, C. A., Daentl, D., and Lupski, J. R. (2001a). EGR2 mutation R359W causes a spectrum of Dejerine-Sottas neuropathy. Neurogenetics *3*, 153-157.

Boerkoel, C. F., Takashima, H., Garcia, C. A., Olney, R. K., Johnson, J., Berry, K., Russo, P., Kennedy, S., Teebi, A. S., Scavina, M., *et al.* (2002). Charcot-Marie-Tooth disease and related neuropathies: mutation distribution and genotype-phenotype correlation. Ann Neurol *51*, 190-201.

Boerkoel, C. F., Takashima, H., Stankiewicz, P., Garcia, C. A., Leber, S. M., Rhee-Morris, L., and Lupski, J. R. (2001b). Periaxin mutations cause recessive Dejerine-Sottas neuropathy. Am J Hum Genet *68*, 325-333.

Bolino, A., Lonie, L. J., Zimmer, M., Boerkoel, C. F., Takashima, H., Monaco, A. P., and Lupski, J. R. (2001). Denaturing high-performance liquid chromatography of the myotubularin- related 2 gene (MTMR2) in unrelated patients with Charcot-Marie-Tooth disease suggests a low frequency of mutation in inherited neuropathy. Neurogenetics *3*, 107-109.

Bolino, A., Muglia, M., Conforti, F. L., LeGuern, E., Salih, M. A., Georgiou, D. M., Christodoulou, K., Hausmanowa-Petrusewicz, I., Mandich, P., Schenone, A., *et al.* (2000). Charcot-Marie-Tooth type 4B is caused by mutations in the gene encoding myotubularin-related protein-2. Nat Genet *25*, 17-19.

Bomont, P., Cavalier, L., Blondeau, F., Ben Hamida, C., Belal, S., Tazir, M., Demir, E., Topaloglu, H., Korinthenberg, R., Tuysuz, B., *et al.* (2000). The gene encoding gigaxonin, a new member of the cytoskeletal BTB/kelch repeat family, is mutated in giant axonal neuropathy. Nat Genet *26*, 370-374.

Bonne, G., Di Barletta, M. R., Varnous, S., Becane, H. M., Hammouda, E. H., Merlini, L., Muntoni, F., Greenberg, C. R., Gary, F., Urtizberea, J. A., *et al.* (1999). Mutations in the gene encoding lamin A/C cause autosomal dominant Emery-Dreifuss muscular dystrophy. Nat Genet *21*, 285-288.

Bouhouche, A., Benomar, A., Birouk, N., Mularoni, A., Meggouh, F., Tassin, J., Grid, D., Vandenberghe, A., Yahyaoui, M., Chkili, T., *et al.* (1999). A locus for an axonal form of autosomal recessive Charcot-Marie-Tooth disease maps to chromosome 1q21.2-q21.3. Am J Hum Genet *65*, 722-727.

Boyle, M. E., Berglund, E. O., Murai, K. K., Weber, L., Peles, E., and Ranscht, B. (2001). Contactin orchestrates assembly of the septate-like junctions at the paranode in myelinated peripheral nerve. Neuron *30*, 385-397.

Breitschopf, K., Bengal, E., Ziv, T., Admon, A., and Ciechanover, A. (1998). A novel site for ubiquitination: the N-terminal residue, and not internal lysines of MyoD, is essential for conjugation and degradation of the protein. EMBO J *17*, 5964-5973.

Bridge, P. M., Ball, D. J., Mackinnon, S. E., Nakao, Y., Brandt, K., Hunter, D. A., and Hertl, C. (1994). Nerve crush injuries--a model for axonotmesis. Exp Neurol *127*, 284-290.

Brown, M. C., and Hardman, V. J. (1987). A reassessment of the accuracy of reinnervation by motoneurons following crushing or freezing of the sciatic or lumbar spinal nerves of rats. Brain *110*, 695-705.

Bunge, R. P. (1993). Expanding roles for the Schwann cell: ensheathment, myelination, trophism and regeneration. Curr Opin Neurobiol *3*, 805-809.

Bunge, R. P., Bunge, M. B., and Bates, M. (1989). Movements of the Schwann cell nucleus implicate progression of the inner (axon-related) Schwann cell process during myelination. J Cell Biol *109*, 273-284.

Carey, D. J., Todd, M. S., and Rafferty, C. M. (1986). Schwann cell myelination: induction by exogenous basement membrane-like extracellular matrix. J Cell Biol *102*, 2254-2263.

Carmo-Fonseca, M. (2002). The contribution of nuclear compartmentalization to gene regulation. Cell *108*, 513-521.

Carpenter, D. A., and Ip, W. (1996). Neurofilament triplet protein interactions: evidence for the preferred formation of NF-L-containing dimers and a putative function for the end domains. J Cell Sci *109*, 2493-2498.

Carrano, A. C., and Pagano, M. (2001). Role of the F-box protein Skp2 in adhesion-dependent cell cycle progression. J Cell Biol *153*, 1381-1390.

Cattoretti, G., Becker, M. H., Key, G., Duchrow, M., Schluter, C., Galle, J., and Gerdes, J. (1992). Monoclonal antibodies against recombinant parts of the Ki-67 antigen (MIB 1 and MIB 3) detect proliferating cells in microwave-processed formalin-fixed paraffin sections. J Pathol *168*, 357-363.

Cenciarelli, C., Chiaur, D. S., Guardavaccaro, D., Parks, W., Vidal, M., and Pagano, M. (1999). Identification of a family of human F-box proteins. Curr Biol *9*, 1177-1179.

Ceuterick-de Groote, C., De Jonghe, P., Timmerman, V., Van Goethem, G., Lofgren, A., Ceulemans, B., Van Broeckhoven, C., and Martin, J. J. (2001). Infantile demyelinating neuropathy associated with a de novo point mutation on Ser72 in PMP22 and basal lamina onion bulbs in skin biopsy. Pathol Res Pract *197*, 193-198.

Chance, P. F., Alderson, M. K., Leppig, K. A., Lensch, M. W., Matsunami, N., Smith, B., Swanson, P. D., Odelberg, S. J., Disteche, C. M., and Bird, T. D. (1993). DNA deletion associated with hereditary neuropathy with liability to pressure palsies. Cell *72*, 143-151.

Charles, P., Tait, S., Faivre-Sarrailh, C., Barbin, G., Gunn-Moore, F., Denisenko-Nehrbass, N., Guennoc, A. M., Girault, J. A., Brophy, P. J., and Lubetzki, C. (2002). Neurofascin is a glial receptor for the paranodin/Caspr-contactin axonal complex at the axoglial junction. Curr Biol *12*, 217-220.

Chen, A., Wu, K., Fuchs, S. Y., Tan, P., Gomez, C., and Pan, Z. Q. (2000). The conserved RING-H2 finger of ROC1 is required for ubiquitin ligation. J Biol Chem *275*, 15432-15439.

Christodoulou, K., Kyriakides, T., Hristova, A. H., Georgiou, D. M., Kalaydjieva, L., Yshpekova, B., Ivanova, T., Weber, J. L., and Middleton, L. T. (1995). Mapping of a distal form of spinal muscular atrophy with upper limb predominance to chromosome 7p. Hum Mol Genet *4*, 1629-1632.

Ciechanover, A. (1998). The ubiquitin-proteasome pathway: on protein death and cell life. EMBO J *17*, 7151-7160.

Cleveland, D. W., and Rothstein, J. D. (2001). From Charcot to Lou Gehrig: deciphering selective motor neuron death in ALS. Nat Rev Neurosci *2*, 806-819.

Cluskey, S., and Ramsden, D. B. (2001). Mechanisms of neurodegeneration in amyotrophic lateral sclerosis. Mol Pathol *54*, 386-392.

Cohen, L., Henzel, W. J., and Baeuerle, P. A. (1998). IKAP is a scaffold protein of the IkappaB kinase complex. Nature *395*, 292-296.

Craig, K. L., and Tyers, M. (1999). The F-box: a new motif for ubiquitin dependent proteolysis in cell cycle regulation and signal transduction. Prog Biophys Mol Biol *72*, 299-328.

Cuesta, A., Pedrola, L., Sevilla, T., Garcia-Planells, J., Chumillas, M. J., Mayordomo, F., LeGuern, E., Marin, I., Vilchez, J. J., and Palau, F. (2002). The gene encoding ganglioside-induced differentiation-associated protein 1 is mutated in axonal Charcot-Marie-Tooth type 4A disease. Nat Genet *30*, 22-25.

Dawkins, J. L., Hulme, D. J., Brahmbhatt, S. B., Auer-Grumbach, M., and Nicholson, G. A. (2001). Mutations in SPTLC1, encoding serine palmitoyltransferase, long chain base subunit-1, cause hereditary sensory neuropathy type I. Nat Genet *27*, 309-312.

De Jonghe, P., Mersivanova, I., Nelis, E., Del Favero, J., Martin, J. J., Van Broeckhoven, C., Evgrafov, O., and Timmerman, V. (2001). Further evidence that neurofilament light chain gene mutations can cause Charcot-Marie-Tooth disease type 2E. Ann Neurol *49*, 245-249.

De Jonghe, P., Timmerman, V., Ceuterick, C., Nelis, E., De Vriendt, E., Lofgren, A., Vercruyssen, A., Verellen, C., Van Maldergem, L., Martin, J. J., and Van Broeckhoven, C. (1999). The Thr124Met mutation in the peripheral myelin protein zero (MPZ) gene is associated with a clinically distinct Charcot-Marie-Tooth phenotype. Brain *122*, 281-290.

De Jonghe, P., Timmerman, V., FitzPatrick, D., Spoelders, P., Martin, J. J., and Van Broeckhoven, C. (1997). Mutilating neuropathic ulcerations in a chromosome 3q13-q22 linked Charcot-Marie-Tooth disease type 2B family. J Neurol Neurosurg Psychiatry *62*, 570-573.

De Sandre-Giovannoli, A., Chaouch, M., Kozlov, S., Vallat, J. M., Tazir, M., Kassouri, N., Szepetowski, P., Hammadouche, T., Vandenberghe, A., Stewart, C. L., *et al.* (2002). Homozygous Defects in LMNA, Encoding Lamin A/C Nuclear-Envelope Proteins, Cause Autosomal Recessive Axonal Neuropathy in Human (Charcot- Marie-Tooth Disorder Type 2) and Mouse. Am J Hum Genet *70*, 726-736.

de Waegh, S. M., Lee, V. M., and Brady, S. T. (1992). Local modulation of neurofilament phosphorylation, axonal caliber, and slow axonal transport by myelinating Schwann cells. Cell *68*, 451-463.

Delague, V., Bareil, C., Tuffery, S., Bouvagnet, P., Chouery, E., Koussa, S., Maisonobe, T., Loiselet, J., Megarbane, A., and Claustres, M. (2000). Mapping of a new locus for autosomal recessive demyelinating Charcot- Marie-Tooth disease to 19q13.1-13.3 in a large consanguineous Lebanese family: exclusion of MAG as a candidate gene. Am J Hum Genet *67*, 236-243.

Deshaies, R. J. (1999). SCF and Cullin/Ring H2-based ubiquitin ligases. Annu Rev Cell Dev Biol *15*, 435-467.

Diemel, L. T., Cai, F., Anand, P., Warner, G., Kopelman, P. G., Fernyhough, P., and Tomlinson, D. R. (1999). Increased nerve growth factor mRNA in lateral calf skin biopsies from diabetic patients. Diabet Med *16*, 113-118.

Doyu, M., Sobue, G., Ken, E., Kimata, K., Shinomura, T., Yamada, Y., Mitsuma, T., and Takahashi, A. (1993). Laminin A, B1, and B2 chain gene expression in transected and regenerating nerves: regulation by axonal signals. J Neurochem *60*, 543-551.

Dubois, M., Strazielle, C., Eyer, J., and Lalonde, R. (2002). Sensorimotor functions in transgenic mice expressing the neurofilament/heavy-LacZ fusion protein on two genetic backgrounds. Neuroscience *112*, 447-454.

Dupree, J. L., Girault, J. A., and Popko, B. (1999). Axo-glial interactions regulate the localization of axonal paranodal proteins. J Cell Biol *147*, 1145-1152.

D'Urso, D., Ehrhardt, P., and Muller, H. W. (1999). Peripheral myelin protein 22 and protein zero: a novel association in peripheral nervous system myelin. J Neurosci *19*, 3396-3403.

Dyck, P. J., and Lambert, E. H. (1968). Lower motor and primary sensory neuron diseases with peroneal muscular atrophy. I. Neurologic, genetic, and electrophysiologic findings in hereditary polyneuropathies. Arch Neurol *18*, 603-618.

Dytrych, L., Sherman, D. L., Gillespie, C. S., and Brophy, P. J. (1998). Two PDZ domain proteins encoded by the murine periaxin gene are the result of alternative intron retention and are differentially targeted in Schwann cells. J Biol Chem *273*, 5794-5800.

Einheber, S., Zanazzi, G., Ching, W., Scherer, S., Milner, T. A., Peles, E., and Salzer, J. L. (1997). The axonal membrane protein Caspr, a homologue of neurexin

IV, is a component of the septate-like paranodal junctions that assemble during myelination. J Cell Biol *139*, 1495-1506.

Eldridge, C. F., Bunge, M. B., and Bunge, R. P. (1989). Differentiation of axon-related Schwann cells in vitro: II. Control of myelin formation by basal lamina. J Neurosci *9*, 625-638.

Fabrizi, G. M., Simonati, A., Taioli, F., Cavallaro, T., Ferrarini, M., Rigatelli, F., Pini, A., Mostacciuolo, M. L., and Rizzuto, N. (2001). PMP22 related congenital hypomyelination neuropathy. J Neurol Neurosurg Psychiatry *70*, 123-126.

Facer, P., Mathur, R., Pandya, S. S., Ladiwala, U., Singhal, B. S., and Anand, P. (1998). Correlation of quantitative tests of nerve and target organ dysfunction with skin immunohistology in leprosy. Brain *121*, 2239-2247.

Fatkin, D., MacRae, C., Sasaki, T., Wolff, M. R., Porcu, M., Frenneaux, M., Atherton, J., Vidaillet, H. J., Jr., Spudich, S., De Girolami, U., *et al.* (1999). Missense mutations in the rod domain of the lamin A/C gene as causes of dilated cardiomyopathy and conduction-system disease. N Engl J Med *341*, 1715-1724.

Feltri, M. L., Graus Porta, D., Previtali, S. C., Nodari, A., Migliavacca, B., Cassetti, A., Littlewood-Evans, A., Reichardt, L. F., Messing, A., Quattrini, A., *et al.* (2002). Conditional disruption of beta 1 integrin in Schwann cells impedes interactions with axons. J Cell Biol *156*, 199-209.

Fernandez-Valle, C., Gwynn, L., Wood, P. M., Carbonetto, S., and Bunge, M. B. (1994). Anti-beta 1 integrin antibody inhibits Schwann cell myelination. J Neurobiol *25*, 1207-1226.

Forghani, R., Garofalo, L., Foran, D. R., Farhadi, H. F., Lepage, P., Hudson, T. J., Tretjakoff, I., Valera, P., and Peterson, A. (2001). A distal upstream enhancer from the myelin basic protein gene regulates expression in myelin-forming schwann cells. J Neurosci *21*, 3780-3787.

Furukawa, K., Inagaki, H., and Hotta, Y. (1994). Identification and cloning of an mRNA coding for a germ cell-specific A- type lamin in mice. Exp Cell Res *212*, 426-430.

Galan, J. M., and Peter, M. (1999). Ubiquitin-dependent degradation of multiple F-box proteins by an autocatalytic mechanism. Proc Natl Acad Sci U S A *96*, 9124-9129.

Garcia, C. A., Malamut, R. E., England, J. D., Parry, G. S., Liu, P., and Lupski, J. R. (1995). Clinical variability in two pairs of identical twins with the Charcot- Marie-Tooth disease type 1A duplication. Neurology *45*, 2090-2093.

Gaullier, J. M., Simonsen, A., D'Arrigo, A., Bremnes, B., Stenmark, H., and Aasland, R. (1998). FYVE fingers bind PtdIns(3)P. Nature *394*, 432-433.

Giannini, C., and Dyck, P. J. (1990). The fate of Schwann cell basement membranes in permanently transected nerves. J Neuropathol Exp Neurol *49*, 550-563.

Giese, K. P., Martini, R., Lemke, G., Soriano, P., and Schachner, M. (1992). Mouse P0 gene disruption leads to hypomyelination, abnormal expression of recognition molecules, and degeneration of myelin and axons. Cell *71*, 565-576.

Gillespie, C. S., Lee, M., Fantes, J. F., and Brophy, P. J. (1997). The gene encoding the Schwann cell protein periaxin localizes on mouse chromosome 7 (Prx). Genomics *41*, 297-298.

Gillespie, C. S., Sherman, D. L., Blair, G. E., and Brophy, P. J. (1994). Periaxin, a novel protein of myelinating Schwann cells with a possible role in axonal ensheathment. Neuron *12*, 497-508.

Gillespie, C. S., Sherman, D. L., Fleetwood-Walker, S. M., Cottrell, D. F., Tait, S., Garry, E. M., Wallace, V. C., Ure, J., Griffiths, I. R., Smith, A., and Brophy, P. J. (2000). Peripheral demyelination and neuropathic pain behavior in periaxin-deficient mice. Neuron *26*, 523-531.

Gong, Y. H., Parsadanian, A. S., Andreeva, A., Snider, W. D., and Elliott, J. L. (2000). Restricted expression of G86R Cu/Zn superoxide dismutase in astrocytes results in astrocytosis but does not cause motoneuron degeneration. J Neurosci *20*, 660-665.

Gossen, M., and Bujard, H. (1992). Tight control of gene expression in mammalian cells by tetracycline- responsive promoters. Proc Natl Acad Sci U S A *89*, 5547-5551.

Griffin, J. W., Li, C. Y., Macko, C., Ho, T. W., Hsieh, S. T., Xue, P., Wang, F. A., Cornblath, D. R., McKhann, G. M., and Asbury, A. K. (1996). Early nodal changes in the acute motor axonal neuropathy pattern of the Guillain-Barre syndrome. J Neurocytol *25*, 33-51.

Griffin, J. W., McArthur, J. C., and Polydefkis, M. (2001). Assessment of cutaneous innervation by skin biopsies. Curr Opin Neurol *14*, 655-659.

Grohmann, K., Schuelke, M., Diers, A., Hoffmann, K., Lucke, B., Adams, C., Bertini, E., Leonhardt-Horti, H., Muntoni, F., Ouvrier, R., *et al.* (2001). Mutations in the gene encoding immunoglobulin mu-binding protein 2 cause spinal muscular atrophy with respiratory distress type 1. Nat Genet *29*, 75-77.

Groll, M., Ditzel, L., Lowe, J., Stock, D., Bochtler, M., Bartunik, H. D., and Huber, R. (1997). Structure of 20S proteasome from yeast at 2.4 A resolution. Nature *386*, 463-471.

Guilbot, A., Williams, A., Ravise, N., Verny, C., Brice, A., Sherman, D. L., Brophy, P. J., LeGuern, E., Delague, V., Bareil, C., *et al.* (2001). A mutation in periaxin is responsible for CMT4F, an autosomal recessive form of Charcot-Marie-Tooth disease. Hum Mol Genet *10*, 415-421.

Gumbiner, B. M. (1995). Signal transduction of beta-catenin. Curr Opin Cell Biol *7*, 634-640.

Hanada, K., Hara, T., Nishijima, M., Kuge, O., Dickson, R. C., and Nagiec, M. M. (1997). A mammalian homolog of the yeast LCB1 encodes a component of serine palmitoyltransferase, the enzyme catalyzing the first step in sphingolipid synthesis. J Biol Chem *272*, 32108-32114.

Harati, Y., and Butler, I. J. (1985). Congenital hypomyelinating neuropathy. J Neurol Neurosurg Psychiatry *48*, 1269-1276.

Harding, A. E., and Thomas, P. K. (1980a). The clinical features of hereditary motor and sensory neuropathy types I and II. Brain *103*, 259-280.

Harding, A. E., and Thomas, P. K. (1980b). Hereditary distal spinal muscular atrophy. A report on 34 cases and a review of the literature. J Neurol Sci *45*, 337-348.

Hayasaka, K., Himoro, M., Sato, W., Takada, G., Uyemura, K., Shimizu, N., Bird, T. D., Conneally, P. M., and Chance, P. F. (1993). Charcot-Marie-Tooth neuropathy type 1B is associated with mutations of the myelin P0 gene. Nat Genet *5*, 31-34.

Hayes, J. D., and Pulford, D. J. (1995). The glutathione S-transferase supergene family: regulation of GST and the contribution of the isoenzymes to cancer chemoprotection and drug resistance. Crit Rev Biochem Mol Biol *30*, 445-600.

Henderson, J. E., Amizuka, N., Warshawsky, H., Biasotto, D., Lanske, B. M., Goltzman, D., and Karaplis, A. C. (1995). Nucleolar localization of parathyroid hormone-related peptide enhances survival of chondrocytes under conditions that promote apoptotic cell death. Mol Cell Biol *15*, 4064-4075.

Herget, T., Esdar, C., Oehrlein, S. A., Heinrich, M., Schutze, S., Maelicke, A., and van Echten-Deckert, G. (2000). Production of ceramides causes apoptosis during early neural differentiation in vitro. J Biol Chem *275*, 30344-30354.

Hershko, A., and Ciechanover, A. (1998). The ubiquitin system. Annu Rev Biochem *67*, 425-479.

Hershko, A., Ciechanover, A., Heller, H., Haas, A. L., and Rose, I. A. (1980). Proposed role of ATP in protein breakdown: conjugation of protein with multiple chains of the polypeptide of ATP-dependent proteolysis. Proc Natl Acad Sci U S A *77*, 1783-1786.

Hirokawa, N. (1998). Kinesin and dynein superfamily proteins and the mechanism of organelle transport. Science *279*, 519-526.

Houlden, H., King, R. H., Hashemi-Nejad, A., Wood, N. W., Mathias, C. J., Reilly, M., and Thomas, P. K. (2001). A novel TRK A (NTRK1) mutation associated with hereditary sensory and autonomic neuropathy type V. Ann Neurol *49*, 521-525.

Huber, O., Korn, R., McLaughlin, J., Ohsugi, M., Herrmann, B. G., and Kemler, R. (1996). Nuclear localization of beta-catenin by interaction with transcription factor LEF-1. Mech Dev *59*, 3-10.

Huxley, C., Passage, E., Manson, A., Putzu, G., Figarella-Branger, D., Pellissier, J. F., and Fontes, M. (1996). Construction of a mouse model of Charcot-Marie-Tooth disease type 1A by pronuclear injection of human YAC DNA. Hum Mol Genet *5*, 563-569.

Huxley, C., Passage, E., Robertson, A. M., Youl, B., Huston, S., Manson, A., Saberan-Djoniedi, D., Figarella-Branger, D., Pellissier, J. F., Thomas, P. K., and Fontes, M. (1998). Correlation between varying levels of PMP22 expression and the degree of demyelination and reduction in nerve conduction velocity in transgenic mice. Hum Mol Genet *7*, 449-458.

Ikeda, S., Kishida, S., Yamamoto, H., Murai, H., Koyama, S., and Kikuchi, A. (1998). Axin, a negative regulator of the Wnt signaling pathway, forms a complex with GSK-3beta and beta-catenin and promotes GSK-3beta- dependent phosphorylation of beta-catenin. EMBO J *17*, 1371-1384.

Indo, Y. (2001). Molecular basis of congenital insensitivity to pain with anhidrosis (CIPA): mutations and polymorphisms in TRKA (NTRK1) gene encoding the receptor tyrosine kinase for nerve growth factor. Hum Mutat *18*, 462-471.

Indo, Y., Tsuruta, M., Hayashida, Y., Karim, M. A., Ohta, K., Kawano, T., Mitsubuchi, H., Tonoki, H., Awaya, Y., and Matsuda, I. (1996). Mutations in the TRKA/NGF receptor gene in patients with congenital insensitivity to pain with anhidrosis. Nat Genet *13*, 485-488.

Inoue, K., Tanabe, Y., and Lupski, J. R. (1999). Myelin deficiencies in both the central and the peripheral nervous systems associated with a SOX10 mutation. Ann Neurol *46*, 313-318.

Ionasescu, V., Searby, C., Sheffield, V. C., Roklina, T., Nishimura, D., and Ionasescu, R. (1996). Autosomal dominant Charcot-Marie-Tooth axonal neuropathy mapped on chromosome 7p (CMT2D). Hum Mol Genet *5*, 1373-1375.

Ionasescu, V. V. (1995). Charcot-Marie-Tooth neuropathies: from clinical description to molecular genetics. Muscle Nerve *18*, 267-275.

Ismailov, S. M., Fedotov, V. P., Dadali, E. L., Polyakov, A. V., Van Broeckhoven, C., Ivanov, V. I., De Jonghe, P., Timmerman, V., and Evgrafov, O. V. (2001). A new locus for autosomal dominant Charcot-Marie-Tooth disease type 2 (CMT2F) maps to chromosome 7q11-q21. Eur J Hum Genet *9*, 646-650.

Ito, N., Phillips, S. E., Yadav, K. D., and Knowles, P. F. (1994). Crystal structure of a free radical enzyme, galactose oxidase. J Mol Biol *238*, 794-814.

Itoh, K., Wakabayashi, N., Katoh, Y., Ishii, T., Igarashi, K., Engel, J. D., and Yamamoto, M. (1999). Keap1 represses nuclear activation of antioxidant responsive

elements by Nrf2 through binding to the amino-terminal Neh2 domain. Genes Dev *13*, 76-86.

Jessen, K. R., and Mirsky, R. (1999). Schwann cells and their precursors emerge as major regulators of nerve development. Trends Neurosci *22*, 402-410.

Jestico, J. V., Urry, P. A., and Efphimiou, J. (1985). An hereditary sensory and autonomic neuropathy transmitted as an X- linked recessive trait. J Neurol Neurosurg Psychiatry *48*, 1259-1264.

Joazeiro, C. A., and Weissman, A. M. (2000). RING finger proteins: mediators of ubiquitin ligase activity. Cell *102*, 549-552.

Julien, J. P. (1999). Neurofilament functions in health and disease. Curr Opin Neurobiol *9*, 554-560.

Kalaydjieva, L., Gresham, D., Gooding, R., Heather, L., Baas, F., de Jonge, R., Blechschmidt, K., Angelicheva, D., Chandler, D., Worsley, P., *et al.* (2000). N-myc downstream-regulated gene 1 is mutated in hereditary motor and sensory neuropathy-Lom. Am J Hum Genet *67*, 47-58.

Kalaydjieva, L., Hallmayer, J., Chandler, D., Savov, A., Nikolova, A., Angelicheva, D., King, R. H., Ishpekova, B., Honeyman, K., Calafell, F., *et al.* (1996). Gene mapping in Gypsies identifies a novel demyelinating neuropathy on chromosome 8q24. Nat Genet *14*, 214-217.

Kennedy, A. J., Wellmer, A., Facer, P., Saldanha, G., Kopelman, P., Lindsay, R. M., and Anand, P. (1998). Neurotrophin-3 is increased in skin in human diabetic neuropathy. J Neurol Neurosurg Psychiatry *65*, 393-395.

Kennerson, M. L., Zhu, D., Gardner, R. J., Storey, E., Merory, J., Robertson, S. P., and Nicholson, G. A. (2001). Dominant intermediate charcot-marie-tooth neuropathy maps to chromosome 19p12-p13.2. Am J Hum Genet *69*, 883-888.

Kerns, J. M., Braverman, B., Mathew, A., Lucchinetti, C., and Ivankovich, A. D. (1991). A comparison of cryoprobe and crush lesions in the rat sciatic nerve. Pain *47*, 31-39.

Kim, S. A., Taylor, G. S., Torgersen, K. M., and Dixon, J. E. (2002). Myotubularin and MTMR2, phosphatidylinositol 3-phosphatases mutated in myotubular myopathy and type 4B Charcot-Marie-Tooth disease. J Biol Chem *277*, 4526-4531.

Kipreos, E. T., and Pagano, M. (2000). The F-box protein family. Genome Biol *1*.

Kirkpatrick, L. L., Witt, A. S., Payne, H. R., Shine, H. D., and Brady, S. T. (2001). Changes in microtubule stability and density in myelin-deficient shiverer mouse CNS axons. J Neurosci *21*, 2288-2297.

Kobe, B., and Deisenhofer, J. (1995). A structural basis of the interactions between leucine-rich repeats and protein ligands. Nature *374*, 183-186.

Kornau, H. C., Schenker, L. T., Kennedy, M. B., and Seeburg, P. H. (1995). Domain interaction between NMDA receptor subunits and the postsynaptic density protein PSD-95. Science *269*, 1737-1740.

Krajewski, K. M., Lewis, R. A., Fuerst, D. R., Turansky, C., Hinderer, S. R., Garbern, J., Kamholz, J., and Shy, M. E. (2000). Neurological dysfunction and axonal degeneration in Charcot-Marie-Tooth disease type 1A. Brain *123*, 1516-1527.

Krappmann, D., Hatada, E. N., Tegethoff, S., Li, J., Klippel, A., Giese, K., Baeuerle, P. A., and Scheidereit, C. (2000). The I kappa B kinase (IKK) complex is tripartite and contains IKK gamma but not IKAP as a regular component. J Biol Chem *275*, 29779-29787.

Kriz, J., Zhu, Q., Julien, J. P., and Padjen, A. L. (2000). Electrophysiological properties of axons in mice lacking neurofilament subunit genes: disparity between conduction velocity and axon diameter in absence of NF-H. Brain Res *885*, 32-44.

Kuhlbrodt, K., Herbarth, B., Sock, E., Hermans-Borgmeyer, I., and Wegner, M. (1998). Sox10, a novel transcriptional modulator in glial cells. J Neurosci *18*, 237-250.

Kwon, J. M., Elliott, J. L., Yee, W. C., Ivanovich, J., Scavarda, N. J., Moolsintong, P. J., and Goodfellow, P. J. (1995). Assignment of a second Charcot-Marie-Tooth type II locus to chromosome 3q. Am J Hum Genet *57*, 853-858.

Laporte, J., Biancalana, V., Tanner, S. M., Kress, W., Schneider, V., Wallgren-Pettersson, C., Herger, F., Buj-Bello, A., Blondeau, F., Liechti-Gallati, S., and Mandel, J. L. (2000). MTM1 mutations in X-linked myotubular myopathy. Hum Mutat *15*, 393-409.

Le Douarin, N., Dulac, C., Dupin, E., and Cameron-Curry, P. (1991). Glial cell lineages in the neural crest. Glia *4*, 175-184.

Le, T. B., Aszmann, O., Chen, Y. G., Royall, R. M., and Brushart, T. M. (2001). Effects of pathway and neuronal aging on the specificity of motor axon regeneration. Exp Neurol *167*, 126-132.

Leal, A., Morera, B., Del Valle, G., Heuss, D., Kayser, C., Berghoff, M., Villegas, R., Hernandez, E., Mendez, M., Hennies, H. C., *et al.* (2001). A second locus for an axonal form of autosomal recessive Charcot-Marie- Tooth disease maps to chromosome 19q13.3. Am J Hum Genet *68*, 269-274.

LeGuern, E., Guilbot, A., Kessali, M., Ravise, N., Tassin, J., Maisonobe, T., Grid, D., and Brice, A. (1996). Homozygosity mapping of an autosomal recessive form of demyelinating Charcot-Marie-Tooth disease to chromosome 5q23-q33. Hum Mol Genet *5*, 1685-1688.

Lemke, G., Lamar, E., and Patterson, J. (1988). Isolation and analysis of the gene encoding peripheral myelin protein zero. Neuron *1*, 73-83.

Liu, H., Nakagawa, T., Kanematsu, T., Uchida, T., and Tsuji, S. (1999). Isolation of 10 differentially expressed cDNAs in differentiated Neuro2a cells induced through controlled expression of the GD3 synthase gene. J Neurochem *72*, 1781-1790.

Llanos, S., Clark, P. A., Rowe, J., and Peters, G. (2001). Stabilization of p53 by p14ARF without relocation of MDM2 to the nucleolus. Nat Cell Biol *3*, 445-452.

Lohrum, M. A., Ashcroft, M., Kubbutat, M. H., and Vousden, K. H. (2000). Identification of a cryptic nucleolar-localization signal in MDM2. Nat Cell Biol *2*, 179-181.

Lupski, J. R., de Oca-Luna, R. M., Slaugenhaupt, S., Pentao, L., Guzzetta, V., Trask, B. J., Saucedo-Cardenas, O., Barker, D. F., Killian, J. M., Garcia, C. A., and et al. (1991). DNA duplication associated with Charcot-Marie-Tooth disease type 1A. Cell *66*, 219-232.

Lykke-Andersen, J. (2001). mRNA quality control: Marking the message for life or death. Curr Biol *11*, R88-91.

Lyon, G. (1969). Ultrastructural study of a nerve biopsy from a case of early infantile chronic neuropathy. Acta Neuropathol *13*, 131-142.

Maayan, C., Kaplan, E., Shachar, S., Peleg, O., and Godfrey, S. (1987). Incidence of familial dysautonomia in Israel 1977-1981. Clin Genet *32*, 106-108.

Machiels, B. M., Zorenc, A. H., Endert, J. M., Kuijpers, H. J., van Eys, G. J., Ramaekers, F. C., and Broers, J. L. (1996). An alternative splicing product of the lamin A/C gene lacks exon 10. J Biol Chem *271*, 9249-9253.

Mandich, P., Mancardi, G. L., Varese, A., Soriani, S., Di Maria, E., Bellone, E., Bado, M., Gross, L., Windebank, A. J., Ajmar, F., and Schenone, A. (1999). Congenital hypomyelination due to myelin protein zero Q215X mutation. Ann Neurol *45*, 676-678.

Maniatis, T. (1999). A ubiquitin ligase complex essential for the NF-kappaB, Wnt/Wingless, and Hedgehog signaling pathways. Genes Dev *13*, 505-510.

Marques, W., Jr., Hanna, M. G., Marques, S. R., Sweeney, M. G., Thomas, P. K., and Wood, N. W. (1999). Phenotypic variation of a new P0 mutation in genetically identical twins. J Neurol *246*, 596-599.

Martinello, F., Fardin, P., Ottina, M., Ricchieri, G. L., Koenig, M., Cavalier, L., and Trevisan, C. P. (1998). Supplemental therapy in isolated vitamin E deficiency improves the peripheral neuropathy and prevents the progression of ataxia. J Neurol Sci *156*, 177-179.

Mayer, C., Quasthoff, S., and Grafe, P. (1998). Differences in the sensitivity to purinergic stimulation of myelinating and non-myelinating Schwann cells in peripheral human and rat nerve. Glia *23*, 374-382.

McEntagart, M., Norton, N., Williams, H., Teare, M. D., Dunstan, M., Baker, P., Houlden, H., Reilly, M., Wood, N., Harper, P. S., *et al.* (2001). Localization of the gene for distal hereditary motor neuronopathy VII (dHMN-VII) to chromosome 2q14. Am J Hum Genet *68*, 1270-1276.

Menegoz, M., Gaspar, P., Le Bert, M., Galvez, T., Burgaya, F., Palfrey, C., Ezan, P., Arnos, F., and Girault, J. A. (1997). Paranodin, a glycoprotein of neuronal paranodal membranes. Neuron *19*, 319-331.

Mersiyanova, I. V., Perepelov, A. V., Polyakov, A. V., Sitnikov, V. F., Dadali, E. L., Oparin, R. B., Petrin, A. N., and Evgrafov, O. V. (2000). A new variant of Charcot-Marie-Tooth disease type 2 is probably the result of a mutation in the neurofilament-light gene. Am J Hum Genet *67*, 37-46.

Muchir, A., Bonne, G., van der Kooi, A. J., van Meegen, M., Baas, F., Bolhuis, P. A., de Visser, M., and Schwartz, K. (2000). Identification of mutations in the gene encoding lamins A/C in autosomal dominant limb girdle muscular dystrophy with atrioventricular conduction disturbances (LGMD1B). Hum Mol Genet *9*, 1453-1459.

Naef, R., and Suter, U. (1999). Impaired intracellular trafficking is a common disease mechanism of PMP22 point mutations in peripheral neuropathies. Neurobiol Dis *6*, 1-14.

Nagano, A., and Arahata, K. (2000). Nuclear envelope proteins and associated diseases. Curr Opin Neurol *13*, 533-539.

Nagarajan, R., Svaren, J., Le, N., Araki, T., Watson, M., and Milbrandt, J. (2001). EGR2 mutations in inherited neuropathies dominant-negatively inhibit myelin gene expression. Neuron *30*, 355-368.

Nawwar, A. M., Sherif, M. F., and Barakat, N. G. (1995). Instrumented forceps for measurement of nerve compression forces. J Biomech Eng *117*, 53-58.

Nelis, E., Haites, N., and Van Broeckhoven, C. (1999a). Mutations in the peripheral myelin genes and associated genes in inherited peripheral neuropathies. Hum Mutat *13*, 11-28.

Nelis, E., Timmerman, V., De Jonghe, P., Van Broeckhoven, C., and Rautenstrauss, B. (1999b). Molecular genetics and biology of inherited peripheral neuropathies: a fast-moving field. Neurogenetics *2*, 137-148.

Nelis, E., Van Broeckhoven, C., De Jonghe, P., Lofgren, A., Vandenberghe, A., Latour, P., Le Guern, E., Brice, A., Mostacciuolo, M. L., Schiavon, F., *et al.* (1996). Estimation of the mutation frequencies in Charcot-Marie-Tooth disease type 1 and hereditary neuropathy with liability to pressure palsies: a European collaborative study. Eur J Hum Genet *4*, 25-33.

Notterpek, L., Ryan, M. C., Tobler, A. R., and Shooter, E. M. (1999). PMP22 accumulation in aggresomes: implications for CMT1A pathology. Neurobiol Dis *6*, 450-460.

Othmane, K. B., Johnson, E., Menold, M., Graham, F. L., Hamida, M. B., Hasegawa, O., Rogala, A. D., Ohnishi, A., Pericak-Vance, M., Hentati, F., and Vance, J. M. (1999). Identification of a new locus for autosomal recessive Charcot-Marie- Tooth disease with focally folded myelin on chromosome 11p15. Genomics *62*, 344-349.

Ouvrier, R. A., McLeod, J. G., and Conchin, T. E. (1987). The hypertrophic forms of hereditary motor and sensory neuropathy. A study of hypertrophic Charcot-Marie-Tooth disease (HMSN type I) and Dejerine-Sottas disease (HMSN type III) in childhood. Brain *110*, 121-148.

Patel, P. I., Roa, B. B., Welcher, A. A., Schoener-Scott, R., Trask, B. J., Pentao, L., Snipes, G. J., Garcia, C. A., Francke, U., Shooter, E. M., and et al. (1992). The gene for the peripheral myelin protein PMP-22 is a candidate for Charcot-Marie-Tooth disease type 1A. Nat Genet *1*, 159-165.

Pennisi, E. (1998). How a growth control path takes a wrong turn to cancer. Science *281*, 1438-1439, 1441.

Perea, J., Robertson, A., Tolmachova, T., Muddle, J., King, R. H., Ponsford, S., Thomas, P. K., and Huxley, C. (2001). Induced myelination and demyelination in a conditional mouse model of Charcot-Marie-Tooth disease type 1A. Hum Mol Genet *10*, 1007-1018.

Pham-Dinh, D., Popot, J. L., Boespflug-Tanguy, O., Landrieu, P., Deleuze, J. F., Boue, J., Jolles, P., and Dautigny, A. (1991). Pelizaeus-Merzbacher disease: a valine to phenylalanine point mutation in a putative extracellular loop of myelin proteolipid. Proc Natl Acad Sci U S A *88*, 7562-7566.

Pingault, V., Bondurand, N., Kuhlbrodt, K., Goerich, D. E., Prehu, M. O., Puliti, A., Herbarth, B., Hermans-Borgmeyer, I., Legius, E., Matthijs, G., *et al.* (1998). SOX10 mutations in patients with Waardenburg-Hirschsprung disease. Nat Genet *18*, 171-173.

Pingault, V., Guiochon-Mantel, A., Bondurand, N., Faure, C., Lacroix, C., Lyonnet, S., Goossens, M., and Landrieu, P. (2000). Peripheral neuropathy with hypomyelination, chronic intestinal pseudo- obstruction and deafness: a developmental "neural crest syndrome" related to a SOX10 mutation. Ann Neurol *48*, 671-676.

Podratz, J. L., Rodriguez, E., and Windebank, A. J. (2001). Role of the extracellular matrix in myelination of peripheral nerve. Glia *35*, 35-40.

Postma, T. J., Benard, B. A., Huijgens, P. C., Ossenkoppele, G. J., and Heimans, J. J. (1993). Long-term effects of vincristine on the peripheral nervous system. J Neurooncol *15*, 23-27.

Quasthoff, S., and Hartung, H. P. (2002). Chemotherapy-induced peripheral neuropathy. J Neurol *249*, 9-17.

Quattrone, A., Gambardella, A., Bono, F., Aguglia, U., Bolino, A., Bruni, A. C., Montesi, M. P., Oliveri, R. L., Sabatelli, M., Tamburrini, O., *et al.* (1996). Autosomal recessive hereditary motor and sensory neuropathy with focally folded myelin sheaths: clinical, electrophysiologic, and genetic aspects of a large family. Neurology *46*, 1318-1324.

Rasband, M. N., Peles, E., Trimmer, J. S., Levinson, S. R., Lux, S. E., and Shrager, P. (1999). Dependence of nodal sodium channel clustering on paranodal axoglial contact in the developing CNS. J Neurosci *19*, 7516-7528.

Ray, D. E. (1997). Function in neurotoxicity: index of effect and also determinant of vulnerability. Clin Exp Pharmacol Physiol *24*, 857-860.

Reilly, M. M. (1998). Genetically determined neuropathies. J Neurol *245*, 6-13.

Riley, C. M., Day, R.L., Greely, D., Langford, W.S. (1949). Central autonomic dysfunction with defective lacrimation. Pediatrics *3*, 468-477.

Roa, B. B., Dyck, P. J., Marks, H. G., Chance, P. F., and Lupski, J. R. (1993a). Dejerine-Sottas syndrome associated with point mutation in the peripheral myelin protein 22 (PMP22) gene. Nat Genet *5*, 269-273.

Roa, B. B., Garcia, C. A., Suter, U., Kulpa, D. A., Wise, C. A., Mueller, J., Welcher, A. A., Snipes, G. J., Shooter, E. M., Patel, P. I., and et al. (1993b). Charcot-Marie-Tooth disease type 1A. Association with a spontaneous point mutation in the PMP22 gene. N Engl J Med *329*, 96-101.

Roberts, R. G. (2001). Dystrophins and dystrobrevins. Genome Biol *2*.

Rogers, T., Chandler, D., Angelicheva, D., Thomas, P. K., Youl, B., Tournev, I., Gergelcheva, V., and Kalaydjieva, L. (2000). A novel locus for autosomal recessive peripheral neuropathy in the EGR2 region on 10q23. Am J Hum Genet *67*, 664-671.

Saam, J. R., and Gordon, J. I. (1999). Inducible gene knockouts in the small intestinal and colonic epithelium. J Biol Chem *274*, 38071-38082.

Sadot, E., Simcha, I., Iwai, K., Ciechanover, A., Geiger, B., and Ben-Ze'ev, A. (2000). Differential interaction of plakoglobin and beta-catenin with the ubiquitin-proteasome system. Oncogene *19*, 1992-2001.

Sahenk, Z. (1999). Abnormal Schwann cell-axon interactions in CMT neuropathies. The effects of mutant Schwann cells on the axonal cytoskeleton and regeneration-associated myelination. Ann N Y Acad Sci *883*, 415-426.

Salinas, A. E., and Wong, M. G. (1999). Glutathione S-transferases--a review. Curr Med Chem *6*, 279-309.

Santoro, L., Manganelli, F., Di Maio, L., Barbieri, F., Carella, M., D'Adamo, P., and Casari, G. (2002). Charcot-Marie-Tooth disease type 2C: a distinct genetic entity.

Clinical and molecular characterization of the first European family. Neuromuscul Disord *12*, 399-404.

Scherer, S. S., Xu, Y. T., Bannerman, P. G., Sherman, D. L., and Brophy, P. J. (1995). Periaxin expression in myelinating Schwann cells: modulation by axon- glial interactions and polarized localization during development. Development *121*, 4265-4273.

Scott, M., Boisvert, F. M., Vieyra, D., Johnston, R. N., Bazett-Jones, D. P., and Riabowol, K. (2001). UV induces nucleolar translocation of ING1 through two distinct nucleolar targeting sequences. Nucleic Acids Res *29*, 2052-2058.

Senderek, J., Ramaekers, V. T., Zerres, K., Rudnik-Schoneborn, S., Schroder, J. M., and Bergmann, C. (2001). Phenotypic variation of a novel nonsense mutation in the P0 intracellular domain. J Neurol Sci *192*, 49-51.

Shackleton, S., Lloyd, D. J., Jackson, S. N., Evans, R., Niermeijer, M. F., Singh, B. M., Schmidt, H., Brabant, G., Kumar, S., Durrington, P. N., *et al.* (2000). LMNA, encoding lamin A/C, is mutated in partial lipodystrophy. Nat Genet *24*, 153-156.

Shatzky, S., Moses, S., Levy, J., Pinsk, V., Hershkovitz, E., Herzog, L., Shorer, Z., Luder, A., and Parvari, R. (2000). Congenital insensitivity to pain with anhidrosis (CIPA) in Israeli- Bedouins: genetic heterogeneity, novel mutations in the TRKA/NGF receptor gene, clinical findings, and results of nerve conduction studies. Am J Med Genet *92*, 353-360.

Sheng, M. (1996). PDZs and receptor/channel clustering: rounding up the latest suspects. Neuron *17*, 575-578.

Sherman, D. L., and Brophy, P. J. (2000). A tripartite nuclear localization signal in the PDZ-domain protein L- periaxin. J Biol Chem *275*, 4537-4540.

Sherman, D. L., Fabrizi, C., Gillespie, C. S., and Brophy, P. J. (2001). Specific disruption of a schwann cell dystrophin-related protein complex in a demyelinating neuropathy. Neuron *30*, 677-687.

Shusterman, V., Usiene, I., Harrigal, C., Lee, J. S., Kubota, T., Feldman, A. M., and London, B. (2002). Strain-specific patterns of autonomic nervous system activity and heart failure susceptibility in mice. Am J Physiol Heart Circ Physiol *282*, H2076-2083.

Simonati, A., Fabrizi, G. M., Pasquinelli, A., Taioli, F., Cavallaro, T., Morbin, M., Marcon, G., Papini, M., and Rizzuto, N. (1999). Congenital hypomyelination neuropathy with Ser72Leu substitution in PMP22. Neuromuscul Disord *9*, 257-261.

Skre, H. (1974). Genetic and clinical aspects of Charcot-Marie-Tooth's disease. Clin Genet *6*, 98-118.

Slaugenhaupt, S. A., Blumenfeld, A., Gill, S. P., Leyne, M., Mull, J., Cuajungco, M. P., Liebert, C. B., Chadwick, B., Idelson, M., Reznik, L., *et al.* (2001). Tissue-

specific expression of a splicing mutation in the IKBKAP gene causes familial dysautonomia. Am J Hum Genet *68*, 598-605.

Smith, A. G., Ramachandran, P., Tripp, S., and Singleton, J. R. (2001). Epidermal nerve innervation in impaired glucose tolerance and diabetes- associated neuropathy. Neurology *57*, 1701-1704.

Soltysik-Espanola, M., Rogers, R. A., Jiang, S., Kim, T. A., Gaedigk, R., White, R. A., Avraham, H., and Avraham, S. (1999). Characterization of Mayven, a novel actin-binding protein predominantly expressed in brain. Mol Biol Cell *10*, 2361-2375.

Southard-Smith, E. M., Kos, L., and Pavan, W. J. (1998). Sox10 mutation disrupts neural crest development in Dom Hirschsprung mouse model. Nat Genet *18*, 60-64.

Spiegelman, V. S., Slaga, T. J., Pagano, M., Minamoto, T., Ronai, Z., and Fuchs, S. Y. (2000). Wnt/beta-catenin signaling induces the expression and activity of betaTrCP ubiquitin ligase receptor. Mol Cell *5*, 877-882.

Sternberg, N., and Hamilton, D. (1981). Bacteriophage P1 site-specific recombination. I. Recombination between loxP sites. J Mol Biol *150*, 467-486.

Street, V. A., Goldy, J. D., Golden, A. S., Tempel, B. L., Bird, T. D., and Chance, P. F. (2002). Mapping of Charcot-Marie-Tooth disease type 1C to chromosome 16p identifies a novel locus for demyelinating neuropathies. Am J Hum Genet *70*, 244-250.

Sullivan, T., Escalante-Alcalde, D., Bhatt, H., Anver, M., Bhat, N., Nagashima, K., Stewart, C. L., and Burke, B. (1999). Loss of A-type lamin expression compromises nuclear envelope integrity leading to muscular dystrophy. J Cell Biol *147*, 913-920.

Sunderland, S. (1951). Classification of peripheral nerve injuries producing loss of function. Brain *74*, 491.

Suter, U., Moskow, J. J., Welcher, A. A., Snipes, G. J., Kosaras, B., Sidman, R. L., Buchberg, A. M., and Shooter, E. M. (1992a). A leucine-to-proline mutation in the putative first transmembrane domain of the 22-kDa peripheral myelin protein in the trembler-J mouse. Proc Natl Acad Sci U S A *89*, 4382-4386.

Suter, U., Welcher, A. A., Ozcelik, T., Snipes, G. J., Kosaras, B., Francke, U., Billings-Gagliardi, S., Sidman, R. L., and Shooter, E. M. (1992b). Trembler mouse carries a point mutation in a myelin gene. Nature *356*, 241-244.

Tait, S., Gunn-Moore, F., Collinson, J. M., Huang, J., Lubetzki, C., Pedraza, L., Sherman, D. L., Colman, D. R., and Brophy, P. J. (2000). An oligodendrocyte cell adhesion molecule at the site of assembly of the paranodal axo-glial junction. J Cell Biol *150*, 657-666.

Takashima, H., Boerkoel, C. F., De Jonghe, P., Ceuterick, C., Martin, J. J., Voit, T., Schroder, J. M., Williams, A., Brophy, P. J., Timmerman, V., and Lupski, J. R.

(2002). Periaxin mutations cause a broad spectrum of demyelinating neuropathies. Ann Neurol *51*, 709-715.

Takashima, H., Nakagawa, M., Suehara, M., Saito, M., Saito, A., Kanzato, N., Matsuzaki, T., Hirata, K., Terwilliger, J. D., and Osame, M. (1999). Gene for hereditary motor and sensory neuropathy (proximal dominant form) mapped to 3q13.1. Neuromuscul Disord *9*, 368-371.

Tao, W., and Levine, A. J. (1999). P19(ARF) stabilizes p53 by blocking nucleo-cytoplasmic shuttling of Mdm2. Proc Natl Acad Sci U S A *96*, 6937-6941.

Tate, P., Lee, M., Tweedie, S., Skarnes, W. C., and Bickmore, W. A. (1998). Capturing novel mouse genes encoding chromosomal and other nuclear proteins. J Cell Sci *111*, 2575-2585.

Taylor, G. S., Maehama, T., and Dixon, J. E. (2000). Inaugural article: myotubularin, a protein tyrosine phosphatase mutated in myotubular myopathy, dephosphorylates the lipid second messenger, phosphatidylinositol 3-phosphate. Proc Natl Acad Sci U S A *97*, 8910-8915.

Thomas, P. K., Marques, W., Jr., Davis, M. B., Sweeney, M. G., King, R. H., Bradley, J. L., Muddle, J. R., Tyson, J., Malcolm, S., and Harding, A. E. (1997). The phenotypic manifestations of chromosome 17p11.2 duplication. Brain *120*, 465-478.

Timmerman, V., De Jonghe, P., Ceuterick, C., De Vriendt, E., Lofgren, A., Nelis, E., Warner, L. E., Lupski, J. R., Martin, J. J., and Van Broeckhoven, C. (1999). Novel missense mutation in the early growth response 2 gene associated with Dejerine-Sottas syndrome phenotype. Neurology *52*, 1827-1832.

Timmerman, V., De Jonghe, P., Simokovic, S., Lofgren, A., Beuten, J., Nelis, E., Ceuterick, C., Martin, J. J., and Van Broeckhoven, C. (1996a). Distal hereditary motor neuropathy type II (distal HMN II): mapping of a locus to chromosome 12q24. Hum Mol Genet *5*, 1065-1069.

Timmerman, V., De Jonghe, P., Spoelders, P., Simokovic, S., Lofgren, A., Nelis, E., Vance, J., Martin, J. J., and Van Broeckhoven, C. (1996b). Linkage and mutation analysis of Charcot-Marie-Tooth neuropathy type 2 families with chromosomes 1p35-p36 and Xq13. Neurology *46*, 1311-1318.

Timmerman, V., Nelis, E., Van Hul, W., Nieuwenhuijsen, B. W., Chen, K. L., Wang, S., Ben Othman, K., Cullen, B., Leach, R. J., Hanemann, C. O., and et al. (1992). The peripheral myelin protein gene PMP-22 is contained within the Charcot-Marie-Tooth disease type 1A duplication. Nat Genet *1*, 171-175.

Topilko, P., Levi, G., Merlo, G., Mantero, S., Desmarquet, C., Mancardi, G., and Charnay, P. (1997). Differential regulation of the zinc finger genes Krox-20 and Krox-24 (Egr-1) suggests antagonistic roles in Schwann cells. J Neurosci Res *50*, 702-712.

Topilko, P., Schneider-Maunoury, S., Levi, G., Baron-Van Evercooren, A., Chennoufi, A. B., Seitanidou, T., Babinet, C., and Charnay, P. (1994). Krox-20 controls myelination in the peripheral nervous system. Nature *371*, 796-799.

Ulrich, H. D., and Jentsch, S. (2000). Two RING finger proteins mediate cooperation between ubiquitin- conjugating enzymes in DNA repair. EMBO J *19*, 3388-3397.

Umehara, F., Tate, G., Itoh, K., Yamaguchi, N., Douchi, T., Mitsuya, T., and Osame, M. (2000). A novel mutation of desert hedgehog in a patient with 46,XY partial gonadal dysgenesis accompanied by minifascicular neuropathy. Am J Hum Genet *67*, 1302-1305.

Uziyel, Y., Hall, S., and Cohen, J. (2000). Influence of laminin-2 on Schwann cell-axon interactions. Glia *32*, 109-121.

Vance, J. M. (2000). The many faces of Charcot-Marie-Tooth disease. Arch Neurol *57*, 638-640.

Verhoeven, K., Villanova, M., Rossi, A., Malandrini, A., De Jonghe, P., and Timmerman, V. (2001). Localization of the gene for the intermediate form of charcot-marie- tooth to chromosome 10q24.1-q25.1. Am J Hum Genet *69*, 889-894.

Wachtler, J., Mayer, C., Quasthoff, S., Adelsberger, H., and Grafe, P. (1996). P2 purinoceptor-mediated intracellular Ca2+ transients in human sural nerve. Neuroreport *7*, 1289-1292.

Warner, L. E., Hilz, M. J., Appel, S. H., Killian, J. M., Kolodry, E. H., Karpati, G., Carpenter, S., Watters, G. V., Wheeler, C., Witt, D., *et al.* (1996a). Clinical phenotypes of different MPZ (P0) mutations may include Charcot- Marie-Tooth type 1B, Dejerine-Sottas, and congenital hypomyelination. Neuron *17*, 451-460.

Warner, L. E., Mancias, P., Butler, I. J., McDonald, C. M., Keppen, L., Koob, K. G., and Lupski, J. R. (1998). Mutations in the early growth response 2 (EGR2) gene are associated with hereditary myelinopathies. Nat Genet *18*, 382-384.

Warner, L. E., Reiter, L. T., Murakami, T., and Lupski, J. R. (1996b). Molecular mechanisms for Charcot-Marie-Tooth disease and related demyelinating peripheral neuropathies. Cold Spring Harb Symp Quant Biol *61*, 659-671.

Warner, L. E., Svaren, J., Milbrandt, J., and Lupski, J. R. (1999). Functional consequences of mutations in the early growth response 2 gene (EGR2) correlate with severity of human myelinopathies. Hum Mol Genet *8*, 1245-1251.

Watson, D. F., Nachtman, F. N., Kuncl, R. W., and Griffin, J. W. (1994). Altered neurofilament phosphorylation and beta tubulin isotypes in Charcot-Marie-Tooth disease type 1. Neurology *44*, 2383-2387.

Weber, J. D., Taylor, L. J., Roussel, M. F., Sherr, C. J., and Bar-Sagi, D. (1999). Nucleolar Arf sequesters Mdm2 and activates p53. Nat Cell Biol *1*, 20-26.

Webster (1984). Peripheral Neuropathy. In Peripheral Neuropathy, P. J. Dyck, ed., pp. 329-359.

Wegner, M. (2000). Transcriptional control in myelinating glia: the basic recipe. Glia *29*, 118-123.

Williams, A. C., and Brophy, P. J. (2002). The function of the Periaxin gene during nerve repair in a model of CMT4F. J Anat *200*, 323-330.

Winston, J. T., Koepp, D. M., Zhu, C., Elledge, S. J., and Harper, J. W. (1999). A family of mammalian F-box proteins. Curr Biol *9*, 1180-1182.

Wrabetz, L., and Feltri, M. L. (2001). Do Schwann cells stop, DR(o)P2, and roll? Neuron *30*, 642-644.

Wrabetz, L., Feltri, M. L., Quattrini, A., Imperiale, D., Previtali, S., D'Antonio, M., Martini, R., Yin, X., Trapp, B. D., Zhou, L., *et al.* (2000). P(0) glycoprotein overexpression causes congenital hypomyelination of peripheral nerves. J Cell Biol *148*, 1021-1034.

Xirodimas, D., Saville, M. K., Edling, C., Lane, D. P., and Lain, S. (2001). Different effects of p14ARF on the levels of ubiquitinated p53 and Mdm2 in vivo. Oncogene *20*, 4972-4983.

Yoshikawa, H., Nishimura, T., Nakatsuji, Y., Fujimura, H., Himoro, M., Hayasaka, K., Sakoda, S., and Yanagihara, T. (1994). Elevated expression of messenger RNA for peripheral myelin protein 22 in biopsied peripheral nerves of patients with Charcot-Marie-Tooth disease type 1A. Ann Neurol *35*, 445-450.

Young, P., and Suter, U. (2001). Disease mechanisms and potential therapeutic strategies in Charcot- Marie-Tooth disease. Brain Res Brain Res Rev *36*, 213-221.

Zhang, Y., and Xiong, Y. (1999). Mutations in human ARF exon 2 disrupt its nucleolar localization and impair its ability to block nuclear export of MDM2 and p53. Mol Cell *3*, 579-591.

Zhao, C., Takita, J., Tanaka, Y., Setou, M., Nakagawa, T., Takeda, S., Yang, H. W., Terada, S., Nakata, T., Takei, Y., *et al.* (2001). Charcot-Marie-Tooth disease type 2A caused by mutation in a microtubule motor KIF1Bbeta. Cell *105*, 587-597.

Zhu, Q., Couillard-Despres, S., and Julien, J. P. (1997). Delayed maturation of regenerating myelinated axons in mice lacking neurofilaments. Exp Neurol *148*, 299-316.